Alma Mater Studiorum · University of Bologna

School of Science
Department of Physics and Astronomy
Master's Degree in Physics

Improving Delivery Time for Breath-Hold Proton Therapy via Combination of Advanced Spot Positioning Algorithms and Ridge Filter

Supervisor:

Prof. Mauro Villa

Co-supervisors:

Isabella Colizzi, PhD

Nicola Bizzocchi, Medical Physicist

Submitted by:

Martina Bonomi

Academic Year 2022/2023

ALMA MATER STUDIORUM - UNIVERSITY OF BOLOGNA

Abstract

Pencil beam scanning (PBS) is particularly susceptible to respiration-induced tumor motions, which can result in unnecessary dose exposure of healthy tissues or inadequate dosing of the target. Various motion mitigation techniques, such as rescanning, gating, and breath-hold, are used to address this issue. However, breath-hold's widespread use in proton therapy, particularly for scanned delivery, is limited due to the need for rapid treatment delivery.

In this study, we aimed at assessing the feasibility of delivering an entire field dose within one single breath-hold in PSI's Gantry 2 by examining the advantages and limitations of combining a novel designed Ridge filter (RF) with various spot placement techniques to reduce the treatment delivery time, trying to achieve delivery times per field (in case of small tumors) or per patch (in case of large tumors that require the patching technique used by Gantry 2) of approximately less than 20 seconds. To achieve our goal, treatment plans were created on a cohort of 12 breath-hold cases using as spot placement algorithms a fixed gird-based algorithm (Fixed Grid configuration), an energy-dependent algorithm based on the beam's size in air at the isocenter (Air configuration) and an energy-dependent algorithm based on the beam's size in water at the Bragg peak (Water configuration). Configurations performances were then compared in terms of plans quality, clinical acceptability and delivery time reduction for each patient.

Results indicated that the Fixed Grid configuration showed the best performance, by meeting all medical prescriptions and robustness criteria. The Air and Water configurations, instead, performed poorly, with the Water configuration showing the worst results and not yelding any acceptable plans due to excessive dosing of the target and nearby organs at risk. Furthermore, it was demonstrated that the combination of the Ridge filter with different spot placement algorithms significantly reduced the dead time during dose delivery compared to the clinical setups currently used at PSI's proton therapy center. Finally, in terms of breath-hold feasibility, it was determined that, out of the clinically acceptable plans we created, the delivery of an entire field dose within a single breath-hold was feasible for small tumors, while for extended tumor volumes performing one breath-hold per patch was a feasible solution.

In conclusion, we found that by combining the RF with a spot placement algorithm based on a fixed grid, we can obtain clinically acceptable plans and achieve mean delivery times per field or per patch of less than 20 seconds enabling breath-hold techniques with PSI's Gantry 2.

Acknowledgements

Premessa: non sono brava con le parole a ringraziare le persone. Di solito sto zitta e apprezzo in silenzio, anche se non si nota. Se devo essere sincera, comunico molto meglio con la mia collezione di sticker di Whatsapp. E odio le cose sdolcinate. Ah, poi non so nemmeno più scrivere in italiano. Non che sia mai stata una gran scrittrice. Ne sono la prova i miei temi del liceo scritti a caratteri cubitali per occupare spazio e riempire le pagine. Ma ci proverò lo stesso. Anche perché in un qualche modo 120 pagine di tesi le ho riempite.

Per prima cosa, vorrei ringraziare la mia PAZIENZA nell'usare e creare piani con il treatment planning system del PSI, la mia carissima FIonA. Che dire. Grazie. Mi hai insegnato a diventare zen. Ho imparato che nient'altro potrà farmi innervosire d'ora in poi. Ringrazio anche la mia playlist di Spotify "botta di vita", che mi ha supportata durante la mia lunga relazione con FIonA. Se non fosse stato per te, avrei terminato la relazione molto prima.

Simpatia a parte, ringrazio dal profondo del mio cuore i miei genitori, che hanno sempre creduto in me e nelle mie capacità, e mi hanno sempre incoraggiata a fare ciò che mi piaceva. Sono la persona che sono ora soprattutto grazie a voi e grazie al vostro amore. Mi sento fortunata ad essere vostra figlia, non vi deluderò. Vi voglio bene.

Ringrazio tutte le mie amiche e i miei amici, che siete sparsi un po' per tutta Italia e tutto il mondo. Grazie per tutti i mille ricordi e risate in tutti questi anni, non vi cambierei con nulla al mondo. Ad altrettanti momenti passati insieme (magari a Cuba? Io la butto lì...)

Ringrazio il mio relatore, Mauro Villa, che mi ha seguito in ogni step della realizzazione di questa tesi.

Ringrazio Isabella, la miglior supervisor che potessi avere. Questi tesi in realtà è anche un po' tua. Grazie per aver sopportato costantemente le mie lamentele sulla pioggia perenne della Svizzera, ma a quanto pare sono io che faccio piovere ovunque vada. Ma soprattutto, grazie per avermi insegnato, tra gossip e drama, più cose di quanto mi sarei mai immaginata durante la mia permanenza al PSI. Prima di andarmene da Zurigo mi hai fatto i complimenti per la mia motivazione e mi hai detto di puntare in alto perché ne ho le capacità. Grazie, lo farò. (Cuba...?)

Ringrazio Nicola Bizzocchi, altro mio supervisor al Paul Scherrer Institute, che è sempre stato disponibile per qualsiasi cosa durante la mia permanenza in Svizzera, e tutti i PhD students e Master's students con cui ho condiviso l'ufficio per quattro mesi. È stato un piacere passare del tempo con voi (e mangiare tutti i dolci che portavamo in ufficio).

Vorrei anche ringraziare Fabio, per l'opportunità che mi ha dato di lavorare con il suo team e per quella che mi sta dando per il mio futuro. Sei stata la prima persona a farmi sentire apprezzata veramente per il lavoro che faccio, e di questi tempi non è affatto scontato. PhD o no, ci si vede a Sydney!

Infine, (call me selfish, but) vorrei dedicare questa tesi a nessun altro se non a me stessa e alla mia determinazione. Nonostante qualsiasi cosa, non mi sono mai arresa e anzi mi sono impegnata sempre di piu nel raggiungere i miei obiettivi (essere testardi non sempre è un difetto). Alla fine di questo percorso sono fiera di me stessa e di poter dire di essere diventata una persona diversa, migliore, sia dal punto di vista accademico che personale.

Contents

Nomenclature

BH **B**reath **H**old

BP **B**ragg **P**eak

CPT **C**enter **P**roton **T**herapy

CTV **C**linical **T**arget **V**olume

CT **C**omputed **T**omography

DIBH **D**eep **I**nspiration **B**reath **H**old

DVH **D**ose-**V**olume **H**istogram

EC **E**nforced **C**onstraint

EM **E**lectro **M**agnetic

FB **F**ree **B**reathing

FWHM **F**ull **W**idth **H**alf **M**aximum

HS **H**ot-**S**pot

ICRU **I**nternational **C**ommission on **R**adiation **U**nits and Measurements

IMPT **I**ntensity **M**odulated **P**roton **T**herapy

LET **L**inear **E**nergy **T**ransfer

MCS **M**ultiple **C**oulomb **S**cattering

MFO **M**ultiple **F**ield **O**ptimization

NSCLC **N**on **S**mall **C**ell **L**ung **C**ancer

OAR **O**rgan **A**t **R**isk

OP **O**ptimization **P**oint

OS **O**verall **S**urvival

PBS **P**encil **B**eam **S**canning

PBT **P**roton **B**eam **T**herapy

PSI **P**aul **S**cherrer **I**nstitute

PSPT **P**assive **S**cattering **P**roton **T**herapy

PSP **P**roton **S**topping **P**ower

PS **P**assive **S**cattering

PTCOG **P**article **T**herapy **C**o-**O**perative **G**roup

PTV **P**lanning **T**arget **V**olume

RBE **R**elative **B**iological **E**ffectiveness

RF **R**idge **F**ilter

RT **R**adiation **T**herapy

SCLC **S**mall **C**ell **L**ung **C**ancer

SFO **S**ingle **F**ield **O**ptimization

SMF **S**pot **M**argin **F**actor

SOBP **S**pread **O**ut **B**ragg **P**eak

SSF **S**pot **S**pacing **F**actor

TPS **T**reatment **P**lanning **S**ystem

VMAT **V**olumetric **M**odulated **A**rc **T**herapy

WHO **W**orld **H**ealth **O**rganization

Chapter 1

Introduction to Proton Therapy

Cancer is one of the leading causes of death worldwide. In 2020, it was estimated that there were 19.3 million new cases of cancer and 10 million cancer-related deaths globally [1].

Cancer is caused by DNA mutations or changes in cells, which can start almost anywhere in the human body, and can lead to uncontrolled cell growth and division. In normal conditions, human cells grow and multiply to substitute older, damaged, or dead cells as the body needs them. The control of human cell division is a highly regulated process involving the coordination of many different proteins and mechanisms: any disruption to these processes can lead to abnormalities in cell division, which can contribute to the development of cancerous cells. Some cancers are caused by inherited genetic mutations, which are passed down from parents to their children. However, most cancers are caused by acquired mutations, which occur during a person's lifetime as a result of exposure to various environmental or lifestyle factors, such as exposure to specific chemicals or radiation, viral infections, and lifestyle choices like smoking, drinking alcohol, and eating poorly [2].

There are many different types of cancer, each with its own unique risk factors, symptoms, and available treatments. The methods used to treat cancer vary based on the type and stage of the disease, but surgery, chemotherapy, immunotherapy, and radiation therapy are the mainly used methods.

Surgery involves the removal of the cancerous mass or tissue from the body. Depending on the position of the tumor inside the patient, this procedure can either be minimally

invasive or not. In the majority of cases, surgery is combined with chemotherapy or radiotherapy. Chemotherapy aims at killing or slowing down the growth of cancerous cells by means of drugs, which work by targeting rapidly dividing cells including cancerous ones, but also other healthy cells in the body that divide quickly, such as those in the bone marrow, hair follicles, and digestive tract, causing several collateral effects to the patient. Immunotherapy uses the body's immune system to recognize and attack abnormal cells, such as cancerous cells. The most common immunotherapy treatments involve the use of checkpoint inhibitors, CAR-T cells, monoclonal antibodies, and cancer vaccines. Radiation therapy, instead, uses radiation (with energies on the order of MeV/MV) to damage the DNA of cancerous cells, which will prevent them from growing and dividing and eventually kill them. Cancerous cells are more susceptible to radiation than normal cells because they divide more rapidly and they are less able to repair DNA damage. Two different kinds of radiation are used to treat cancer: photons (conventional radiotherapy) and protons or carbon ions (hadron therapy).

For the purposes of this study, we will focus only on proton therapy.

1.1 Basic Quantities Used in Proton Therapy

Before getting into the specifics of proton treatment, it's worthwhile introducing some fundamental quantities utilized in proton therapy.

Protons are elementary particles with a positive charge $\mathrm{e} = +1.602 \times 10^{-19}\mathrm{C}$ and a rest energy $\mathrm{mc}^2 = 938.27$ MeV.

We can define the fluence Φ as the number of protons, during a given exposure of treatment, crossing an infinitesimal element of area dA normal to the beam's direction, namely

$$\Phi \equiv \frac{\mathrm{d}N}{\mathrm{d}A}\left[\frac{\text{protons}}{\mathrm{cm}^2}\right] \tag{1.1}$$

The stopping power is the rate at which a single proton loses kinetic energy:

$$S \equiv -\frac{\mathrm{d}E}{\mathrm{d}x}\left[\frac{\mathrm{MeV}}{\mathrm{cm}}\right] \tag{1.2}$$

The mass stopping power is the stopping power normalized to the density of the medium traversed:

$$\frac{S}{\rho} \equiv -\frac{1}{\rho}\frac{\mathrm{d}E}{\mathrm{d}x}\left[\frac{\mathrm{MeV}}{\mathrm{g/cm^2}}\right] \tag{1.3}$$

where ρ (g/cm^3) is the local density of the medium crossed.

If the material crossed is not homogeneous, we can model it as a succession of very thin sheets of each constituent element. The mass stopping power will then be given by the sum of the contributions of each different element:

$$\frac{S}{\rho} = \sum_i w_i \left(\frac{S}{\rho}\right)_i \tag{1.4}$$

The physical absorbed dose D at some point in a radiation field is the energy absorbed per unit target mass. In SI units, it is defined as:

$$D \equiv \frac{\mathrm{d}E}{\mathrm{d}m}\left[\frac{\mathrm{J}}{\mathrm{kg}}\right] \tag{1.5}$$

The unit of the dose used in radiation therapy is the Gray: 1 Gy $\equiv$ 1 J/kg. Generally, a complete proton therapy treatment delivers $\approx$ 70 Gy to $\approx$ 1000 cm^3 of target volume given in $\approx$ 35 fractions of $\approx$ 2 Gy each. However, hypofractionated radiotherapy has been increasingly utilized in recent years [3], in which larger doses per fraction are delivered and therefore fewer fractions are prescribed in a given treatment course.

The physical absorbed dose, the fluence, and the stopping power are related in the following way:

$$D = \Phi\frac{S}{\rho} = 0.1602 \cdot \Phi\frac{S}{\rho}[\mathrm{Gy}] \tag{1.6}$$

It's important to keep in mind that the energy lost by a proton beam exceeds the energy absorbed locally by the patient, as a portion of the beam's energy is converted into neutral secondaries like γ-rays and neutrons, which can escape the patient body and therefore can deposit their energy elsewhere in the shielding or the treatment room.

Lastly, when working with a certain type of radiation that differs from conventional X-rays, the relative biological effectiveness (RBE) for a radiation of type R on a tissue is defined as

$$RBE = \frac{D_X}{D_R} \tag{1.7}$$

where D_X is a reference absorbed dose of radiation of a standard type X, usually X-rays, and D_R is the absorbed dose of radiation of type R that causes the same amount of biological damage. Generally, proton dosages are specified in GyRBE, which are given by multiplying the equivalent photon dose in Gy by the RBE factor, i.e., Gy $\times$ RBE. For proton therapy, the RBE is assumed to be a constant value of 1.1, as it is the standard value used in many institutions, including the Paul Scherrer Institute (PSI) [4].

1.2 Photon Therapy vs. Proton Therapy

Radiation therapy is a medical treatment that uses high-energy radiation, such as X-rays or protons, to kill cancerous cells by damaging their DNA, making it difficult or impossible for them to grow and divide.

Photons and protons interact with matter in different ways due to their different properties: indeed, photons are elementary neutral particles, while protons are subatomic particles with a positive electric charge. This leads to different treatment outcomes when comparing photon therapy with proton therapy. Figure 1.1 shows the contrasting behavior of photons and protons in terms of energy release in matter as a function of the distance traveled in water. Photons exhibit a dose buildup followed by an exponential decay. As they travel inside the patient, they interact mainly by Compton scattering and pair production for energies on the order of MeV, releasing their energy to the electrons of the crossed matter. At the entrance region, the dose deposited by electrons to surrounding tissues increases with depth due to a lack of charged particles equilibrium [5]. This phenomenon creates the buildup region on the left of the curve, which is considered to be clinically beneficial since it protects the skin [6]. Once equilibrium is reached, the intensity of the beam is then attenuated following an exponential trend. For charged

particles, instead, the number of particles only decreases slightly with depth when interacting with matter by electromagnetic (EM) or nuclear interactions, while the energy of each one decreases continuously, making thus the entire beam stop at approximately the same depth. Additionally, charged particles lose more energy per cm as they slow down, such that there's a large dose enhancement just before they stop: this is referred to as "Bragg peak" (BP). The physical mechanism that lead to the formation of the BP will be discussed in Section 1.3.

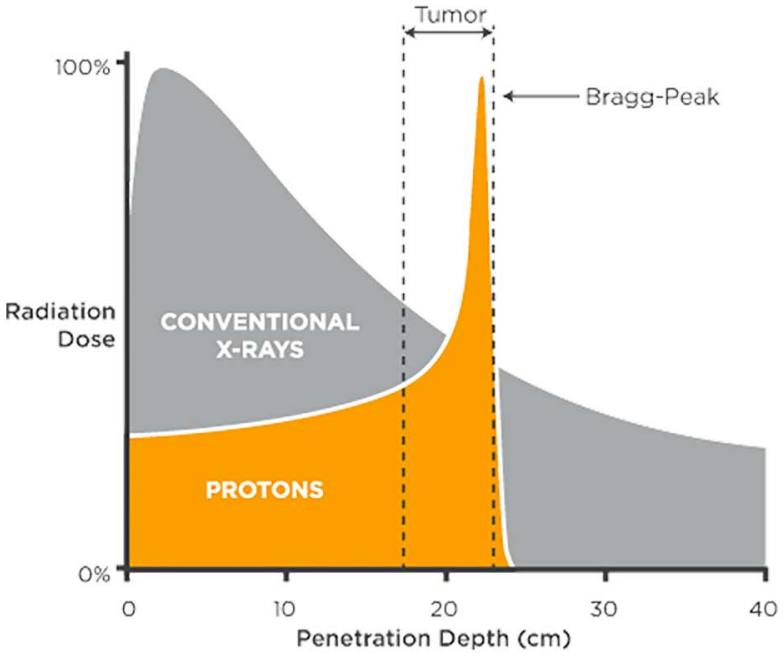

FIGURE 1.1: Depth-dose distribution for photons (grey area) and quasi-monoenergetic Bragg peak for protons (orange area). Photons have an exponential decay, which makes them deliver radiation even to healthy tissues beyond the tumor. Protons, instead, deliver the majority of their energy to the target at a specific depth and stop there, sparing beyond tissues [7].

Two important features when using radiation therapy are the lateral penumbra (well defined for both photons and protons) and the distal penumbra (only defined for protons), which are essential for sparing critical organs adjacent to the target volume. These are defined as $d_{20} - d_{80}$, where d_{20} and d_{80} are the values of the lateral position (for lateral penumbra) or depth (for distal penumbra) at which 20% and 80% of the dose is delivered.

The lateral penumbra that can be achieved in the patient is determined by the design of the beam delivery system as well as the nature of the interaction between radiation particles and tissues in the patient. Figure 1.2 shows the lateral penumbra for a 6 MeV

photon beam and that for a scattered proton beam at different depths (4 and 10 cm): overall, the lateral penumbra for protons is much sharper than the one for photons. However, it increases rapidly with depth, becoming larger than photons' penumbra at depths greater than $\sim$ 20 cm [6].

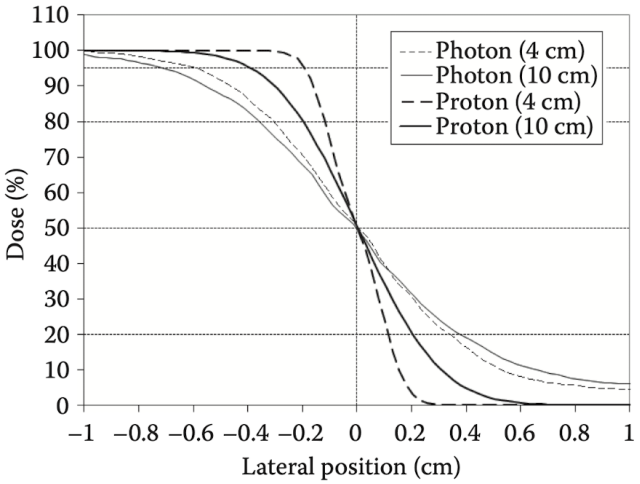

FIGURE 1.2: Lateral penumbra profiles comparison for a 6 MeV photon beam and a scattered proton beam. Proton beams show a steeper lateral penumbra with respect to photon beams, at least for not too big depths [6].

The distal penumbra, instead, results from the formation of the BP, and it is an additional degree of freedom that can be used when planning with protons which is not present with photons. In a medium with quite homogeneous tissue density, the distal beam penumbra is always much sharper than the lateral one, and it increases with energy (for reasons that will be better explained in Section 1.3). However, if the beam travels through a region with a high-gradient tissue inhomogeneity, the distal penumbra can be degraded and may be much greater than the lateral penumbra. It should be pointed out that while the distal beam penumbra is substantially sharper than the lateral one, it is not typically employed clinically for tight margin sparing due to problems in predicting the beam range in the patient.

These different behavior in both the energy release as a function of depth and the lateral and distal penumbras make protons an attractive alternative to conventional radiotherapy, as the potential of proton therapy is the ability to increase the radiation dose to the tumor while simultaneously decreasing the radiation dose to surrounding healthy tissues. Indeed, conventional radiotherapy delivers a dose to the tumor and beyond,

harming healthy tissues and having serious consequences, whereas proton therapy delivers a beam of proton particles that stops at the tumor location, sparing organs at risk.

1.3 Protons' Characteristics

In this section, we will describe all the main features that characterize protons and lead to the formation of the BP, which is the key aspect that distinguishes proton therapy from photon therapy.

1.3.1 Protons-Matter Interactions

As previously mentioned, protons (and charged particles in general) undergo electromagnetic (EM) interactions or nuclear interactions. The most important EM interaction between charged particles and matter is multiple Coulomb scattering (MCS). Except in rare cases, the deflection of a charged particle by a single atomic nucleus is extremely small: therefore, the observed angular spread of a proton beam crossing matter is mainly due to the random combination of several such deflections. In addition to MCS, protons may interact with the atomic nucleus through elastic or non-elastic nuclear reactions: in the latter case the nucleus is permanently altered, and the proton undergoes processes in which it is absorbed by the nucleus and one or more nucleons are released. These secondary particles that escape the nucleus have considerably lower energy than the entering proton and will deliver a certain amount of dose at the reaction site to the surrounding tissues.

1.3.2 Energy Loss

As the interaction of a particle with matter is a stochastic process, protons in a monoenergetic beam crossing the same depth of material will not release the same amount of energy. The Bethe-Bloch formula (Eq. 1.8) gives the average value of those energy losses (or stopping power):

$$-\frac{\mathrm{d}E}{\mathrm{d}x} = \frac{\rho Z}{A}\frac{4\pi N_A m_\mathrm{e} c^2}{M_U}\left(\frac{e^2}{4\pi\epsilon_0 m_\mathrm{e} c^2}\right)^2 \frac{z^2}{\beta^2}\left[\ln\left(\frac{2m_\mathrm{e}c^2\beta^2}{I(1-\beta^2)}\right) - \beta^2 - \frac{\delta}{2} - \frac{C}{Z}\right] \tag{1.8}$$

From Eq. 1.8, we can see that the energy loss depends on both the properties of the medium crossed, i.e. the material density ρ, the atomic number Z, the mass number A and the ionization potential of the material I, and the characteristics of the beam, i.e. the beam atomic number z and the beam velocity β. It is important to notice from this equation that the rate at which protons lose their energy and transfer it to the surrounding matter increases as protons slow down since in a given proton-electron interaction, the longer the proton stays closer to the electron, the more momentum is transferred to it. As a result, the majority of the proton's energy is released near the end of the range when the particle is traveling at extremely low speeds before stopping completely, giving rise to a pronounced peak (see Figure 1.1).

1.3.3 Mean Penetration Depth

As a consequence of the stochastic nature of particles' interactions with matter, all protons will come to rest at approximately (but not exactly) the same depth. We define the mean projected range of a proton beam with initial energy E_{initial} as the mean penetration depth measured along a straight line parallel to the original direction of motion of the charged particles, it is calculated by summing the energy loss in very thin slabs until the energy reaches E_{final}:

$$R_{\text{proj}}(E_{\text{initial}}) = \int_{E_{\text{initial}}}^{E_{\text{final}}} \langle \cos\chi \rangle \left(\frac{1}{\rho} \frac{\mathrm{d}E}{\mathrm{d}x} \right)^{-1} \mathrm{d}E \tag{1.9}$$

where $\langle \cos\chi \rangle$ is the mean value of the cosine of the scattering angle. As we can see from Eq. 1.9, the range of protons (and charged particles in general) is determined by their kinetic energy, allowing them to reach deeper or more superficial regions, which is unique to proton treatment. For clinical purposes, the range of energies used for proton beams is between 3-300 MeV, as within this range we can cover the entire thickness of the human body (see Table 1.1).

Kinetic Energy [MeV]	1	3	10	30	100	300
Range [cm H_2O]	0.002	0.014	0.123	0.885	7.718	51.45

TABLE 1.1: Range-energy table values for water [6].

The slight dispersion in the stopping point that occurs when the incident beam has an energy spread is referred to as "range straggling" (see Figure 1.3) and it is an essential factor that must be taken into consideration when delivering a dose to a tumor in front of an organ at risk. In current practice, range uncertainty is addressed in treatment planning by adding a margin to the tumour contour, typically 3.5%, to avoid any target undershooting [6]. Although this ensures that the distal element of the target volume is covered, it also risks overdosing the normal tissue behind the target volume.

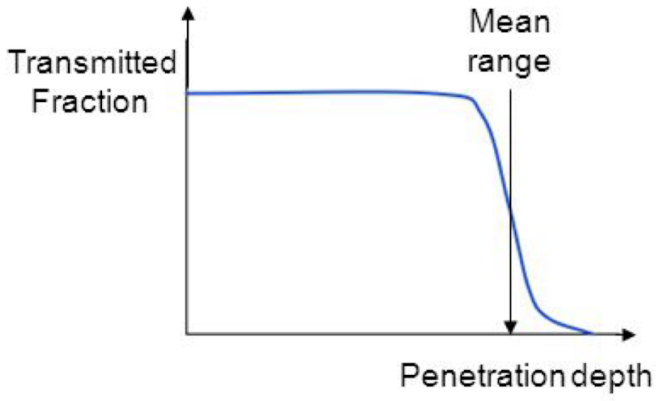

FIGURE 1.3: Transmitted fraction of protons as a function of the penetration depth, showing the so-called "range straggling", which is due to the stochastic behaviour of charged particles' energy loss.

1.3.4 Bragg Peak

All the protons' features described above come together to determine the characteristic shape of the Bragg Peak, which is defined as the integral depth-dose distribution in water of a broad quasi-monoenergetic proton beam.

The width of the Bragg peak region is given by the contribution of both the range straggling $\sigma_{RS} \sim 0.012 \times$ range and the beam's energy spread σ_{beam}, and it changes with the beam's energy. For cyclotron based facilities, when using a degrader followed by beam analysis, as in the case of PSI's Gantry 2 and Gantry 3, at higher energies the beam can travel deeper in matter and, as a consequence, the number of scattering events will be higher and the energy spread of the beam will be greater. This will cause the peak to enlarge in width and decrease in height with respect to a beam traveling at lower energies, as can be seen in Figure 1.4. Moreover, as the range straggling σ_{RS} is directly proportional to the energy of the beam, the lower the energy, the steeper the distal penumbra of the peak and vice-versa.

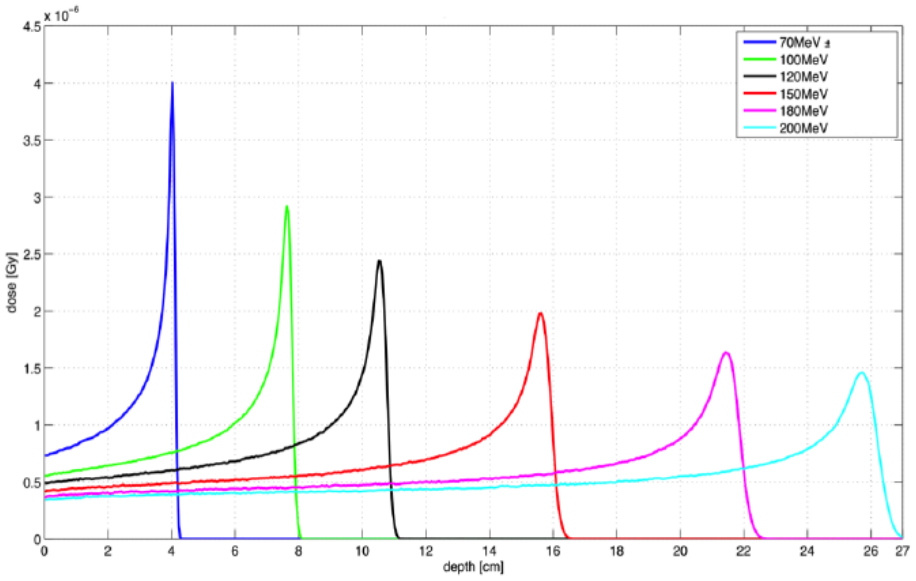

FIGURE 1.4: Shape of the BPs at different energies measured at PSI's Gantry 2: at low energies, BPs are sharper, taller, and have a steeper dose fall-off due to the lower MCS; at higher energies BPs are broader and less steep due to the higher MCS and larger range straggling [8].

1.4 Pencil Beam's Characteristics

During proton treatment, the accelerator and beam transport system can deliver a quasi mono-energetic pencil beam with a variable size to the patient at any given moment. A pencil beam can be described in the longitudinal dimension by the depth–dose distribution (BP), and in the transversal dimension by a Gaussian distribution, as shown in Figure 1.5.

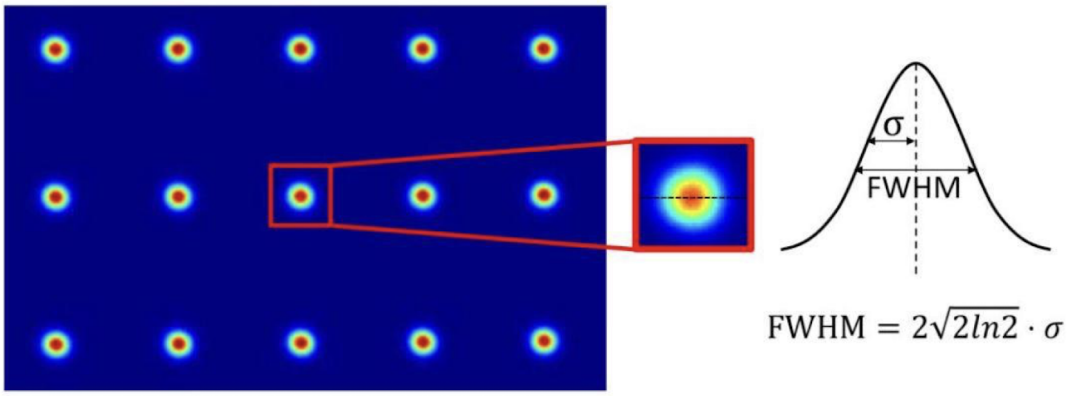

FIGURE 1.5: Gaussian shape of a pristine proton beam. On the left, the 2-dimensional visualization of the beam (scanning map); on the right the 1-dimensional Gaussian shape characterized by the parameter σ [9].

A point P inside a pristine BP at a water equivalent depth w and at a position described by (t, u) in the transverse plane (see Figure 1.6) is described by:

$$P = \frac{D_P(w)}{2\pi\sigma_t\sigma_u} \mathrm{e}^{-\frac{t^2}{2\sigma_t^2}} \mathrm{e}^{-\frac{u^2}{2\sigma_u^2}} \tag{1.10}$$

where $D_P(w)$ is the integral dose at depth w, and σ_t and σ_u are the parameters that characterize the Gaussian distributions of the beam in the t and u transverse directions, respectively. The beam's sigma σ is the only parameter that characterizes the Gaussian shape and it depends on the beam's optics: the smaller it is, the sharper the dose fall-off will be, and the better the organs at risk close to the target will be spared.

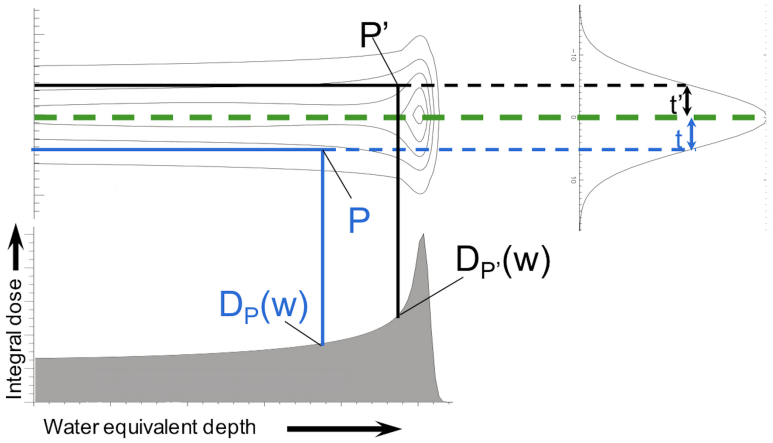

FIGURE 1.6: 3-dimensional visualization of point P inside a pristine proton beam in space and its corresponding integral dose at a certain depth w [9].

1.5 The Spread-Out Bragg Peak (SOBP)

Proton therapy relies on precise adjustments of the BP in order cover the target, and protect healthy tissues as much as possible. As a mono-energetic proton beam is unsuitable in many situations for cancer treatment due to its narrow width, sometimes it is necessary to spread out this peak to provide a uniform dose within the target volume and protect healthy tissues as much as possible. To widen the treatment depth range and create a flat dose distribution, the so-called "spread-out Bragg peak" (SOBP) is created by varying the energy of the incident proton beam with appropriate weights to produce a superposition of several Bragg peaks in the same beam direction (see Figure 1.7).

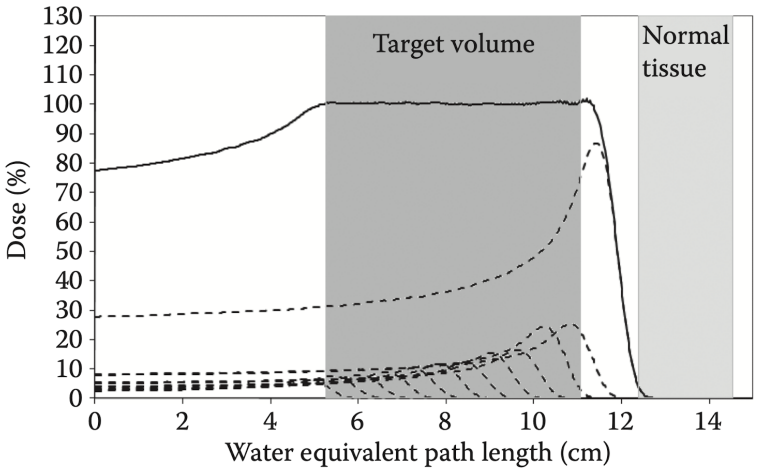

FIGURE 1.7: Spread-out Bragg peak (SOBP): the uniform dose plateau is obtained by adding several BPs with different energies and different weights [6].

The dose distribution in Figure 1.7 shows very important features: first of all, the delivered dose in depth across the target volume is uniform. Second, the SOBP preserves the sharp distal fall of the Bragg peak, thus having the ability to spare normal tissue behind the target volume. However, as each single Bragg peak delivers a certain dose at the entrance (from 10% up to 30%), by summing several BPs to create the SOBP, a considerable dose will be delivered at the entrance region, of about 80% of the total dose. This must be taken into consideration when deciding the direction of the fields used to deliver the treatment, as this dose may damage other tissues when entering inside the patient before reaching the tumor volume.

Finally, the creation of a SOBP depends on the beam's source: for cyclotron-based facilities, it is obtained by using degraders or range shifters to change the energy of the beam, as cyclotrons can only provide a fixed energy beam, whereas synchrotron-based facilities can provide beams of varying energies without the need of using energy degraders.

1.6 Proton Therapy Delivery Methods

After being accelerated by a cyclotron or a synchrotron, protons are transported into the treatment room through the beam line. The proton beam that enters the treatment room is quasi mono-energetic and has just a few millimeters of lateral spread. Without adjustment, this beam would provide a dosage distribution that is clinically ineffective.

The clinical use of the proton beam requires it to be spread to create of a uniform dose distribution both in the lateral and the in the longitudinal directions. Generally, two different proton therapy delivery methods are used: passive scattering and pencil beam scanning. The main difference between the two techniques can be seen in Figure 1.8.

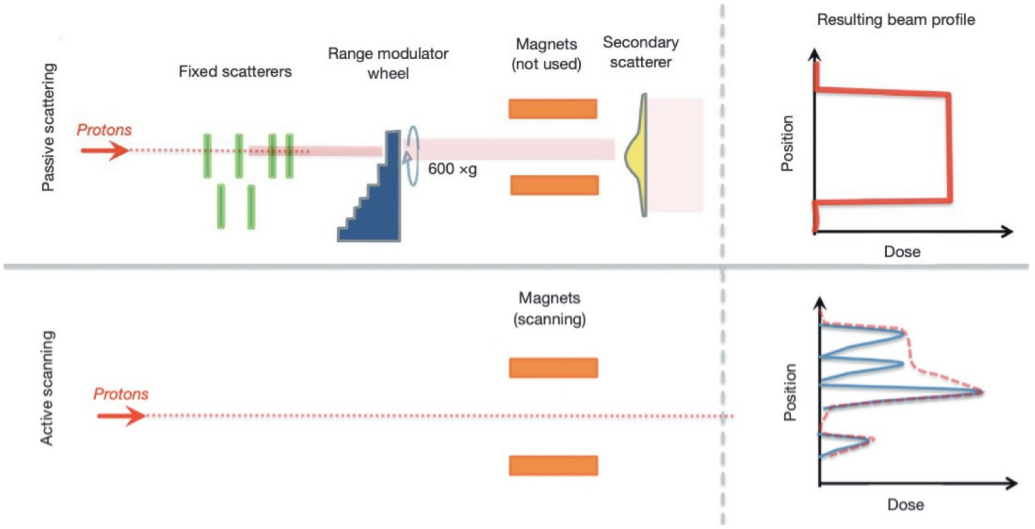

FIGURE 1.8: Differences between passive scattering (PS) (above) and pencil beam scanning (PBS) (below). In PS, the beam is widened by mean of scatterers and the energy is changed by means of Ridge filters or modulator wheels, resulting a uniform beam profile. In PBS, the pristine beam is scanned with magnets all over the target and the energy is changed layer by layer, resulting in a non uniform beam profile conform to the tumor [10].

Passive scattering (PS) is a delivery technique in which the proton beam is spread out both laterally and longitudinally to cover the entire tumor size. Lateral spread of the beam can be achieved by single or double scattering: single scattering can be used for smaller field sizes, whereas for greater uniform field sizes a double scattering system is necessary. Most double scattering systems can create a uniform field distribution for maximal field sizes of up to 25 cm in diameter. Collimators can then shape the radiation field that impinges on the patient by laterally shaping the beam's edges, to adapt it to the tumor's profile. A spinning range modulator wheel allows the beam energy to change with time, resulting in a spread in the protons' energies and in the creation of a SOBP with a uniform dose distribution. The multiple energies are not delivered simultaneously, but rather in a single cycle of a range modulator wheel [10]. Other ways of changing the beam's energy is by mean of Ridge filters (RF), which will be discussed later. The main drawback of passive scattering techniques, however, is that the delivered field has a single depth, which causes dose delivery also to regions that should be spared. To overcome this issue, usually compensators are used [11], which

conform the beam's distal fall-off to the target, thus stopping the beam at the end of the it without delivering additional doses to the organs at risk.

In pencil beam scanning (PBS) (also known as active scanning or spot scanning), a focused beam of protons of varying strength and energy is magnetically scanned over the tumor. This scanning technique allows for conformal dose in the lateral directions (t, u) without using additional hardware. Moreover, the ability to regulate the energy (and hence the depth of penetration of the protons) eliminates the need for field specific range compensators, and the resultant beams can adapt to the target's proximal and distal forms.

Depending on the kind and location of the tumor, either approach should be used: for eye cancers, PS is always used, but for any other tumor location, PBS is currently used worldwide. Several medical studies have been conducted to compare clinical results of PS and PBS proton beam treatments, but different results have been found. Gjyshi et al. [12] showed that patients with toracic malignancies treated with PBS had lower mean radiation doses to the OAR and experienced fewer pulmonary and cardiac toxicities than those treated with PS proton treatment (PSPT). However, Nichols et al. [13] reported that when compared to PS, proton treatment for locally advanced pancreatic cancer utilizing PBS was not linked with clinically relevant reductions in normal tissue dosage, yet PBS resulted in statistically significant improvements in target coverage and may provide enhanced conformality for the treatment of irregular targets. Additonally, Won et al. [14] reported that there were no differences in oncologic outcomes, including overall survival, in-field local control, out-field intrahepatic control, extrahepatic progression-free survival, and complete response rates, or in the toxicity profiles between PS and PBS proton beam therapy (PBT) for primary hepatocellular carcinoma. However, further investigations are necessary.

Since our work is based on PSI's Gantry 2, which uses the PBS delivery method, our focus will be on this latter technique.

1.7 Pencil Beam Scanning

Pencil Beam Scanning (PBS) is the leading method worldwide used in proton therapy. It consists of "painting" the target with narrow spots, which correspond to the position

of the BPs, by steering the beam in both longitudinal and transversal directions to deposit the correct dose at the right position at a proper time. In the longitudinal direction, the beam is moved across the target by changing the beam's energy, and thus its penetration depth. This can be achieved either upstream, by directly changing the energy of the beam exiting the cyclotron, or downstream, by mean of range shifters at the nozzle position in such a way that the beam is slowed down. In the transverse direction, instead, the beam can be scanned either by mechanical motions, by magnetic field variation or by a combination of the two. In the first case, one could physically move the target with respect to a fixed beam position. In the second case, instead, the beam is scanned by varying the magnetic fields to bend the beam's trajectory, as in PSI Gantry 2. Finally, a combination of the two techniques can also be used, for example by scanning the beam magnetically in one dimension and moving the target in the other dimension, as in PSI Gantry 1 [6].

Unlike passive scattering, where a SOBP is generated to produce a uniform depth-dose distribution, in PBS this will be obtained through the superposition of the BPs at different energies used to distribute the dose inside the target volume. For shallower depths, BPs have a narrower width and a steeper distal dose fall-off. When adding them in the longitudinal direction, if the widths are not big enough, this could generate a non-uniform depth-dose distribution. To address this issue, ridge filters or range modulators can be used to slightly widen the BP and generate a more uniform dose distribution. However, this is mainly done for carbon ions as they are characterized by much sharper peaks with respect to protons. The transverse dose distribution, instead, is given by a superposition of the transverse raw beam profiles.

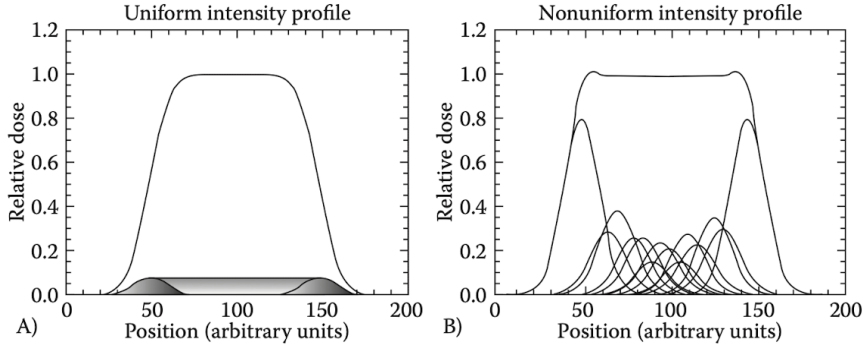

FIGURE 1.9: Superposition of equally spaced Gaussian beams with same amplitudes (A) and non-uniformly spaced and modulated Gaussian beams (B) to obtain a uniform overall dose distribution [6].

As mentioned before, a pristine beam has a Gaussian distribution: a key feature of Gaussian curves is that, assuming the curves are not too far apart, the sum of equally spaced Gaussian distributions yields a uniform distribution. Therefore, by adding beams together in the transverse direction, a flat dose distribution can be obtained, as shown in Figure 1.9. The relative intensity of the pencil beams can change to have a sharper lateral penumbra, even if the delivered dose will not be perfectly uniform (edge enhancement).

The events that take place during a scanning sequence will influence the time required to deliver the treatment plan, and depending on motion effects, will determine the actual delivered dose distribution. There are two types of existing scanning patterns used to deliver the dose to a target volume: in one case (Figure 1.10), the beam scans the transverse cross-section first and then changes the range (energy). In the other case (Figure 1.11), instead, the beam scans a horizontal layer by varying the energy, before moving to another layer in the transverse direction [6]. Depending on the different scanning patterns, the delivery time is different. Indeed, the first method is much faster than the second one, as it takes more time to change the energy to deliver the dose at different depths with respect to changing the transversal position. At PSI, the first technique is used.

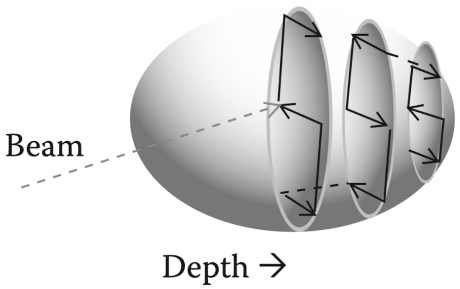

FIGURE 1.10: Scanning in the longitudinal direction: the beam is first scanned on the transversal $u-t$ plane and then energy is changed layer by layer [6].

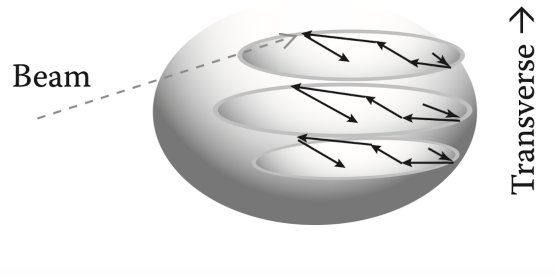

FIGURE 1.11: Scanning in the transversal direction: the beam is first scanned in the horizontal direction while changing energy, and then it is moved in the vertical direction to scan the next layer [6].

1.8 Clinical Results Using Proton Therapy for Thoracic Malignancies

The number of cancer patients who are being treated with proton therapy has been following a growing trend in the past two decades thanks to the innovative studies and positive outcomes. According to the Particle Therapy Co-Operative Group (PTCOG) [15], the number of patients treated with proton therapy increased from $\sim$ 50.000 in 2007 up to $\sim$ 280.000 in 2021. Particle therapy is considered to be safer and just as effective as traditional radiation therapy for adults with advanced cancer thanks to the reduction in the delivered integral dose. However, it remains to be well investigated how much clinical benefit this reduction achieves for patients. According to W. Levin and T. DeLaney [16], with minimization of the normal tissue dose protons may allow for better tolerance of combined chemotherapy and radiation therapy regimens.

For the purposes of this thesis, we will be focusing on the clinical results of proton therapy used for treating thoracic malignancies, in particular non-small cell lung cancer (NSCLC). While there is evidence that lung cancer rates are decreasing, it is still considered the largest cause of cancer-related mortality. In 2010, 28% of patients were diagnosed with stage III disease, and this number has slightly decreased in recent years as more patients were identified with early stages (I and II) and later stages (IV) [17]. Despite advances in therapy and technology, lung cancer still has a low overall survival (OS). People with NSCLC account for more than 80% of all lung cancer patients, with small cell lung cancer (SCLC) accounting for the remainder. SCLC is more aggressive than NSCLC, frequently appearing with bulkier disease near dose-limiting mediastinal structures, having a 5-year survival rate of around 6%, compared to 23% for NSCLC [18].

The main advantages of using protons over photons for thoracic neoplasms are improved organs-at-risk (OAR) sparing in the chest, reduced risks of radiation-induced toxicities, safer deposition of curative irradiation doses to tumors, and lower total integral dose, which reduces the risk of secondary malignancies in patients who are expected to live long enough to potentially experience significant morbidity [17] [19]. Indeed, in contrast to photon-based intensity-modulated radiation therapy (IMRT) or volumetric modulated arc therapy (VMAT), which typically need 5 to >12 beam fields, in intensity-modulated

proton therapy (IMPT) only 2 to 4 fields are needed. When compared to photon therapy, recent dosimetry studies have shown that proton therapy has an advantage compared to photon therapy both theoretically and clinically [18] [19], as it significantly reduces the dose to normal tissues, particularly lungs, heart, and esophagus, while maintaining similar robust target volume coverage to the clinical target volume (CTV) in both early and advanced NSCLC, with a more homogeneous dose distribution when PBS proton therapy is applied with respect to PSPT [12]. However, as the majority of studies comparing the effectiveness and safety of proton treatment to traditional photon therapy had small sample sizes and were single-arm studies missing a direct comparison, the advantages of proton therapy still need to be fully investigated.

Apart from dosimetric differences from photons, protons may be different also from a radio-biologically point of view. Preclinical results suggest that the biological reactions of protons and photons may differ, with proton beam therapy (PBT) being more efficient than photons at sensitizing NSCLC cells [19]. Furthermore, preliminary in-vitro studies show that PBT may have an immunogenic benefit, as researchers discovered that protons can boost cytotoxic T-lymphocyte death of tumor cells, even in cells that are normally resistant to photon radiation therapy (RT) [20].

1.9 Proton Therapy Limitations

Despite the dosimetric benefits of PBS proton therapy over traditional radiation therapy mentioned above, issues in treating moving targets persist, as do concerns about the technique's high costs.

1.9.1 Treatment of Moving Targets

Target motion is a substantially greater problem for proton treatment than for photon therapy, particularly when utilizing a scanning delivery mode. Complex treatment plans with steep dose gradients necessitate measures for mitigating and compensating for motion effects in general, particularly breathing movements. Indeed, the relative movements of the proton beam and the intrafractional breathing-related motion overlap, resulting in a distortion of the patient's dose distribution, the so-called "interplay

effects". These are patient-specific and depend on the target size, tumor motion amplitude and frequency.

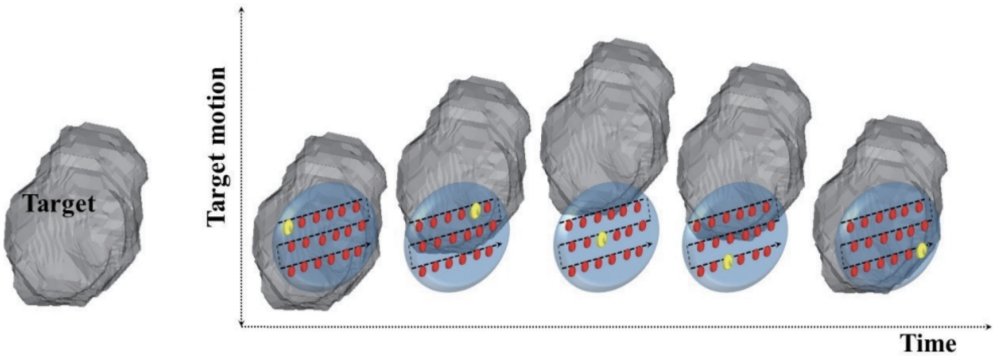

FIGURE 1.12: Schematic representation showing the relative motion between the target and the beam, leading to interplay effects. The red colored spots represent the planned spot sequence and the yellow colored spot represent the dose being irradiated at a specific time [21].

Many studies have found that while interplay effects in proton treatment have little influence on the mean target dose, they cause a significant decrease in dose homogeneity, which can significantly impact tumor control, with smaller spot sizes being more sensitive to motion and interplay effects compared to bigger spot sizes [3]. According to the World Health Organization (WHO) cancer incidence estimates, breathing motion affects around 55% of potentially lethal tumors requiring treatment. The impact of breathing motion on clinical outcomes differs depending on anatomical position and proximity to the diaphragm [22]. It is therefore critical that future proton treatment systems can detect this motion and adjust beam supply accordingly. Another factor that affects dose uniformity to the target volume is range uncertainty, which necessitates a distinct margin along the beam direction and is affected by patient geometry and beam angle. Because the tumor is frequently surrounded by low-density tissue, these effects are amplified in the lungs.

Despite ongoing attempts to reduce motion effects in both advanced photon treatment and proton therapy in body areas affected by breathing motion with amplitudes of up to 2 to 3 cm, systematic advancements are still required. Several motion mitigation techniques have been developed so far in order to mitigate breathing motion, the most common of which being gating, tracking, rescanning, increasing target's margins and breath-hold [3] [23].

Respiratory gating, also known as free breathing (FB) gating, refers to the restriction of treatment delivery to certain phases of the breathing cycle and requires continuous monitoring. FB gating strategies are typically utilized during end-expiration, which occupies the majority of the breathing cycle (see Figure 1.13). Gating is now the most widely utilized motion mitigation method in particle treatment.

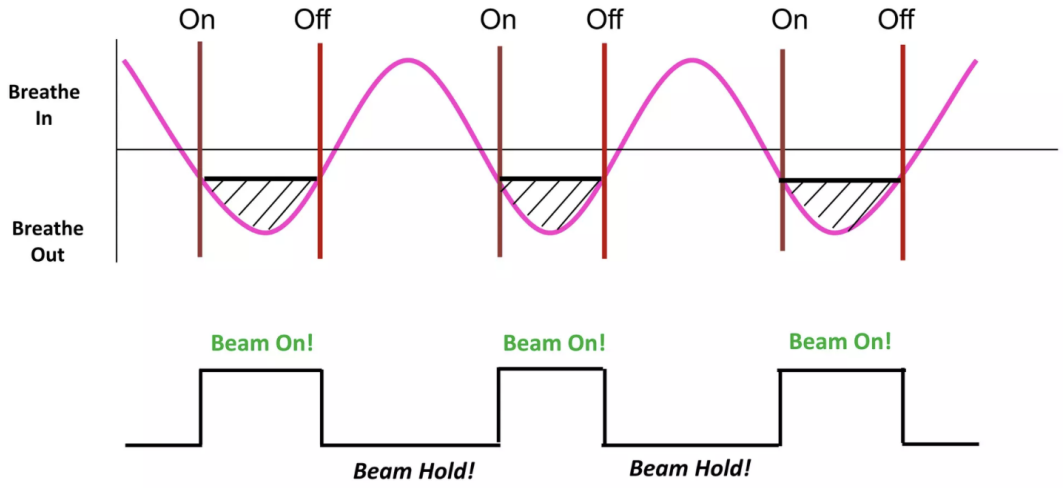

FIGURE 1.13: Visual representation of a breathing cycle used for respiratory gating. During the expiration phase of the respiratory cycle, the beam is turned on and the treatment is delivered, while during inspiration the beam is off [24].

Tracking implies continuous delivery of the treatment while tracking the tumor's path. However, it relies on real-time 3D imaging information of the patient, which is not yet available for particle therapy and thus not yet implemented clinically.

Rescanning is a motion mitigation technique that is unique for scanned particles. It consists of n repeated scans in which the dose is supplied at 1/n of the initial spot weight to reduce interplay effects by statistical averaging. As it requires to deliver several times a small amount of dose, it requires fast transverse scanning and gantries that are able to deliver very small dose elements. The main difference between rescanning and gating is that gating decreases the dosage to normal lungs substantially more than rescanning at the expense of longer treatment times. However, gating and rescanning are frequently used in combination, as is the case at the PSI.

Another method widely used for moving targets consists of increasing the tumor's margins when delivering the dose to the target to account for its movements. In particular, there exist field specific margins that take into consideration target's motion for each

field's direction. It is generally used in combination with the other methods and the margins values may vary depending on how effective other procedures are.

Finally, deep inspiration breath-hold (DIBH) consists of delivering an entire fraction of dose within single or multiple breath holds, generally performed in combination with gating. This can be achieved either by voluntary breath-hold or with computer-controlled devices, which can assist DIBH through airway blocking or feedback. By providing a static condition during treatment, DIBH minimizes interplay effects, which may drastically disrupt particle treatment plans. For the purposes of this thesis, we will be focusing on this latter motion mitigation technique.

Breath-hold (BH) has already been used successfully in conventional radiation treatment settings, but it has yet to be widely employed in proton therapy. Underberg et al. [25] reported the theoretical advantages of conventional radiotherapy for lung cancer in DIBH in 2005, demonstrating that maximally expanded healthy lung tissue allows minimizing lung dose and that complete immobilization of the planning target volume (PTV) allows reduction of PTV margins, which again reduces lung dose. Since then, this approach has become increasingly used for simple and reliable tumor immobilization, lung exposure reduction, and heart protection. Additionally, Georg et al. [26] evaluated PSPT and IMPT plans for shallow breathing with abdominal compression and DIBH. They discovered that the DIBH approach enhanced dose-volume histograms regardless of treatment type. Nevertheless, there were no statistically significant differences between shallow breathing and DIBH. Despite these results, questions were raised concerning the practicality of fully delivering the dose during breath holds. To accomplish so, delivery systems must be rapid enough to give the complete treatment in a short time, as the patient might have some respiratory issues and should be comfortable enough throughout the treatment.

It is interesting to mention a study carried out by Parkes et al. [27] in which they demonstrated a technique that enabled patients with cancer to safely deliver a single prolonged breath-hold of > 5 minutes. 15 patients aged 37-74 undergoing radiotherapy for breast cancer were trained to breath-hold safely with pre-oxygenation and mechanically induced hypocapnia under simulated radiotherapy treatment conditions, and the mean breath-hold duration was 5.3 ± 0.2 min.

1.9.2 High Costs

As mentioned above, proton therapy has been shown to have significant advantages over conventional radiotherapy. However, a limitation of the use and expansion of this technique is its substantial costs, considering both the costs of buildings and operating particle accelerators. In a recent study, the overall expenses and upfront proton therapy costs were predicted to be higher than those of photons, but the decreased incidence of pneumonitis and esophagitis enable protons to recover part of the total costs [18]. Yet, as has already been demonstrated in photon treatment, proton therapy may offer superior cost-effectiveness ratios with safer hypofractionation. Indeed, the cost difference between proton therapy and photon radiation becomes smaller as fewer fractions are delivered. Moreover, proton therapy may delay or prevent the need for extra hospital stays that would otherwise be necessary for patients receiving photon-based radiation, saving money in the long run [17]. Thus, demonstrating the cost-effectiveness and delivering hypofractionated treatments still remains an important financial topic when taking into consideration proton therapy treatments for patients.

1.10 Treatment Delivery Time Reduction

As previously stated, the dose delivery time when treating breath-hold cases should be as short as possible: dead time and beam-on time are the two key factors that determine the entire treatment delivery time. The beam-on time is the amount of time needed to deliver the dose. For cyclotron-based facilities, it relies on the energy and it is directly proportional to the achievable beam current at the isocenter. The dead-time, instead, is the time required by the system to change energy layers and the lateral position of the beam. The time it takes for the energy layers to change varies on the type of proton treatment facility. In cyclotron-based facilities, like the PSI, the extracted energy is fixed, and energy selection is done upstream, with a degrader right after the cyclotron, or downstream, with a range shifter. In Gantry 2, the energy modulation is done upstream using a degrader, which degrades the 250 MeV beam generated by the cyclotron to energies ranging from 70 MeV to 230 MeV, and the time necessary for the energy layer to change is on average 150 ms. The lateral position changing time, instead, is determined by the speed of the scanning magnets, which are the two dipoles located

upstream or downstream of the final bending magnet that deflect the beam transversely across the $x - y$ plane (or $u - t$ plane). For Gantry 2, the spot position-changing time is about 0.3 ms. As the beam-on time depends on the beam tunes' characteristics and safety requirements, attempts to reduce the overall delivery time can be made by reducing the dead-time. To do that, the number of energy layers that must be scanned and the number of spots for each layer can be reduced, for instance by using the Ridge filter and different spot placement algorithms respectively.

1.10.1 Spot Positioning Techniques

To create a proton plan, a set of initial spot positions (corrisponding to the position of the BP) and weights first need to be generated. Afterward, the individual spot weights are optimized to provide a homogenous dose distribution within the target volume, the desired target conformity, and OAR sparing. Throughout the optimization process, the initial generation of spot placements and relative lateral and longitudinal spacing has a significant impact on the quality of a plan. Indeed, spot width σ, interspot distance d, and the number of spots N are the parameters that characterize dose quality and treatment time in proton PBS. A possible way to decrease the delivery time is to reduce the total number of spots that have to be scanned throughout the tumor volume. Yet, the spot placement techniques employed must not only reduce the number of spots used but most importantly satisfy medical prescriptions and target coverage.

A study carried out by Grassberger et al. [28] quantified the impact of respiratory motion on the treatment of lung tumors with spot-scanning proton therapy. They assessed the interaction effects on the dosage distribution in the patient using 4D Monte Carlo simulations. Results pointed out that respiratory motion affects target dose homogeneity, with smaller spot sizes ($\sigma \approx 3$ mm) being naturally more sensitive to motion, reducing target dose homogeneity on average by a factor ~ 2.8 when compared to a larger spot size ($\sigma \approx 13$ mm). Moreover, treatment of large target volumes with small spots would result in an unacceptably large number of spots and associated treatment time, even if more accurate at the distal dose falloff.

For Gantry 2 at PSI, a basic spot placement technique is currently used, which places spots on a regular rectangular with a fixed 0.4 mm $\times$ 0.4 mm spacing. However, there

exist several other spot positioning algorithms characterized by different planning outcomes.

Rehman et al. [29] evaluated quantitative dosimetric measurements of five proton pencil beam spot placement techniques, comparing two grid-based algorithms (a rectilinear grid and a hexagonal grid, both commonly available in commercial planning systems) and three boundary contoured techniques (concentric, hybrid and optimized contours) (see Figure 1.14).

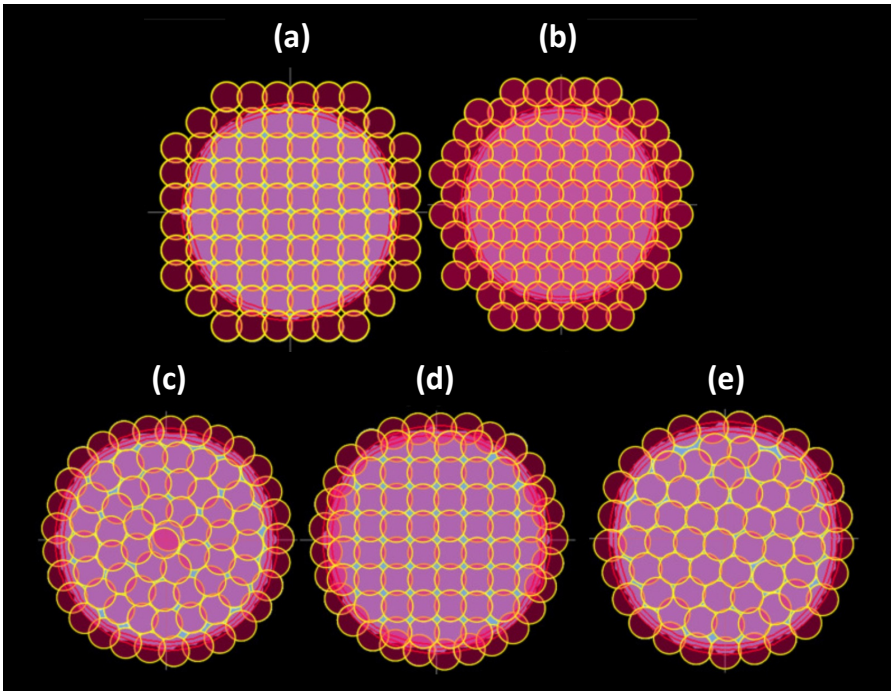

FIGURE 1.14: Spatial distribution of spots using different spot placement techniques: rectilinear grid (a), hexagonal grid (b), concentric contours (c), hybrid (d), and optimized (e) [29].

For all treatment plans, an optimal set of planning criteria was defined, and the influence of spot placement techniques on plan quality was assessed in terms of distal falloff, normal tissue sparing, conformance, homogeneity of dose distributions, and, of course, the number of spots placed. The results showed that over a variety of proton scanning beam spot sizes, boundary-contoured spot placement approaches offer a significant increase in dosimetry metrics when compared to commercially available grid-based techniques. Moreover, when utilizing grid-based approaches, extra spots are necessary to adequately cover the target since some spots fall just within the target boundary, resulting in low dosage at the target borders if additional spots are not used. However, it is worth

noticing that boundary-contoured approaches are not robust enough for thoracic malignancies, where interplay effects play a crucial role in optimal dose delivery, as slight target movements due to breathing can drastically modify the dose distribution to the target.

Van de Water et al. [30] created a new spot reduction algorithm that uses the iterative "pencil beam resampling" process to reduce the number of spots. This involves repeating inverse optimization while adding a small sample of randomly selected spots to each iteration and then eliminating low-weighted spots until plan quality deteriorates. Conclusions reported that the number of spots was reduced by 96% and enabled considerable shortening of the delivery time ($\sim 50\%$) without compromising plan quality or delivery accuracy, and without substantially affecting robustness.

Other spot positioning algorithms are based on the size of the beam in air or in water. A study carried out by N. Bizzocchi [31] at the PSI evaluated the quality of different plans comparing the fixed grid spot placement technique used at PSI with energy dependent spot spacing based on the beam size in air or in water, with the main objective of providing an improved configuration for reducing treatment delivery time while not affecting (and maybe enhancing) dose distribution quality. In the first part of the study, five targets with different shapes and several spot placement configurations (on a fixed grid, in air, and in water, arranging spots on a rectangular or hexagonal grid) have been analyzed. Results showed that when examining the dosage homogeneity value D5-D95, the hexagonal grid spot placement appeared to perform better than the rectangular one for all targets and combinations. Furthermore, the number of spots drops dramatically when going from a fixed grid spot placement technique to a spot positioning in air and water, the latter being the one with the lowest number of spots. The performance of selected configurations was examined for heterogeneous anatomies and by using multiple beams in the second half of the study, demonstrating that spot/layer size-dependent spot placement is beneficial in clinical patient scenarios regardless of the number of deposited spots. Additionally, results show that spot placement in water outperforms the fixed grid for smaller, superficial targets, meanwhile, no reliable trends have been observed for other configurations. Overall, the number of delivered spots and layers drops for each configuration with spot placement in air and water when compared to the fixed grid. As a result, the delivery time is shortened.

1.10.2 Ridge Filter

In PBS the number of stacking layers that have to be scanned might be large, especially in the low-energy region as the BP of the pristine beam is very sharp. When short treatment delivery times are required, the time necessary to change the beam's energy becomes a limiting factor. As previously stated, many particle therapy facilities, such as the PSI, employ cyclotron-based devices that generate a beam with a fixed extraction energy, which must be changed with a degrader in order to cover the entire target volume. The energy changing time for cyclotron-based facilities generally ranges from 80 to 900 ms [32] [33]: if this is too long, the overall delivery time will be long as well. Consequently, lowering the number of energy layers would improve beam delivery efficiency.

One way for reducing the number of energy layers required to cover the whole target is to broaden the BP by mean of a Ridge filter (RF): indeed, when the pristine proton beam passes through it, it crosses different thicknesses leading to the creation of small SOBPs. RFs are typically composed of polymethyl methacrylate (PMMA) or aluminum and have a one or two-dimensional modulated ridged or pyramid structure. However, many different RF designs for particle treatment have been proposed and utilized for medical purposes, some of which are field-specific and patient-specific, and some others more universal. However, one of the main drawbacks of RFs is the increased lateral and distal falloff of the beam, which might affect the dose conformity. Many studies have been conducted to demonstrate the potential benefits of employing RFs to reduce delivery time.

Maradia et al. [32] proposed a novel RF design consisting of two identical dynamic RFs located right before the isocenter that can shift relative to each other to dynamically adjust the BP's properties. They demonstrated that a maximum broadening of the BP of up to 2.5 cm was possible (see Figure 1.15), and that the number of energy layers required to generate different SOBP could be reduced by a factor of three regardless of the maximum energy, resulting in a 50% reduction in delivery time without affecting flatness or penumbra. Furthermore, this approach is easily adaptable for various facilities as it is not patient-specific or beam model-specific.

Fujitaka et al. [34] used a mini-RF to broaden the pristine BP up to a stacked layer thickness of 1 or 2 cm in order to decrease the number of energy layers. They found out

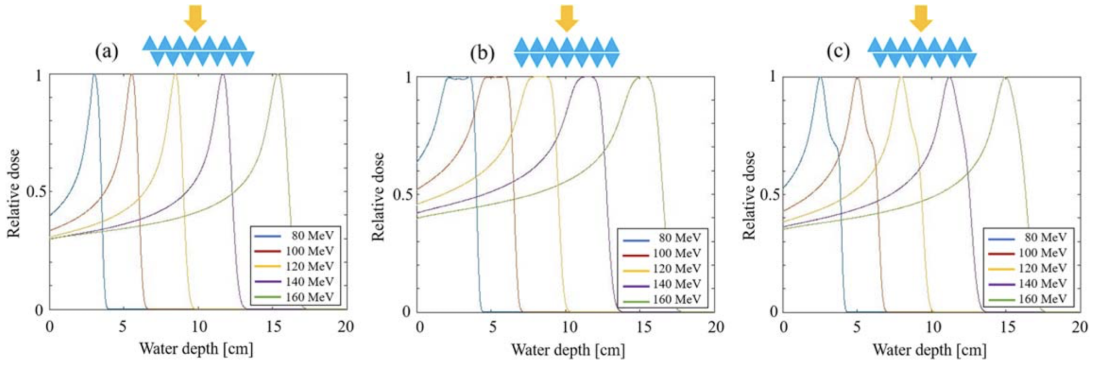

FIGURE 1.15: Monte Carlo simulations of depth dose curves resulting from three different alignments of the dynamic RF [32]. In configuration (a) BPs broadening is negligible, while configuration (b) results in the maximum BP broadening.

that in the case of pristine beam stacking, the number of energy layers can be reduced to 20% or less thanks to the RF.

To mention one more study, Wang et al. [35] conducted a study to determine the feasibility of incorporating a mini-ridge filter as an integral part of the synchrotron nozzle to facilitate the clinical use of mini-ridge filters, as they are frequently used to widen the BP in the longitudinal direction at low energies. Results showed that the integrated mini ridge filter (IMRF) marginally enhanced the dosage to the organs at risk in clinical cases. However, the beam delivery time was reduced from 18.5% to 47.1% for the lung, brain, scalp, and head and neck cases, and target dose uniformity was improved up to 2.9% for these cases, concluding that integrating a mini-ridge filter into a synchrotron nozzle is feasible for improving treatment efficiency without significantly sacrificing plan quality.

It is worth noting that whereas the RF is often used in carbon-ions therapy to increase the width of BPs at low energies [6], it is nearly never used clinically in proton therapy. Indeed, it is only used for experimental purposes or to generate an SOBP of the same dimensions as the tumour by means of patient-specific RFs [36]. Some research has been conducted to determine if the use of the RF for treating patients with proton therapy may provide any benefits, however, none of these studies deeply investigated it on a large cohort of patients.

1.11 Objective of this Thesis

The main purpose of this study is to look at the benefits and drawbacks of using a novel designed Ridge filter in combination with various spot placement techniques to assess if it would be possible to deliver an entire field dose within one single breath-hold, which implies a total delivery time of no more than $\sim$ 20 seconds. To do that, clinical treatment plans will be designed on 12 breath-hold cases using the in-house PSI's treatment planning system called "FIonA", and outcomes will be compared in terms of plan quality and treatment time reduction by using the Ridge filter in combination with a spot placement algorithm based on a fixed grid, currently in use at the proton therapy center at PSI, and two energy dependent spot placement algorithms based on the beam's size in air at the isocenter or in water at the Bragg peak. Thus, we will try to answer two main questions: What is the optimal configuration in terms of clinical acceptance and time reduction when comparing the Ridge filter with various spot placement algorithms? Is it possible to reach a mean treatment delivery time per field $<$ 20 seconds in PSI's Gantry 2?

Chapter 2

Paul Scherrer Institute

Since 1996, the Center for Proton Therapy (CPT) at the Paul Scherrer Institute (PSI) has treated over 2000 patients with deep-tissue tumors (brain, skull base, and spinal column tumors, as well as sarcomas), including over 770 children and adolescents. More than 7900 patients with eye malignancies have been irradiated with protons at PSI's CPT, making it one of the most experienced centers in treating ocular diseases. [37]. PSI can be considered the pioneer of proton therapy with pencil beam scanning as it developed the first scanning gantry in the world in the '90s, Gantry 1, which has been used for treating patients routinely from 1996 until the end of 2018, being able to successfully treat over 1,300 patients during this period of time [38]. However, Optis has been the first-ever treatment room built at the institute, which operated from 1984 to 2010, then updated to Optis 2 in the same year.

PSI currently has four treatment rooms: Gantry 1, which has been permanently closed for patient treatments and is now only used for experiments, Gantry 2, which started clinical service in 2013 and is currently used for both patient treatments and experiments, Gantry 3, supplied by Varian Medical Systems and operating since 2018, and Optis 2, which is dedicated to the treatment of ocular tumors.

2.1 PSI's PROScan Beamline

In Figure 2.1, the PSI's PROScan beamline is shown: it includes a 250 MeV superconducting cyclotron (COMET), four clinical treatment rooms (Gantry 1, Gantry 2, Gantry

3 and Optis 2) and experimental space. The PROScan project was launched in 2007 with the construction of a new 250 MeV superconducting cyclotron dedicated only to proton therapy. Indeed, until that moment, Gantry 1 beam was obtained by splitting a small fraction (0.5% of the beam intensity) of the beam from PSI's ring cyclotron by degrading its energy from 590 MeV down to the required energy for proton treatments, in the range between 120 MeV and 214 MeV [39].

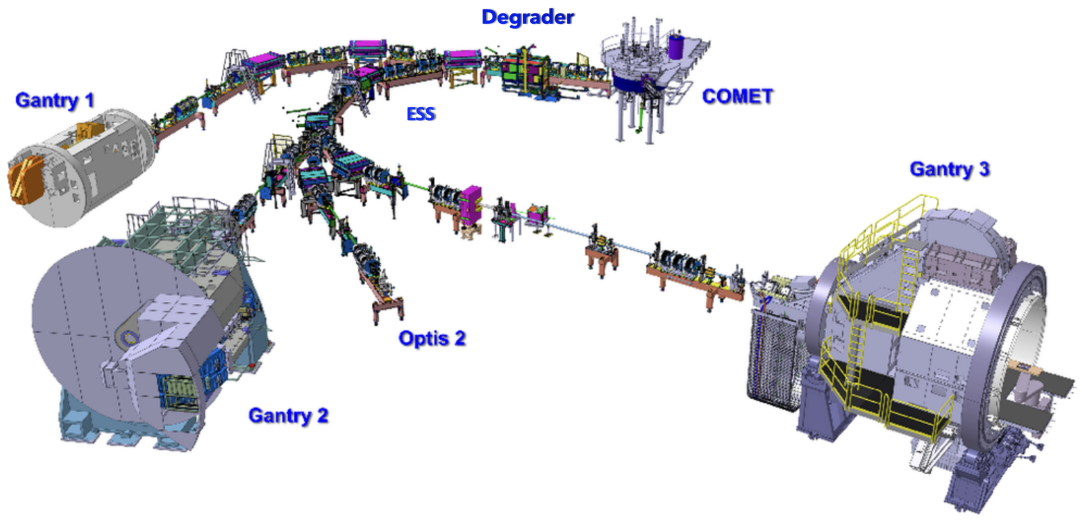

FIGURE 2.1: Schematic layout of PSI's PROScan beamline, showing COMET, Gantry 1, Gantry 2, Gantry 3 and Optis 2 [40].

COMET is a superconducting cyclotron used to generate a 250 MeV proton beam. A quadrupole triplet focuses the beam extracted from the cyclotron onto a degrader made of movable graphite wedges, which enables the delivery of any proton energy between 70 and 230 MeV. After the degrader, two collimators are positioned to restrict the size and the divergence of the scattered beam. Afterward, the Energy Selection System (ESS) reduces the energy (momentum) spread to have a sharper BP before the beam is sent to Gantry 2, Gantry 3, or Optis 2. Instead, for Gantry 1, the energy is selected downstream by means of a series of range shifters within the gantry's nozzle.

2.2 Gantry 1

The Gantry 1 at PSI was brought into clinical service in 1996 and it has been for over a decade the only proton gantry system in the world treating patients with the pencil beam

scanning technique. With just 2 m of radius and an eccentric design, it is still the most compact proton gantry in the world (see Figure 2.2). The transverse movements of the pencil beam are obtained with a fast scanning magnet in one direction, while scanning in the orthogonal direction is achieved with patient-table motion, and the third dimension (depth) is varied adjusting the beam range with range shifter plates. However, this method makes spot-scanning really slow.

Gantry 1 stopped treating patients in 2018, mainly due to its eccentric design, in which the patient was lifted at 2 meters above the ground during treatment, rendering it inaccessible in case of a critical situation. Now it is mainly used for experimental purposes.

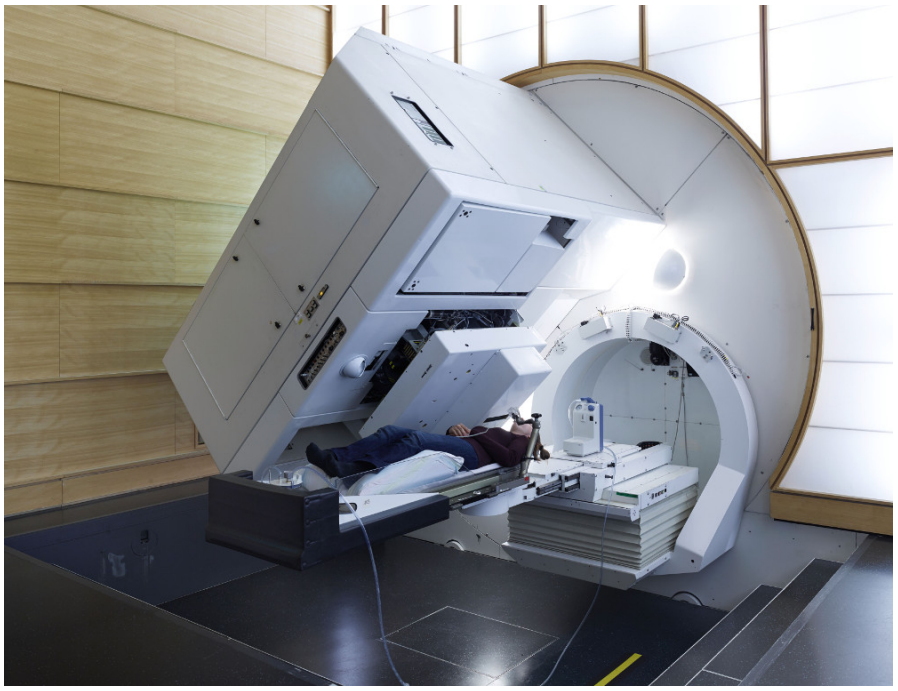

FIGURE 2.2: PSI's Gantry 1 [38].

2.3 Gantry 2

The first patient was treated in Gantry 2 in late 2013. The design of this new gantry is derived from the practical experience of using Gantry 1 but is substantially improved and renewed. As opposed to Gantry 1, which is very compact but eccentric where the patient table is mounted on the gantry and rotates with it, Gantry 2 has been built as an isocentric system. This means that the beams from all angles converge at a single point, the isocenter when the rotation is carried out around a fixed axis. This configuration

allows easy access to the patient table at any time on a fixed floor. A peculiarity of this gantry is its limited rotation. Indeed, it only rotates from -30° to +180° on one side. However, the patient table can rotate from -180° to +180°, allowing for any configuration to be obtained (see Figure 2.3). Moreover, the sweeper magnets are mounted on the gantry before the last bending magnet: in this way, parallel beam scanning in both lateral directions can be provided, significantly reducing the overall radius of the gantry.

FIGURE 2.3: PSI's Gantry 2 [41].

The most important improvement with respect to Gantry 1 is that the beam delivery speed has been reduced: Gantry 2 scans the tumor using two fast magnets that move at rates of 0.5 to 2 cm/msec in the left-to-right and head-to-feet axes, respectively. In the third dimension, energy is changed in only 150 ms to go from one tumor layer to another. As a result, "volumetric repainting" is feasible, which implies that the same volume can be scanned multiple times within the same treatment. This is a useful method for producing dose distributions that are less sensitive to organ movements. Another major advancement is the availability of in-room imaging: an in-room sliding CT is utilized for treatment planning and daily verification of the patient position and includes the ability to provide time-resolved imaging, or "4D imaging" [41].

2.4 Gantry 3

Gantry 3 went into service in July 2018 after four years of planning, building, and commissioning, built-in scientific collaboration with Varian Medical Systems (see Figure 2.4), being the largest machine installed to date at CPT. An onboard integrated imaging system is used to align the patient. Because of the gantry's capacity to give wide irradiation fields, rapid energy changes, and high dose rates, radiation time per patient may be reduced to a minimum. In the future, it is planned to use the 'gating' approach to treat moving tumors at this irradiation facility [42].

FIGURE 2.4: PSI's Gantry 3 [42].

2.5 Optis 2

Optis 2 is a fixed beam line dedicated to the treatment of ocular tumors which employs the PS technique. Clinically operating since 2010, it has treated already over 1800 patients [43]. It uses a horizontal beam line, and the patient is immobilized while seating on a treatment chair (see Figure 2.5). As eye tumors are superficial, the energy required to treat them is around 70 MeV. Unfortunately, more than 99% of the initial protons are lost during the energy degradation from 250 MeV, which is the energy provided by the cyclotron. Thus, in order to improve transmission efficiency, a double-scattering technique is employed. The extracted beam passes through a range shifter, which is

utilized to adjust the range and ensure pre-scattering of the proton pencil beam, as well as to ensure a homogenous field at the isocenter. Dedicated modulator wheels are then used to produce the SOBP.

FIGURE 2.5: PSI's Optis 2 [43].

Chapter 3

Methods

The goal of this study is to investigate the possibility of delivering a field dose within a single breath-hold. To achieve this, we designed plans on breath-hold CTs (i.e., the patient holds his breath during the CT scan) of 12 different patients with lung tumours using the PSI's in-house treatment planning system (TPS) "FIonA". Three plans for each of the 12 patients were created and compared using a novel designed RF in combination with three different spot positioning techniques: spot positioning on a fixed grid and energy-dependent spot positioning based on the beam's size in air at the isocenter and beam's size in water at the Bragg peak. In addition to that, clinical plans for each patient were also created using the standard methodology currently applied for treating patients at PSI's Center for Proton Therapy to compare the delivery time from other plans. The aim is to determine which of these three configurations can achieve a low field delivery time (< 20 seconds) by reducing the number of spots with respect to clinical plans while still satisfying medical prescriptions for both the target and OARs. It is worth mentioning that the results obtained are specific to PSI Gantry 2, but the methodology used (the combination of the RF with unconventional spot placement techniques) can be easily adapted for other facilities.

3.1 Patients and Image Data

The breath-hold CT images of patients used for this study were acquired at the Department of Oncology of the Rigshospitalet Copenhagen University Hospital in Copenhagen,

Denmark between 2012 and 2013, in which patients (median age 67 years, range 46-80) were treated for locally advanced NSCLC with photon radiation therapy with 66 Gy delivered in 33 fractions over a period of 6 to 7 weeks [4]. The patients were prospectively enrolled in a clinical protocol at the photon clinic of the Rigshospitalet Copenhagen University Hospital (local ethics committee approval no. H-2-2011-153) and were included in the present PBS proton therapy planning study.

Table 3.1 summarizes the main characteristics of our cohort, including the patient's ID, the clinical target volume (CTV) and the location of the tumour inside the patient.

Patient	**CTV [cc]**	**Tumor location**
P1	377.40	Right lobe
P2	183.84	Left lobe
P3	143.15	Left lobe
P5	107.44	Right lobe
P6	507.57	Left lobe
P9	144.56	Right lobe
P10	957.94	Right lobe
P11	144.76	Left lobe
P12	75.58	Right lobe
P13	65.99	Left lobe
P14	100.89	Right lobe
P17	175.03	Right lobe

TABLE 3.1: Summary of tumours' characteristics for each patient, reporting the volumes of the clinical targets (CTV) and the tumour's location in the patient.

3.2 Planning Steps

The goal of treatment planning is to deliver a certain amount of dose to the target volume and minimize the dose to healthy tissues. The plans created must satisfy prescriptions,

which are approved by medical doctors, with constraints on the maximum and minimum or mean deliverable dose to organs at risk and to the tumour volume, respectively.

To create a plan, different actions must be taken [44]: first of all, the patient's tumour and surrounding tissues must be accurately contoured, providing information about the location, size, and shape. Subsequently, the plan can be designed using a TPS by following the steps outlined below. The initial step involves selecting the directions of the fields, and then the TPS determines the placement of the spots, where the spot position corresponds to the position of the BP. After that, the plan's optimization is performed to assign spots' weights in the way to achieve a homogeneous dose distribution within the target volume and spare the OARs, and finally, the delivered dose is normalized. In the end, the plan's quality is assessed by checking its robustness against the target's geometrical shifts and range uncertainties and whether all medical prescriptions are satisfied or not. Once the plan is ready and approved, it is delivered to the patient. Since proton dosages are administered in different fractions over a few weeks, the patient's condition is monitored during the course of the treatment duration as the tumour reduces in size. If at some point the tumour shrank too much or changed position, a plan adaptation would be necessary to correctly deliver the remaining fractions of the dose.

For the creation of the treatment plans, the PSI's in-house Flexible Ion-planning Application "FIonA" treatment planning system has been used.

FIGURE 3.1: FIonA treatment planning system.

In the following sections, we will describe in detail all the necessary steps followed for designing plans in FIonA.

3.2.1 Definitions of CTV and PTV

CTV (Clinical Target Volume) and PTV (Planning Target Volume) are important concepts used to define the target area for radiation therapy. The CTV represents the volume of the tumour and surrounding tissues that need to be irradiated to achieve an effective treatment. This volume is typically defined using imaging modalities such as MRI, CT, or PET/CT scans and can be manually contoured by medical doctors or automatically contoured by AI algorithms (still under research and not widely used clinically). The PTV, on the other hand, is an expansion of the CTV that accounts for uncertainties in the treatment delivery process, such as patient setup errors and organ motion, and it aims at guaranteeing that the correct amount of radiation is delivered to the whole CTV. The size of the PTV is determined based on the magnitude of these uncertainties, which can vary depending on the specific treatment site and technique used, usually being of the order of a few millimetres. Generally, when treating lung tumors, the PTV is obtained by expanding the CTV by 8 mm, where 5 mm account for geometrical shifts and 3 mm account for range uncertainties. For our patients, however, the PTVs have been created by expanding the CTV volume only by 5 mm: this choice has been made because we only account for geometrical shifts, as density variations will be taken into consideration by the optimization method used (see Section 3.2.3).

3.2.2 Fields Definition

In the process of planning proton therapy treatments, several factors need to be considered. The number and direction of fields used are dependent on various aspects, including the size and location of the target being treated. For lung tumours, three to four fields are generally used. When deciding the directions of the fields, different considerations have to be made. If the tumour is located close to an organ at risk, such as the esophagus or heart, the direction of fields is chosen in such a way that the OAR is spared as much as possible. To do that, the sharp beam's lateral penumbra is exploited, while the use of distal penumbra is generally avoided due to uncertainties in the range (range straggling) and density variations. Thus, field directions that place the OAR immediately beyond the target are generally avoided. Moreover, if the tumour is located only on one lobe, fields should not deliver doses to the other side to minimize the dose to the other lobe. For female patients, fields directed at the breast must be avoided

due to the high radiosensitivity of mammary glands. Additionally, for the treatment of moving targets, fields coming from the back of the patient are preferred since these directions result to be more robust when delivering the dose as the patient is lying on the table and this region of the body has a smaller motion amplitude.

When defining fields, the TPS determines for each of it the possible set of all deliverable spots within the patient by mean of a spot positioning algorithm (see Section 3.2.8), where each spot position, which corresponds to the position of the BP, is converted from the water equivalent range to the depth in the patient to account for the varying density of tissues. After that, a first spot selection is performed in which all the spots outside of the target volume are removed while all spots within the target volume are preserved. However, spots located within a defined margin from the target are also preserved: this is required to completely cover the target. This margin value can be manually set in FIonA when defining fields with different spot placement algorithms. For algorithms that place spots at a predefined fixed distance, the margins set are constant across all energy layers. However, this margin varies depending on the energy used for energy dependent spot placement algorithms. In that case, the margins are given by $margin = SMF \times SSF$, where SMF is the spot margin factor, which can be varied, and SSF is the spot spacing factor, which depends on the beam's size σ. In our study, for plans utilizing spot placement on a fixed grid were assigned margins ranging from 0.7 cm to 1.5 cm, depending on the size and shape of the target to reach the required coverage. On the other hand, for plans employing spot placement in air and water, we chose a specific SMF such that the margin width was similar to that of the fixed grid plans at 150 MeV, which represents the average energy within the range of depths we considered. For Patient 2, Patient 5, Patient 11, Patient 12, Patient 13 and Patient 17, however, plans using the energy dependent spot positioning algorithm in air were created by increasing the SMF to reach the required target coverage.

Figure 3.2 shows the different fields' arrangements planned for each patient in our study: three fields were employed for all the patients, positioned at different angles to achieve the maximum target coverage. The directions of fields for each plan were approved by a medical physicist at the PSI's Center for Proton Therapy.

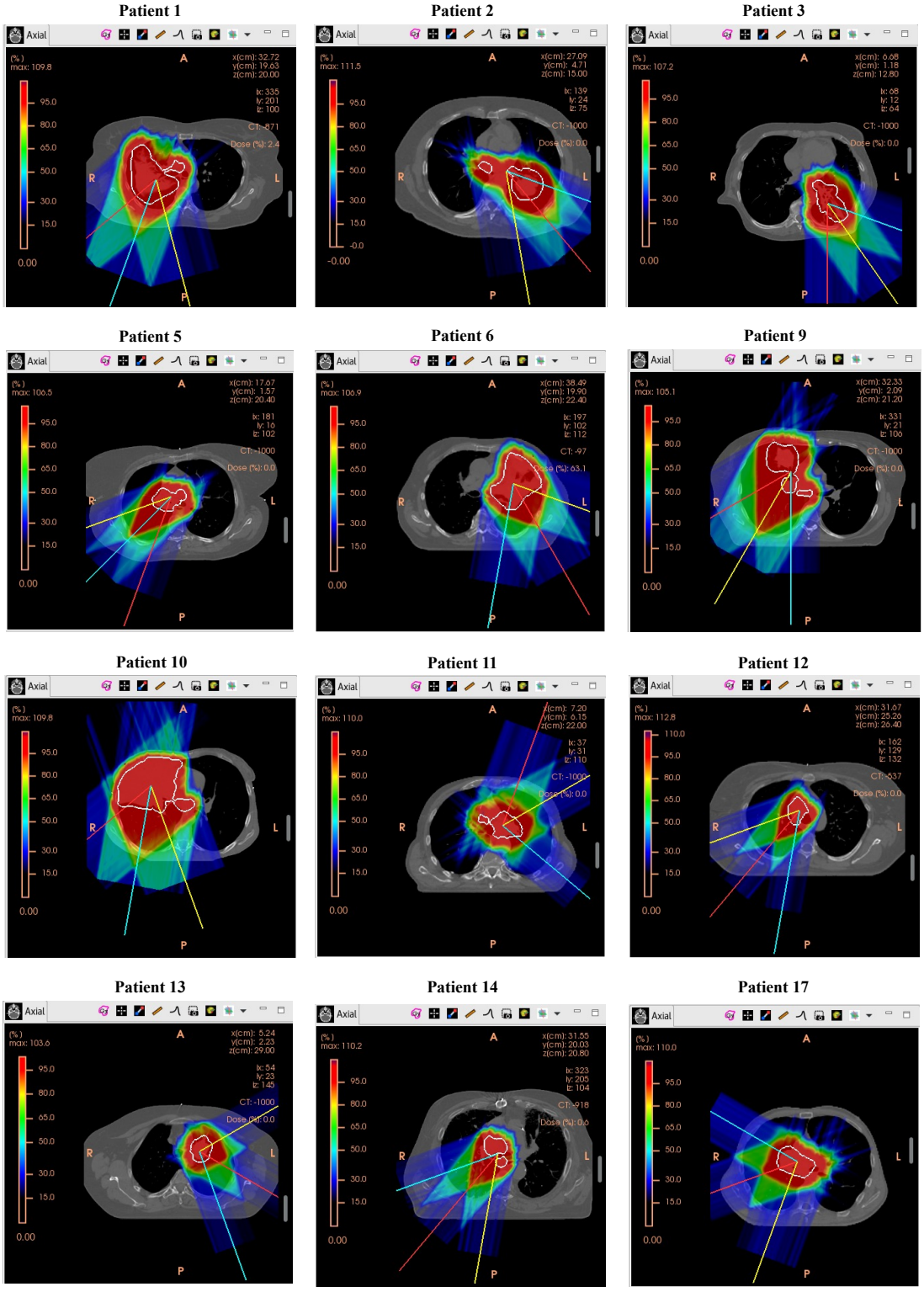

FIGURE 3.2: Visualization of plans created for each patient. The straight lines show the fields' directions, the white contour corresponds to the CTV, while the percentage of dose delivered to the target and surrounding tissues are represented in a coloured dose scale described on the left side of each plan.

3.2.3 Optimization

Once fields' directions have been chosen and spots have been placed, the optimization procedure aims at finding a set of spots' weights that will result in generating a uniform dose distribution inside the target [6]. From a mathematical point of view, the problem consists of finding the minimum value of $||\overrightarrow{P} - \overrightarrow{D}||$, where $\overrightarrow{P}$ is the target dose (dose you want to deliver) and $\overrightarrow{D}$ is the dose you actually deliver [45].

When running the optimization in FIonA, the user can decide whether to perform a single-field optimization (SFO) or a multi-field optimization (MFO). In the SFO, the spot weights are optimized so that each field delivers a homogeneous dose to the target individually. In MFO, instead, the spot weights are optimized so that each field can deliver a highly inhomogeneous dose distribution to the target individually but when all fields are combined, a homogeneous dose distribution is achieved. Since our aim is to investigate whether or not it is possible to deliver an entire field dose within a single breath-hold, we chose to perform an SFO as it is generally more robust, especially for organs that move during treatments, such as lungs.

Three classes of dose calculation algorithms can be used for scanned proton therapy: ray casting, pencil beam decomposition (both analytical approaches), and Monte Carlo [6] [9]. As FIonA uses ray casting, in this section we will describe in detail how this algorithm works for two different types of optimizations available within this TPS: *GPU Based Optimization* (generally used in the clinics) and *Improved Optimization on GPU* (used to optimize our plans) [45] [46].

The dose from a spot j to a given optimization point (OP) i (or voxel) is calculated as:

$$d_{i,j} = \frac{T_j(s_{\mathrm{eq},i})}{2\pi\sigma_t\sigma_u} \mathrm{e}^{-\frac{\Delta t_{i,j}^2}{2\sigma_t^2} - \frac{\Delta u_{i,j}^2}{2\sigma_u^2}} \tag{3.1}$$

where $s_{\mathrm{eq},i}$ denotes the water equivalent depth of the calculation point i, $T_j(s_{\mathrm{eq},i})$ denotes the integral dose for spot j at a given depth in water and $\sigma_{t,u}$ describes the beam size (1σ) in t and u respectively.

The total dose at a given OP i is then given by summing the contribution over all spots weighted by their intensity ω_j:

$$D_i = \sum_{j}^{spots} \omega_j \cdot d_{i,j} \tag{3.2}$$

To find the correct value of ω_j, FIonA's optimization uses an iterative approach, where the spot's weight ω_j is updated using a multiplicative factor where the weight at iteration $k+1$ is calculated from the weight at iteration k.

In the case no constraints are set on doses to deliver to structures (e.g., a maximum or mean dose to a certain volume of an OAR that must be satisfied), the weight ω_j of spot j at iteration $k+1$ is given by:

$$\omega_j(k+1) = \omega_j(k)\frac{\sum_i g_i^2 d_{ij}^2(k)\frac{P_i}{D_i(k)}}{\sum_i g_i^2 d_{ij}^2(k)} = \omega_j(k)\frac{N_j^{\text{target}}(k)}{G_j^{\text{target}}(k)} \tag{3.3}$$

where $\omega_j(k)$ is the weight of spot j at iteration k, g_i is the importance of the OP i, P_i is the target dose at the OP i and $D_i(k)$ is the total dose to the OP i given by all the weighted spots at iteration k. In clinical settings, it is customary to define a predetermined number of iterations, typically 150, to prevent an infinite loop from occurring.

When dose constraints on structures are added (we can also refer to these as "objectives" to be satisfied), an evaluation of the dose objective must be done. To do that, the newly computed dose distribution of the structure under analysis is extracted and the dose corresponding to the volume specified by the objective is calculated. In this case, for the *GPU based optimization*, the spot weight update formula becomes:

$$\omega_j(k+1) = \omega_j(k)\frac{N_j^{\text{target}}(k) + \sum_i\left(\sum_l^{\text{obj}} H\left(D_i(k), \Pi_{i,l}\right)\gamma_{i,l}^2 d_{ij}^2(k)\frac{\Pi_{i,l}}{D_i(k)}\right)}{G_j^{\text{target}}(k) + \sum_i\left(\sum_l^{\text{obj}} H\left(D_i(k), \Pi_{i,l}\right)\gamma_{i,l}^2 d_{ij}^2(k)\right)} \tag{3.4}$$

where l is an objective on a volume (e.g. an OAR), $\gamma_{i,l}$ is the importance of objective l and $\Pi_{i,l}$ is the objective dose at an objective volume. The function $H\left(D_i(k), \Pi_{i,l}\right)$ is denoted as an "objective inclusion function" and it decides if the OP i is "of interest" to fulfil objective l at iteration k. It is defined as:

$$H\left(D_i(k), \Pi_{i,l}\right) = \begin{cases} 0 & \text{if} \quad (i \notin l) \vee (D_i(k) < \Pi_{i,j}) \\ 1 & \text{else} \end{cases} \tag{3.5}$$

As opposed to the *GPU based optimization*, the *Improved Optimization on GPU* uses enforced constraints (EC) accounting for hotspots reduction above a user-defined maximum HS dose D_{HS} (default value is $D_{HS} = 107\%$) and/or range robustness. The spot weight update formula is slightly different with respect to Eq. 3.4 as hotspots (HS) are now included. If only the hotspots reduction is set in the optimization's settings, then the spot weight update formula becomes:

$$\omega_j(k+1) = \omega_j(k) \frac{N_j^{\text{target}}\ (k) + \sum_i \left(g_{\text{HS}}^2 d_{ij}^2(k) \frac{D_{\text{HS}}}{D_i(k)} H_{i,\text{HS}}(k) + \sum_l^{\text{obj}} \gamma_{i,l}^2(k) d_{ij}^2(k) H\big(D_i(k), \Pi_{i,l}\big) \right)}{G_j^{\text{target}}\ (k) + \sum_i \left(g_{\text{HS}}^2 d_{ij}^2(k) H_{i,\text{HS}}(k) + \sum_l^{\text{obj}} \gamma_{i,l}^2(k) d_{ij}^2(k) \right)} \tag{3.6}$$

The objective inclusion function $H\left(D_i(k), \Pi_{i,l}\right)$ is defined here as $\Pi_{i,l}/Di(k)$ if the objective is not satisfied and 1 if it is satisfied. There is an analogue HS reduction "inclusion" formula $H_{i,HS}$, which is 1 if the current dose is larger than a defined HS dose $D_i(k) > D_{HS}$ and 0 otherwise. The HS reduction importance g_{HS} is constant throughout the optimization and user-defined (the default value set in FIonA is 3). An additional difference between this type of optimization (with EC) and the previous one (without EC) is the adaption of the objective importance $\gamma_{i,l}$ through the iterations with the following formula:

$$\gamma_{i,l}(k) = \gamma_{i,l}(k-1) \frac{D_{V/\text{mean},\{i,l\}}(k)}{\Pi_{i,l}} \tag{3.7}$$

where $D_{V/mean,\{i,l\}}(k)$ is the dose at volume objective or mean objective at iteration k for the whole structure considered by objective l (and not only OP i).

When accounting for range robustness, the optimizer considers two additional dose distributions with scaled proton stopping power (PSP) in addition to the nominal dose, considering a range uncertainty of $\pm 3\%$ as the default value. If also this option is selected, then Eq. 3.6 is modified as follows:

$$\begin{aligned} \sum_i &\rightarrow \sum_i \sum_m \\ d_{ij}(k) &\rightarrow d_{ij,m}(k) \\ D_i(k) &\rightarrow D_{i,m}(k) \\ g_i &\rightarrow f_m g_i \\ \gamma_{i,l} &\rightarrow f_m \gamma_{i,l} \end{aligned} \tag{3.8}$$

where m is the scaled PSP scenario and f_m is the scenario's weight, which only multiplies the target and objective terms, implying that the hotspot reduction is independent from scaled-PSP scenarios (f_m is always 1 for the nominal scenario).

When modelling the prescribed dose P_i, the optimizer defines a margin around the target used only during the optimization process and defines a dose at that "optimization margin" (see Figure 3.3). This procedure is done to take into account the dose fall-off induced by BPs. The fall-off is then modelled as a Gaussian function passing through that defined dose at the margin, reaching a maximum dose of 1 and with a standard deviation. The importance of the OP i, or voxel importance, is instead modelled as an exponentially decreasing function. These parameters, such as the margin, the dose at margin and the dose fall-off standard deviation (sigma) used by the optimizer are user-defined during the optimization process. The default parameters values given in FIonA are: margin = 2 mm, dose at margin = 0.9 and sigma = 8 mm. For the optimization of our plans, however, we decided to set margin = 8 mm, dose at margin = 1 and sigma = 2 mm to have a sharper fall-off and a better dose homogeneity.

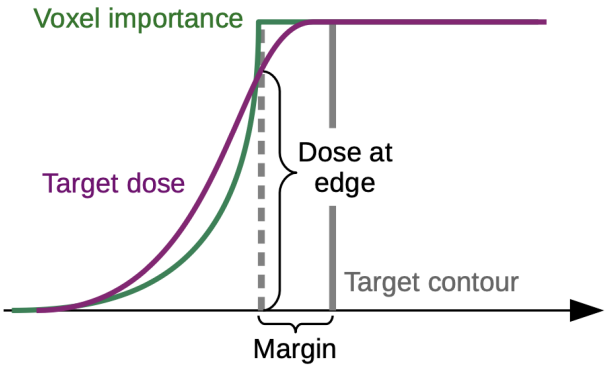

FIGURE 3.3: Visual representation of optimization parameters that can be manually set in FIonA [46]. The grey dotted line represents the optimization margin; the purple line represents the dose fall-off of the prescribed dose (P_i); the green line represents the voxel importance g_i.

Generally, other facilities perform a robust optimization against range uncertainties as well as geometrical shifts, using the CTV as the target of the optimization. However, this cannot be achieved in FIonA due to calculation memory issues. For this reason, at the PSI's CPT a *GPU Based Optimization* (which is not robust) is usually performed setting the PTV as the optimization target instead of the CTV. In this way, the possible variations are taken into account by the PTV. However, since we are treating moving targets, for the optimization of our plans we decided to use the *Improved optimization on GPU* considering both the hotspots reduction and range robustness options with default values, considering the PTV with reduced margin (only 5 mm) as the target of the optimization. This type of optimization is referred to as "hybrid optimization", as it assures robustness for range uncertainties. Further, objectives on structures were set only for a small number of plans when optimizing. To do that, the volumes of the structures of interest were increased by enlarging margins by 3 mm, and the maximum or mean dose constraints were assigned to these new objects. In our scenario, the esophagus and the spinal cord were the only structures that necessitated this procedure.

3.2.4 Dose-Volume Histograms (DVHs)

To evaluate the dose distribution within the target and OAR and to assess the potential effectiveness of a treatment plan, dose-volume histograms (DVHs) are commonly used. DVHs are cumulative dose histograms that represent the percentage of the volume of a particular structure (target or OAR) receiving a certain dose level or greater. The dose is typically plotted on the x-axis, and the volume percentage on the y-axis. A good plan should aim at maximizing the area under the DVHs of target structures (CTV and PTV) and minimizing the area under the DVHs of healthy tissues and OARs. An example of DVHs can be seen in Figure 3.4. The plots of DVHs for the comparison of results have been made using a package of functions specially created for analyzing data from FIonA outputs called *FIonA Plans Analysis*, available on GitHub [47]. To characterize these dose distributions, common dose-volume parameters can be defined: D_V represents the minimum dose [%/Gy] that volume V [%/cc] of a selected organ receives, while V_D represents the volume [%/cc] of a selected organ that receives at least a dose D [%/Gy] [48].

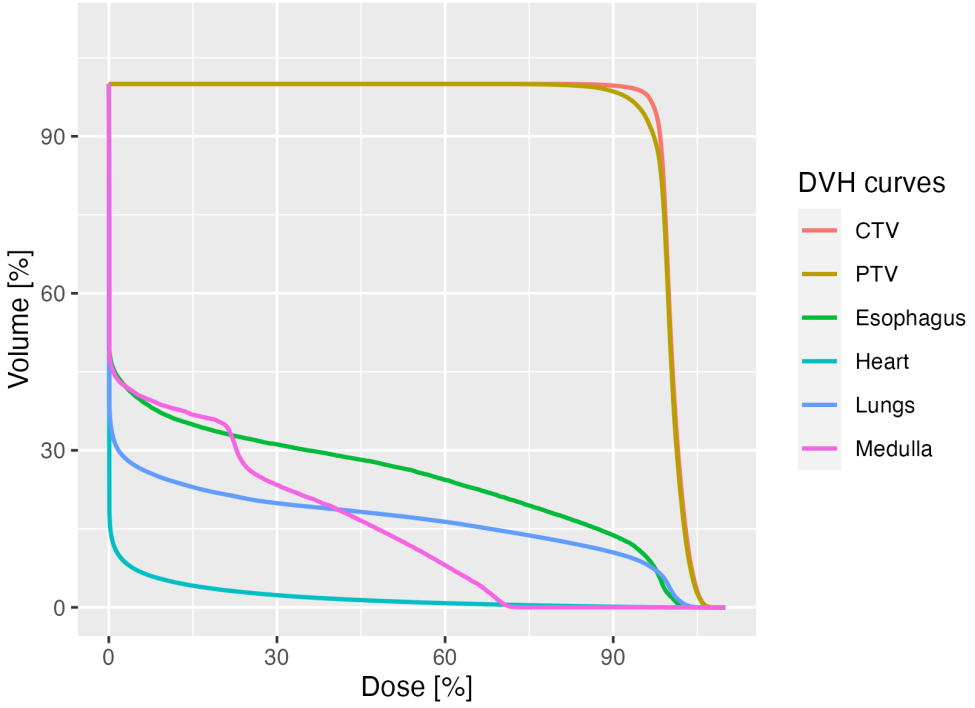

FIGURE 3.4: DVHs for CTV, PTV, heart, lungs, medulla and esophagus of a plan made using the fixed grid spot placement algorithm for Patient 1.

3.2.5 Medical Prescriptions

The total treatment dose that was prescribed to treat our patients was 70 GyRBE, to be delivered in 35 fractions (2 GyRBE/fraction). The medical prescriptions for the target volume and organs at risk that have been followed for the quality evaluation of our plans are listed in Table 3.2. They were approved by a medical doctor at the Center for Proton Therapy at PSI. Moreover, the normalization of the plans' dose was specified to be D95% = 95% on the PTV. These values were not only determined by doctors, but they also conform to the International Commission on Radiation Units and Measurements (ICRU) guidelines for plan quality evaluation [49].

3.2.6 Robustness Evaluation

Robustness evaluation in proton therapy planning involves evaluating the sensitivity of the treatment plan to geometrical shifts of the target to ensure that the plan remains effective in delivering the prescribed dose.

Structure	**Prescription**
CTV	V95% > 97.00%
PTV	V107% < 1.00%
Esophagus	V74.00 GyRBE < 1.00 cc
	Dmean < 34.00 GyRBE
Heart	V45.00 GyRBE < 35.00%
	V30.00 GyRBE < 50.00%
Spinal Cord	Dmax < 54.00 GyRBE
	V50.00 GyRBE < 0.03 cc
Lungs	V5.00 GyRBE < 60.00%
	V20.00 GyRBE < 37.00%
	Dmean < 20.00 GyRBE

TABLE 3.2: Medical prescriptions approved by a medical doctor at PSI's CPT used to obtain optimal plans for each patient.

In our case, by performing the *Improved Optimization on GPU*, we ensured that the plans created were robust for range uncertainties. However, robustness for geometrical shifts in the x, y and z directions must be evaluated as well. To do that, we run the *Calculate robustness DVHs* function in FIonA. For each structure, this function generates 9 DVHs, which correspond to 9 alternative scenarios considered: 6 curves account for geometrical shifts in the ± x, y and z directions, 2 curves account for range uncertainties, while the last curve corresponds to the nominal one output from the optimization process. To assess the robustness of our plans, we used as a constraint that the robustness DVHs for the CTV should satisfy D95% > 95% in the worst-case scenario, i.e. the minimum value between all the 9 DVHs for D95% should be greater than 95%.

Additionally to that, we evaluated the robustness of plans configurations in terms of target coverage within different breath-hold stages by copying on a repeated CT the nominal plan calculated on the planning CT and recalculating the dose. The repeated CT scan was performed on the same patient on a different day, and it was considered as corresponding to a different breath-hold phase. However we did that only for Patient

1, Patient 3, Patient 5, Patient 9 and Patient 13 as repeated CTs for the other patients were not available.

3.2.7 Ridge Filter

As we aim to reduce the treatment delivery time as much as possible while still satisfying medical prescriptions, we would like to have as few spots as possible. To achieve this result, in our study we employed a dynamic RF with a novel design, which is shown in Figure 3.5. The filter is composed by multiple slabs to create the ridge shape, generating a "Gaussian-like" BP. Indeed, depending on the number of slabs, as the quasi-mono-energetic beam passes through, the energy spreads and so the BP broadening changes. The slabs of the filter can be moved in relation to each other to enlarge the BPs, ranging from a minimum broadening of 0.4-1 cm to a maximum broadening of 2-2.5 cm. In our study, we will consider the configuration of maximum broadening only.

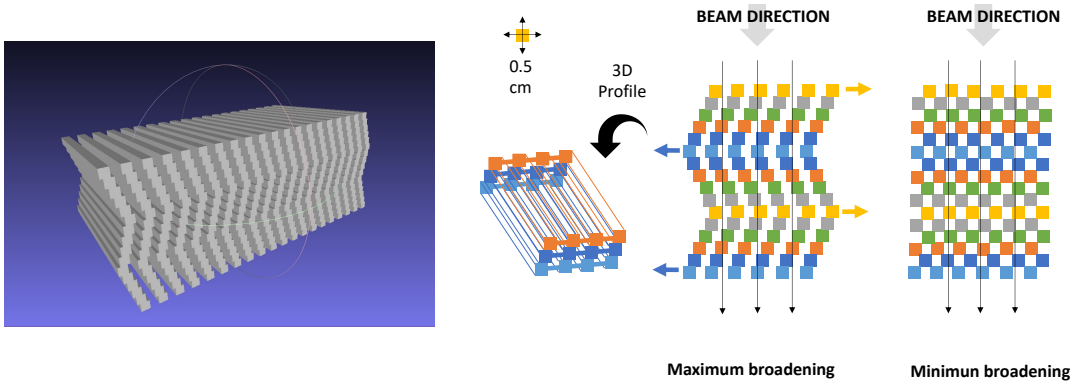

FIGURE 3.5: Ridge filter design used for enlarging the BP to have a Gaussian-like shape. The filter is composed by multiple slabs that can move with respect to each other to achieve different BP broadenings.

The effects of this type of RF on depth-dose curves can be seen in Figure 3.6, which shows the comparison between BPs without the RF and BPs with it. With the RF, the width of BPs enlarges and their intensity decreases, while the distal dose fall-off becomes less steep. The energy layers delivered by Gantry 2 are separated by a fixed step of 2.5 mm [31]. However, since the RF enlarges the width of BPs, considering all the energies would not be optimal. To do that, we set in FIonA an energy step factor of 3 to keep only an energy layer every three: this corresponds to having a distance of 3×2.5 mm between two consecutive layers. In this way, the total number of spots is

highly reduced. However, for the patients with the biggest tumour volumes (Patient 1, Patient 6 and Patient 10), in addition to plans with a 3 factor, we created plans with an energy step factor of 5, which correspond to having a distance of 5 × 2.5 mm between two consecutive layers. The intention behind this approach was to observe the effects of further reducing the number of selected energy layers for larger volumes and to determine the extent of the reduction of delivery time.

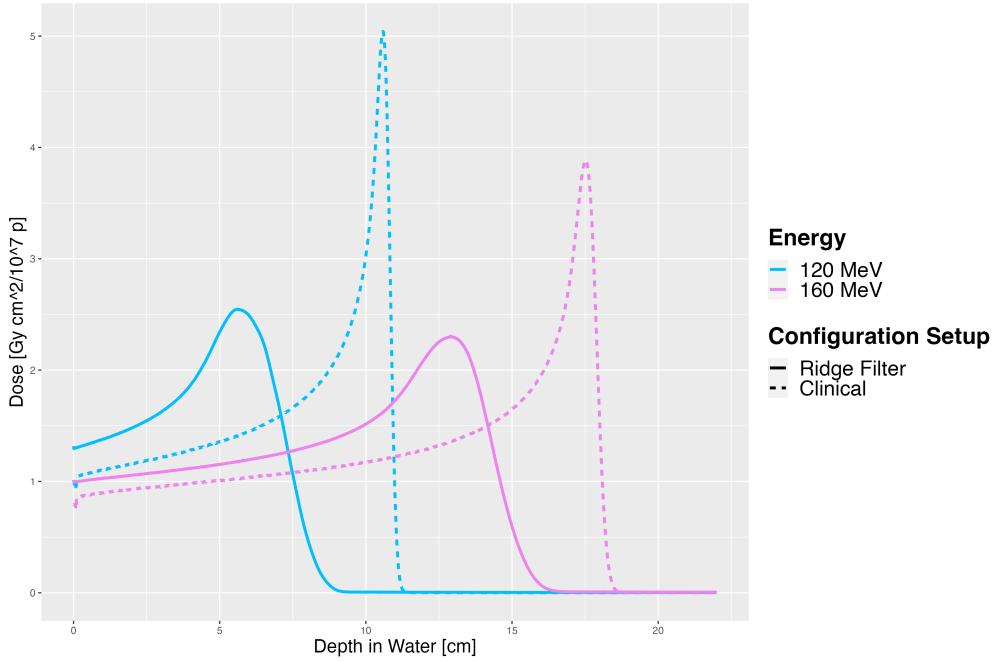

FIGURE 3.6: Comparison between BPs at two different energies (120 MeV and 160 MeV) with the RF (dotted line) and without the RF (continuous line).

3.2.8 Spot Positioning Algorithms

When placing spots, the TPS needs to provide a homogeneous dose distribution: if spots are too far away, the homogeneity is lost, if instead they are too close, an unnecessarily high number of spots is delivered, therefore increasing the delivery time.

In our study, three different spot positioning algorithms implemented in the FIonA treatment planning system were used to create plans: spot positioning on a fixed grid and energy-dependent spot positioning based on the beam size in air at the isocenter and beam's size in water at the Bragg peak. The spot positioning based on a fixed grid is the clinical standard currently employed at the PSI's clinics, and it generally uses a spacing of 0.4 mm × 0.4 mm between spots. However, when using a RF it is necessary to increase the distance between the spots as the beam size is increased: in our case, we set

a grid with a 0.47 × 0.47 mm spacing. The spot positioning based on the beam size in air and in water, instead, are energy dependent: thus, the distance between spots will be different for different energy layers. Figure 3.7 shows the comparison of the clinical beam size of Gantry 2 in terms of full-width-half-maximum (FWHM) at different energies at the gantry isocenter for both situations.

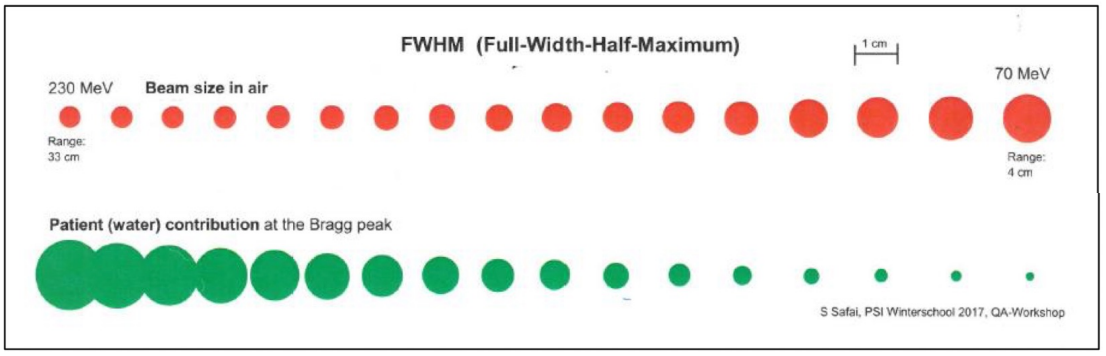

FIGURE 3.7: Comparison of beam size (FWHM) in air and in water at different energies, ranging from 230 MeV to 70 MeV. In the first row, the beam size in the air is shown in red, and in the second row, the beam size in water is shown in green [31].

The beam size in air is simply given by the beam optics contribution:

$$\sigma_{\text{air}} = \sigma_{\text{optics}} \tag{3.9}$$

The beam size in water, instead, is given by two contributions: the beam's optics and multiple Coulomb scattering, which accounts for the interactions of the beam inside the patient, namely

$$\sigma_{\text{water}} = \sqrt{\sigma^2_{\text{optics}} + \sigma^2_{\text{MCS}}} \tag{3.10}$$

At low energies, the scattering contribution is negligible, but at higher energies it becomes meaningful, greatly extending the beam size.

The distance between spots within the same energy layer is given by the product between the beam's σ and a spot spacing factor (SSF) which ranges from 1σ to 1.5σ. Figure 3.8 shows the spot distance as a function of the beam's energy for the three algorithms we used, assuming an SSF = 1.5 for spot positioning in air and an SSF = 1.0 for spot

positioning in the water. In this latter case, we chose a lower SSF since a value of 1.5 would have given a low number of spots, leading to a very low target coverage.

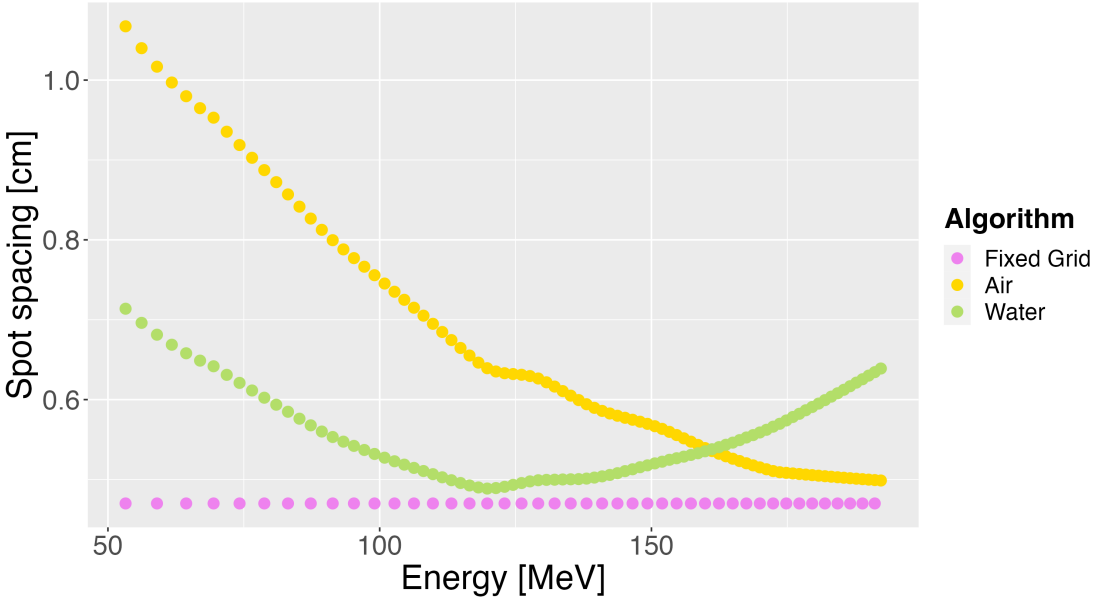

FIGURE 3.8: Spacing between spots as a function of the beam's energy for the three different spot positioning algorithms implemented in FIonA. In this case, a SSF = 1.5 is assumed for spot spacing in air at the isocenter, while a SSF = 1.0 is assumed for spot spacing in water at the Bragg peak.

Finally, Figure 3.9 shows how the TPS places spots inside a volume for the three different configurations. These images were taken from plans created for Patient 1 without the use of the Ridge Filter to better show the different behavior of the three algorithms in the presence of many spots.

For our study, for each patient we created three plans for each of these techniques in combination with the Ridge filter maintaining the same optimization settings to compare how they perform in terms of the number of spots and, consequently, delivery time, while still maintaining a good target coverage. For simplicity, we will refer to these configurations as Fixed Grid configuration, Air configuration and Water configuration.

Additionally, when placing spots, it is common to arrange them in either rectangular or hexagonal grids. For our study, we experimented with both grid types on one patient (Patient 1) to evaluate their performance. However, as we found that the results were comparable, we ultimately decided to use the rectangular grid for all of our other patients.

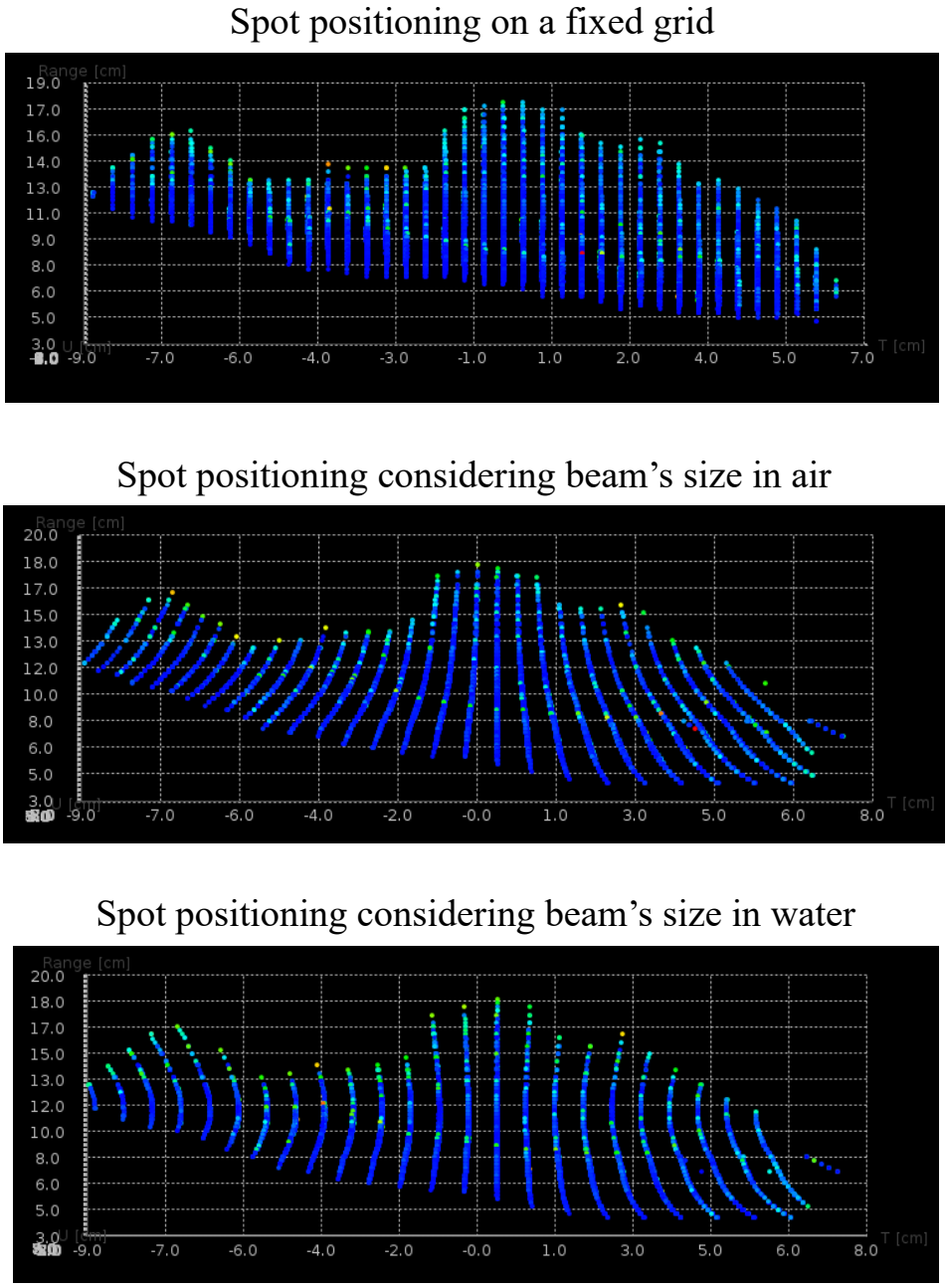

FIGURE 3.9: Comparison of the 3-dimensional distribution of spots inside a volume for the three different spot positioning algorithms (plans were created for Patient 1 without the use of the RF).

3.3 Delivery Time Calculation and Measurements

The calculation of the treatment delivery times made for this study is referred to the time performances of PSI's Gantry 2. The aim of this analysis is to understand how much time it would require to treat a patient with breath-hold in Gantry 2 and what is the difference in terms of delivery time between different planning setup configurations that

employ the RF. Moreover, we would like to see which factor contributes the most to the total delivery time per field. Finally, it would be interesting to have a general idea of the time reduction in the treatment of a patient using the breath-hold technique compared to what is currently done at PSI. Once we analyzed the results from the analysis on plans between the three configurations, we selected only the plans which resulted to be acceptable from a medical point of view, i.e., plans that satisfied all medical prescriptions and were robust, and calculated the delivery time of these plans.

The delivery time for every single field is given by the sum of two contributions: the beam-on time, which is the time when the dose is actually delivered to the target, and the dead time, which is the time necessary to change position inside the target. The latter is given by the sum of two contributions: the spot-changing time, which is the time required to move from one spot to the next one in the transversal direction on the same energy layer, and the energy-changing time, which is the time needed to move from one energy layer to another in the depth direction. When calculating times, we can ignore the time necessary to move the gantry, the table and the nozzle between one field and the next, as the patient can freely breathe during this time.

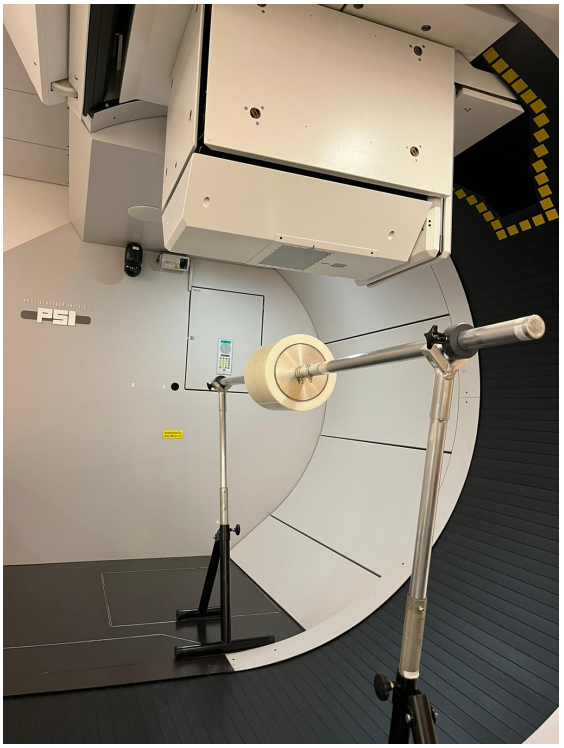

FIGURE 3.10: Setup configuration for measurements in PSI's Gantry 2.

To calculate delivery times, plans were exported from FIonA and a steering file generator (SFGen) was used to generate steering files, which need to be provided to the machine as input to deliver the treatment. From these files, the time required to deliver the dose within every single field can be estimated before the delivery, and the different contributions can be evaluated separately. Further, we measured the actual delivery times of the selected plans in PSI's Gantry 2. Figure 3.10 shows the setup adopted for performing the measurements. The gantry has always been kept in the vertical direction (0°), and a cylindric beam blocker was positioned below the nozzle to absorb the dose delivered during the treatment.

However, it is important to mention that Gantry 2 has a small nozzle window which is only 12 × 20 cm. Thus, for extended tumors, a patching technique is used, in which the tumor volume is divided into two smaller volumes. The process of dividing the tumor volume into patches is done by SFGen when creating steering files (see Figure 3.11).

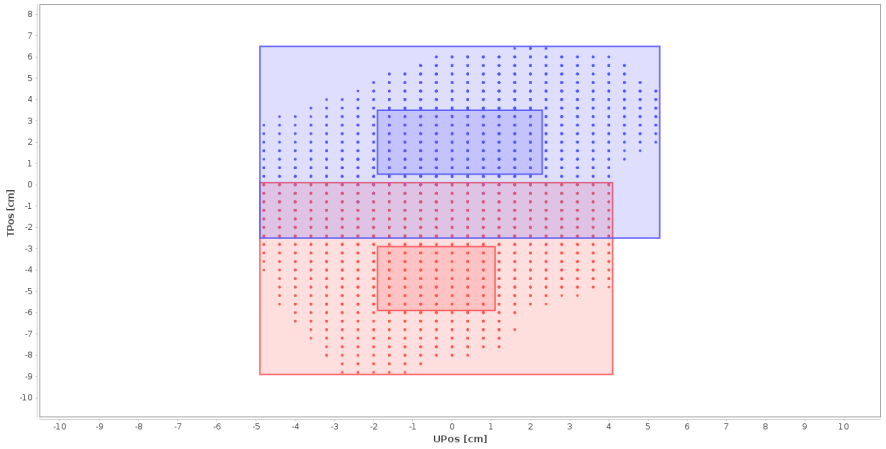

FIGURE 3.11: Visual representation of how SFGen divides the tumor volume into patches. This information is then provided to the machine to deliver the treatment. The figure is referred to Patient 1.

When patching is applied, the gantry delivers the dose to every single patch individually. As we can see from Figure 3.11, patches are slightly overlapped and the dose to the spots in the overlapped region is delivered twice, giving to these spots half of the intensity for each patch. Additionally, to move from one patch to the next one, the table is moved to align the patch to the nozzle window while the gantry is kept fixed. During this process, the beam is turned off. The processes of rescanning and patch-nozzle alignment, including the time required by the control system to give and verify commands, highly increase the field delivery time and it must be taken into account if breath-hold is used.

This patching technique is only used by PSI's Gantry 2, and a few other gantries in the world which have a similar design to this one, e.g. the ones employed at Med Austron in Wien, Austria. The majority of commercial gantries (such as PSI Gantry 3) have nozzle windows sized 30 × 30 cm, and therefore the patching technique is not necessary. Nevertheless, if a patient had an extended tumor which required patching, we could think of performing breath-hold in Gantry 2 anyway considering one breath-hold per patch. This would allow the patient to breathe freely while the table is being moved for alignment between patches, as the time required for aligning the table and preparing for the delivery of the second patch is approximately 8/9 seconds. However, the total duration of the treatment would increase.

We divided the timing analysis into two different parts. In the first part, we focused on calculating delivery times for our configurations for plans that were considered clinically acceptable. However, we made a distinction between patients who did not required patching (i.e., Patient 5, Patient 12, Patient 13, and Patient 14) and those who did. Initially, we estimated from steering files the delivery time for patients without patching and compared these estimates with the measured times obtained from Log files generated by Gantry 2 during the treatment delivery. This was done to assess the accuracy of our timing estimation based on the steering files. As our observations revealed no significant differences between the estimated times and the measured times for these patients, we extended our estimation approach to patients with patching by calculating the average delivery time per patch. It is worth noting that accurately measuring delivery time for patched volumes posed challenges, which led us to solely report the estimated time in our study findings.

In the second part of the analysis, our goal was to determine the contribution of three different timing factors (beam-on time, spots-changing time, and energy-changing time) to the total delivery time per field. However, to obtain more general results and not be limited by patching, we decided to calculate the total delivery time per field from steering files for all patients by excluding the timing contributions related to patching. Subsequently, we roughly estimated the timing associated with each contribution for each plan. It's important to note that precise calculations of the beam on time and spots changing time separately were not possible as steering files only provide the combined sum of these two contributions. However, by making certain assumptions and utilizing measured values as a reference point, we were able to obtain rough estimates for each

individual contribution. Although these approximations are not highly precise, they can still be useful in visualising the time reduction for each contribution. To estimate the beam on time and spot changing time separately, we performed the following steps. We first extrapolated the spot-changing time per spot from Log files for each volume without patches and computed a mean value of this parameter for each configuration. Next, we multiplied the obtained values by the number of spots in each field for the corresponding configurations. This allowed us to estimate the spots changing time per field and to find the average across fields. Finally, to isolate the mean beam-on time, we subtracted the estimated mean spots-changing time from the combined sum of the beam-on time and spots-changing time obtained from the steering files.

Chapter 4

Results

This chapter focuses on the analysis of data obtained from a comparative study of plan performances designed using three different spot positioning algorithms (spot positioning on a fixed grid or energy-dependent spot positioning in air at the isocenter and in water at the Bragg peak), in combination with the Ridge filter, to evaluate their efficacy in facilitating breath-hold procedures. Furthermore, results of the measured treatment delivery times for clinically acceptable plans are compared with the delivery times required by clinical plans, i.e., plans designed using the same settings currently used in the PSI's CPT clinics. For simplicity in presenting the results, we will refer to plans created with the three different algorithms used in combination with the RF as Fixed Grid, Air and Water configurations, respectively.

4.1 Comparison Between Rectangular and Hexagonal Grid

Before creating plans for all patients, we decided to compare the differences between arranging spots on a rectangular or on a hexagonal grid for Patient 1 in terms of dose delivered to the target volume and organs at risk and number of spots. Figure 4.1 shows the comparison of the DVHs between plans designed using the two grid types for each configuration (Fixed Grid, Air and Water), while Figure 4.2 shows the number of spots used for each configuration.

The two grid types show almost the same performances: DVHs for the Fixed Grid and Air configurations are almost perfectly overlapped, showing that doses delivered to both

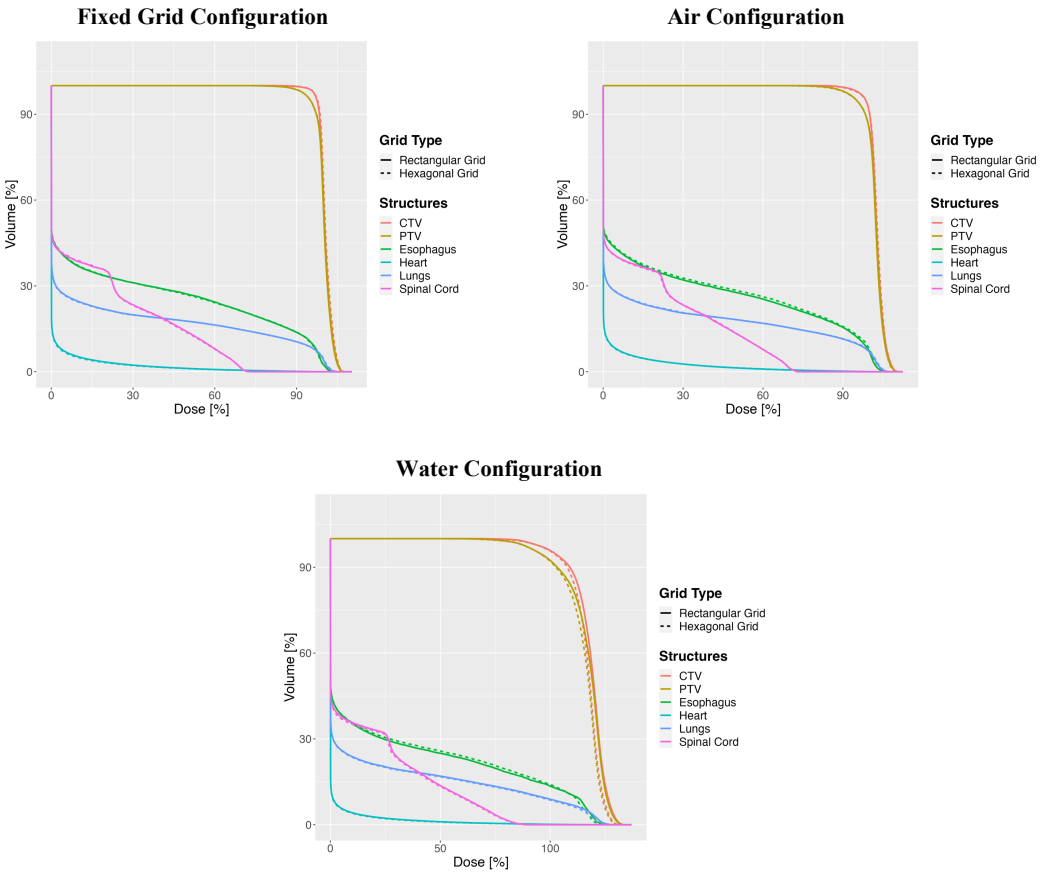

FIGURE 4.1: DVHs comparison of plans created by arranging spots on a rectangular grid and on a hexagonal grid for the Fixed Grid, Air and Water configurations for Patient 1.

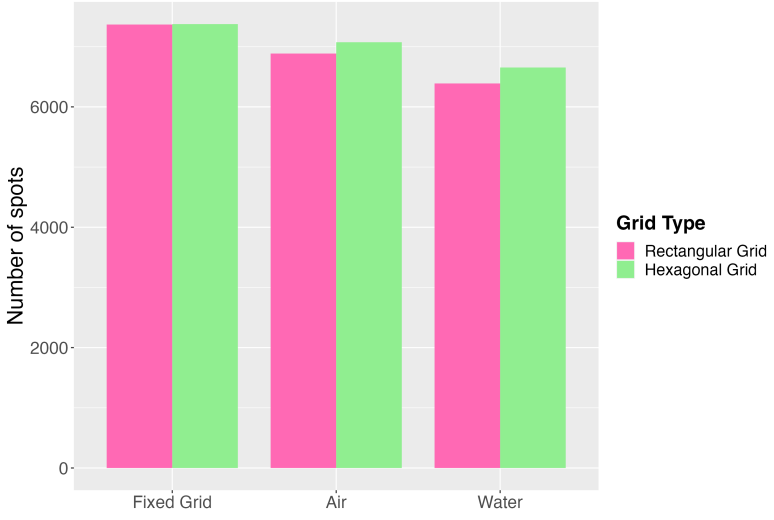

FIGURE 4.2: Comparison of the number of spots used for plans with rectangular and hexagonal grids for the Fixed Grid, Air and Water configurations for Patient 1.

the target and OARs are the same, while for the Water configuration, the plan made with the hexagonal grid delivers slightly less dose to both the target and the OARs, with exception to the esophagus. Furthermore, plans made with the rectangular grid place a slightly lower number of spots when compared to plans with spots arranged hexagonally. Since we did not notice significant differences between plans created with the two grid types, we decided to create plans for all the other patients by arranging spots on layers using the rectangular grid, as this method is also used at PSI's clinics. From now on, all the plans presented and discussed below will be made by arranging spots on a rectangular grid.

4.2 Plans' Comparison Between the Fixed Grid, Air and Water Configurations

In this section, we compare the performances of plans made using the three different spot positioning algorithms in combination with the RF in terms of dose delivered to organs at risk (by comparing their DVHs), prescriptions fulfilment and amount of spots used to deliver the total dose to the target. Furthermore, we calculate for each algorithm the reduction of the number of spots due to the presence of the Ridge filter with respect to Clinical plans.

4.2.1 Comparison of DVHs

To assess which of the Fixed Grid, Air and Water configurations performs better in terms of the delivered dose, we plotted the comparison of DVHs between the three configurations for each patient, as shown in Figures 4.3 and 4.4. All the plans created were normalized to D95% = 95% on the PTV.

If we first look at the DVHs of the target volumes (CTV and PTV), we can notice that plans made with the Water configuration deliver too much dose to the tumor for all patients with respect to the Fixed Grid and Air plans. If we look instead at the DVHs of organs at risk, we are unable to detect a general trend for which one configuration performs better than the others.

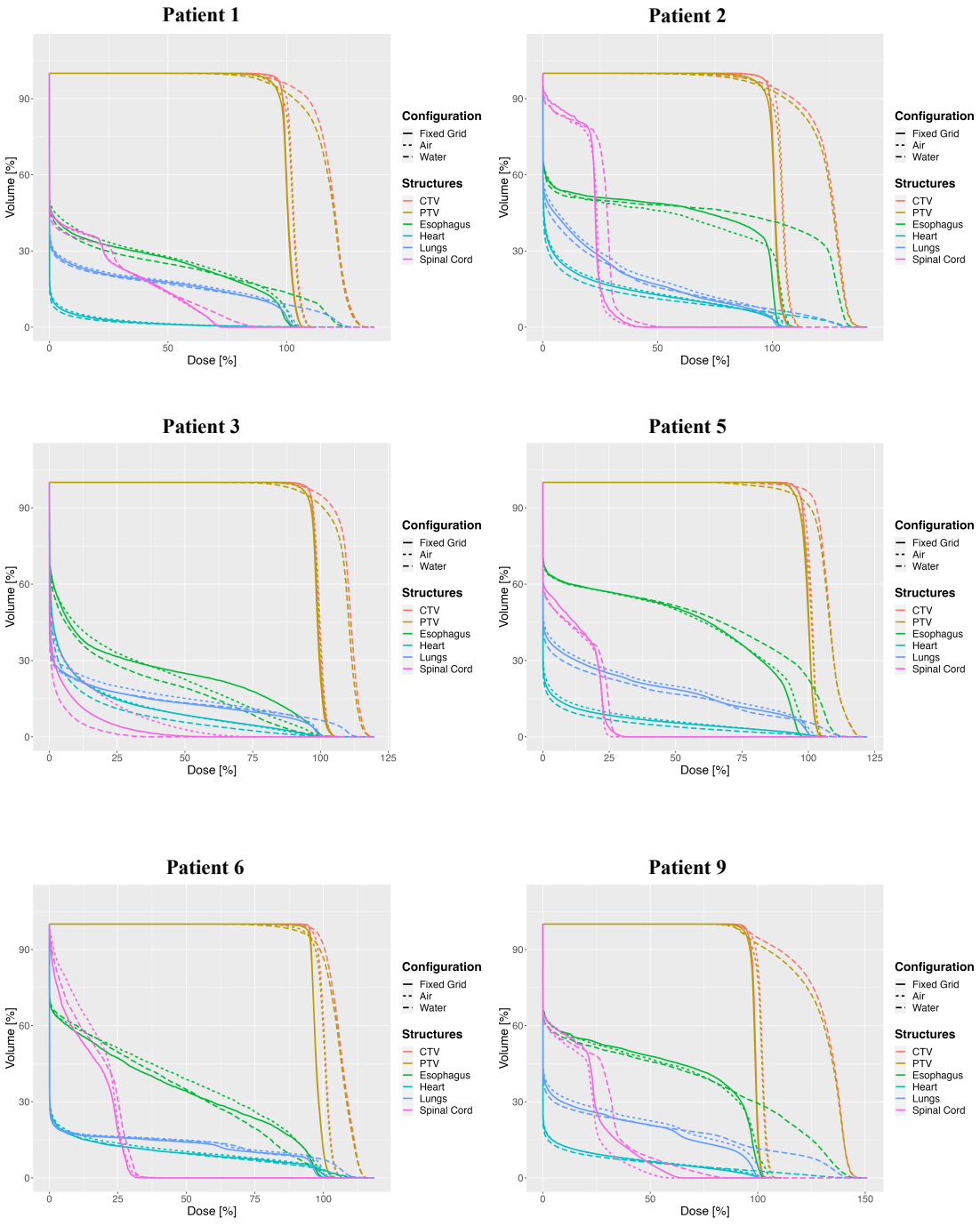

FIGURE 4.3: Comparison of DVHs for the target volumes and organs at risk between plans with Fixed Grid, Air and Water configurations for Patients 1-9.

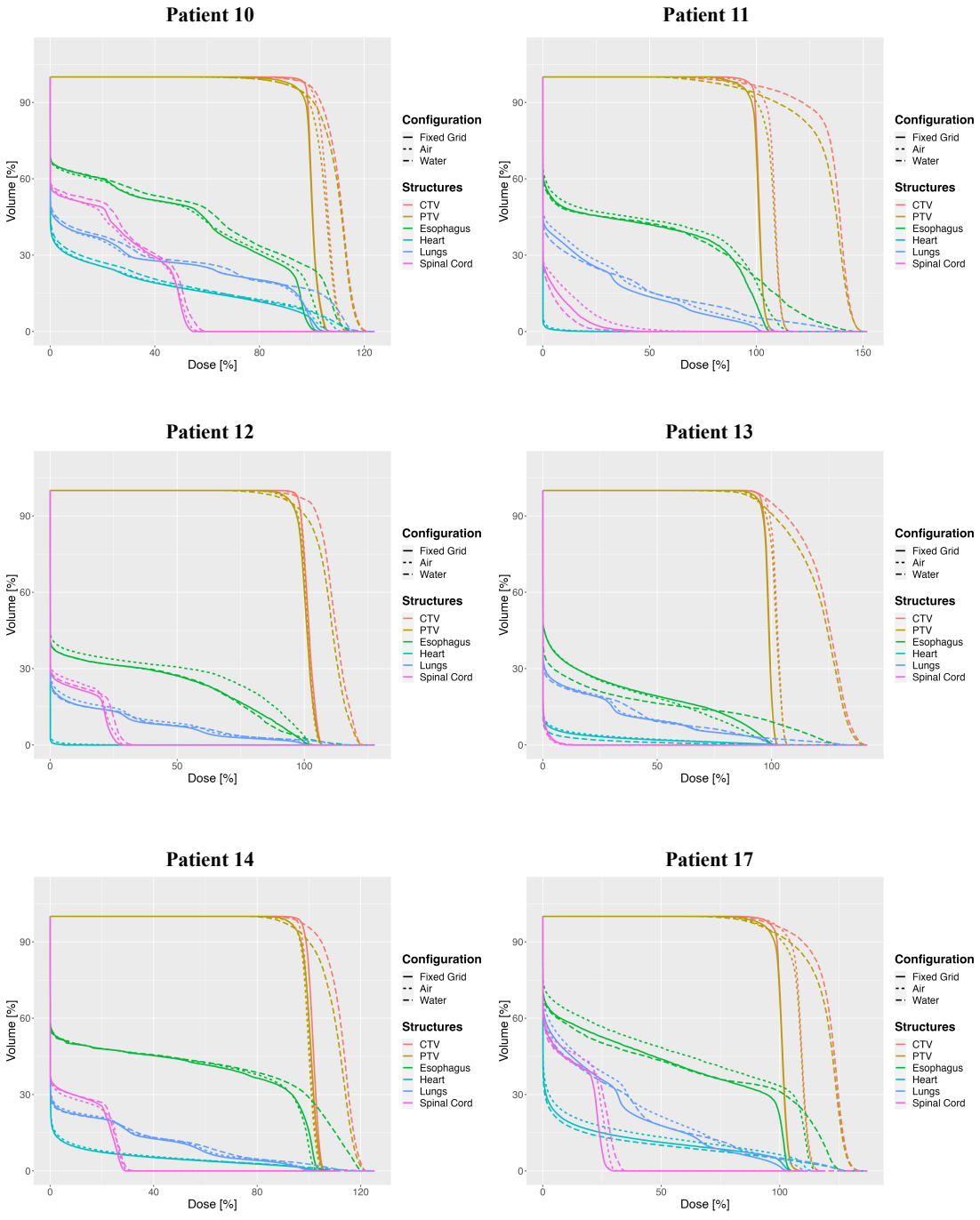

FIGURE 4.4: Comparison of DVHs for the target volumes and organs at risk between plans with Fixed Grid, Air and Water configurations for Patients 10-17.

4.2.2 Prescriptions Fulfillment

To assess the goodness and acceptability of plans, we checked that medical prescriptions (see Table 3.2) were satisfied. The prescription for target coverage was set to be V95% > 97.00% on the CTV, and it was satisfied by all the plans for each configuration, with the exception of the Water plan for Patient 2. The mean values of CTV V95% obtained for the three different configurations were comparable: for Fixed Grid plans the mean value obtained was 98.37% (range 97.38% - 99.56%), for Air plans the mean value was 98.35% (range 97.63% - 99.26%), while for Water plans the mean value was 97.89% (range 96.41% - 98.66%). The values calculated for the three configurations are shown in Figure 4.5.

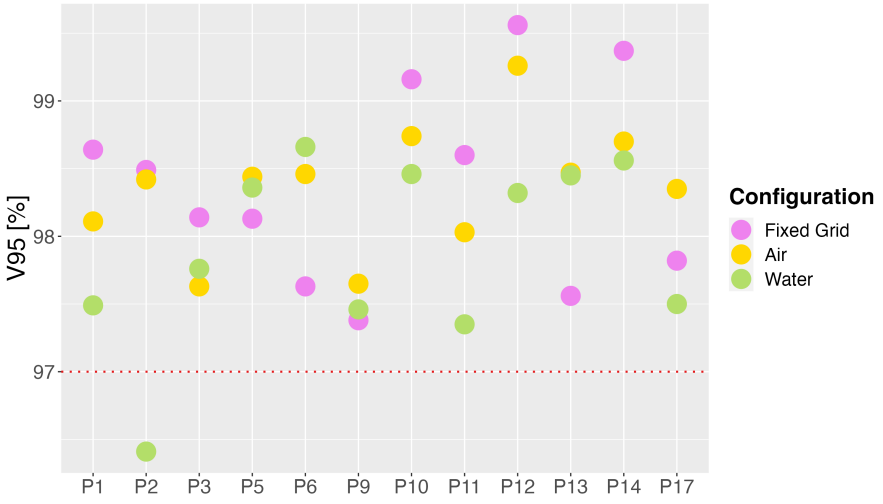

FIGURE 4.5: CTV prescription evaluation: comparison of CTV V95% values between the Fixed Grid, Air and Water configurations for each patient. The red dotted line represents the threshold for satisfying the prescription (V95% > 97.00%).

The requirement for minimizing overdose to the target was set to be V107% < 1.00% on the PTV. For the Fixed Grid configuration, we found a mean value of 0.20% (range 0.00% - 0.81%), with all the plans satisfying the prescription. For the Air configuration, instead, the mean value was 15.44% (range 0.00% - 74.45%), with 5 of 12 plans not meeting the requirement (Patient 1, Patient 2, Patient 10, Patient 11 and Patient 17). For the Water configuration, we obtained a mean value of 76.75% (range 41.37% - 90.99%), with all of the plans significantly exceeding the prescription, as it could be easily seen from PTV DVHs in Figures 4.3 and 4.4. The values measured for the prescription on the PTV between the three configurations are shown in Figure 4.6.

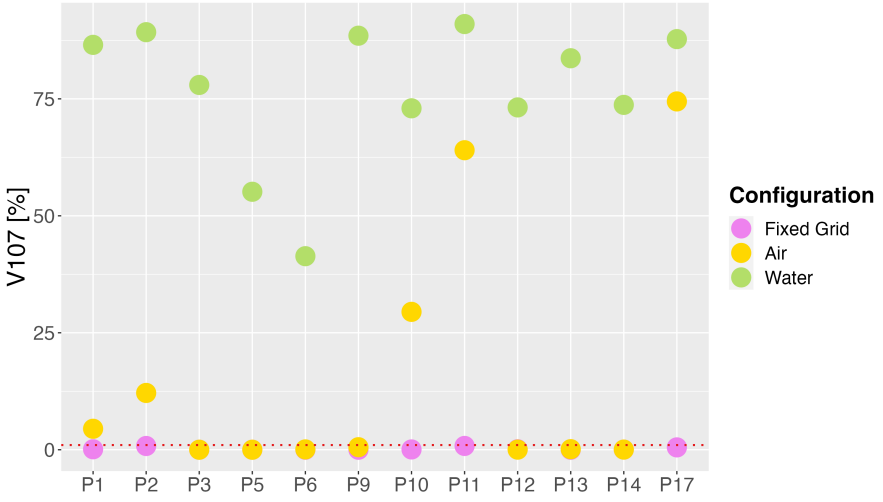

FIGURE 4.6: PTV prescription evaluation: comparison of PTV V107% values between the Fixed Grid, Air and Water configurations for each patient. The red dotted line represents the threshold for satisfying the prescription (V107% $<$ 1.00%).

Additionally to medical prescriptions, another parameter used for assessing the goodness of plans is D5%-D95% (see Figure 4.7), which is used to assess that the dose falloff at the target volume is sharp enough. According to ICRU guidelines for plan quality, this value should satisfy D5%-D95% $<$ 10% for the PTV. All Fixed Grid plans satisfied this requirement, for Air plans only 7 out of 12 plans did (Patient 3, Patient 5, Patient 6, Patient 9, Patient 12, Patient 13 and Patient 14), while for the Water configuration, this value highly exceeded the threshold.

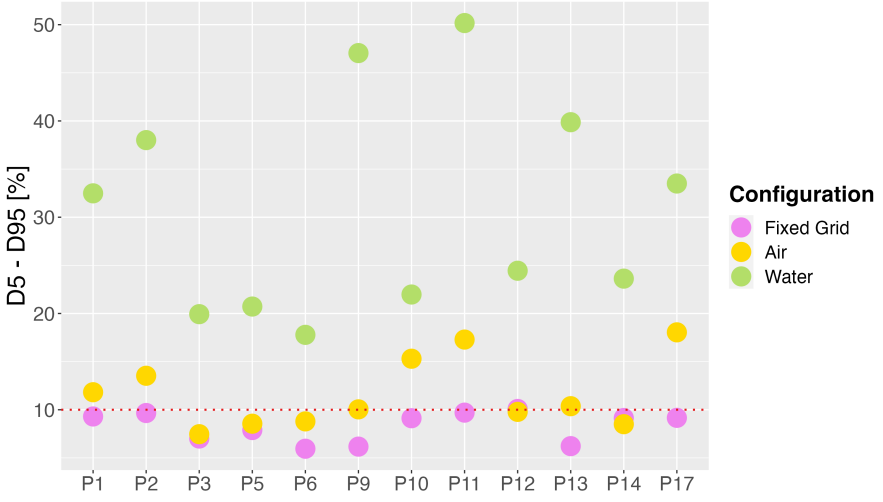

FIGURE 4.7: PTV ICRU guidelines evaluation: comparison of PTV D5%-D95% values between the Fixed Grid, Air and Water configurations for each patient. The red dotted line represents the threshold for satisfying the ICRU guideline requirement (D5%-D95% $<$ 10%).

The delivered dose to organs at risk and the subsequent fulfilment of prescriptions gave different results between patients depending on both the plans' configuration and the size and location of the organs with respect to the tumor volume. Generally, all plans created with the Fixed Grid configuration satisfied all the prescriptions on OARs, while plans with Air and Water configurations did not, with Water plans showing the worst results. A detailed description of the comparison between configurations of prescribed values on OARs for each patient can be found in Appendix A.1.

For the esophagus (see Figure A.1), the prescribed mean dose delivered to the organ (Dmean $<$ 34.00 GyRBE) was not satisfied on 5 patients for Water plans (Patient 2, Patient 5, Patient 9, Patient 10, Patient 17) and on 1 patient for Air plans (Patient 17). The requirement V74.00 GyRBE $<$ 1.0 cc, instead, was not met by 9 plans for the Water configuration (Patient 1, Patient 2, Patient 5, Patient 9, Patient 10, Patient 11, Patient 13, Patient 14, Patient 17), and by 3 plans for the Air configuration (Patient 2, Patient 11, Patient 17).

Prescriptions on the spinal cord (see Figure A.2) were satisfied by all plans for all patients, with the exception for Patient 1 and Patient 9. For Patient 1, the prescription on Dmax (DMax $<$ 54.00 GyRBE) was not satisfied only by the Water configuration plan, while the prescription on V50.00 GyRBE (V50.00 GyRBE $<$ 0.03 cc) was not satisfied by all configuration plans, with Fixed Grid and Air plans slightly exceeding the threshold value. For Patient 9, instead, both prescriptions were not satisfied only by the Water configuration plan.

Prescriptions on lungs (see Figure A.3) were satisfied by all plans for all configurations, with the exception of the Water plan for Patient 10, for which the prescribed Dmean exceeded the threshold value (DMean $<$ 20.00 GyRBE).

Finally, heart prescriptions (see Figure A.4) were satisfied by all plans for all configurations.

4.2.3 Comparison of Number of Spots

Finally, we compared the total number of spots between the three different configurations for each patient (see Figure 4.8).

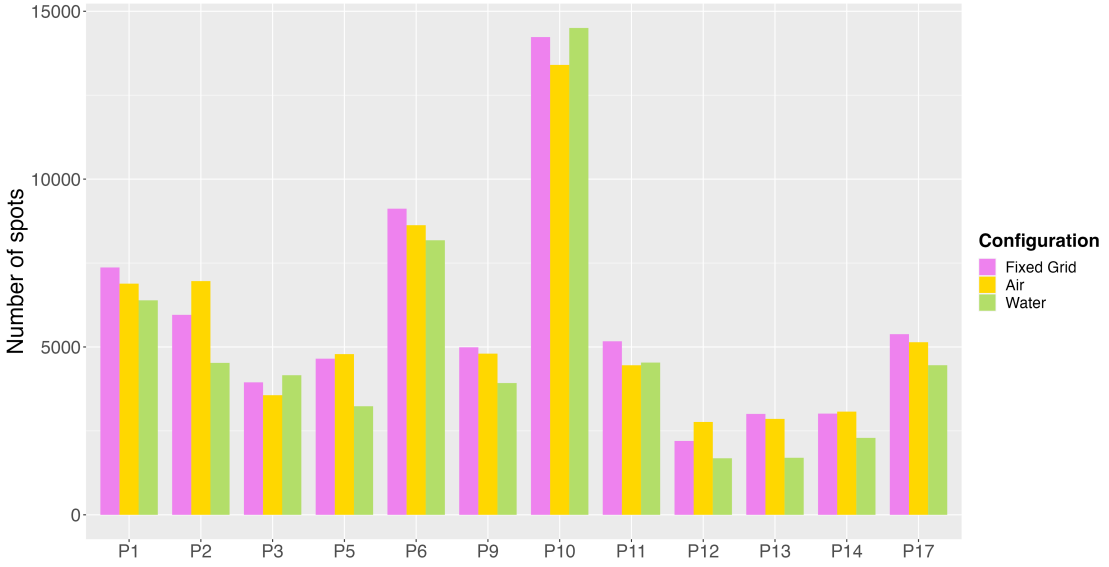

FIGURE 4.8: Comparison of the total number of spots between Fixed Grid, Air and Water plans for each patient.

The number of spots for each plan depends on different factors, including the tumor volume, the spot placement algorithm used and the margin width set for spot arrangement when defining fields to assure target coverage. For Patient 1, Patient 3, Patient 6, Patient 9, Patient 10, Patient 13, and Patient 14, the spot margin factor employed for Air and Water plans was chosen to ensure that the set margins were comparable to those of Fixed Grid plans at 150MeV. It can be noticed that when comparing the three configuration plans for these patients, Fixed Grid plans always assign the highest number of spots on the target, while Water plans always assigns the lowest number of spots, with the exception of Patient 3 and Patient 10, for which the number of spots for Water plans is greater than both Fixed Grid and Air ones. For Patient 2, Patient 5, Patient 11, Patient 12, Patient 13 and Patient 17, instead, Air plans were created by increasing the SMF to reach the required target coverage. By doing so, the number of spots increased, in most cases being higher than the number of spots of plans for the Fixed Grid configuration, as for Patient 2, Patient 5, Patient 12 and Patient 14.

For each plan, we then compared the number of spots of the three configurations with respect to the number of spots of clinical plans and calculated the spot reduction of each configuration with respect to the clinical situation. It has to be reminded that clinical plans do not employ the Ridge filter, while our plans do. Results are shown in Table 4.1. The mean reduction of spots for RF plans compared to clinical plans is 72% for Fixed

Grid plans (range 61% - 83%), while for Air plans the mean reduction is 73% (range 54% - 84%), and for Water plans it is 77% (range 67% - 84%).

	Clinical	**Fixed Grid**		**Air**		**Water**	
Patient	***N. Spots***	***N. Spots***	***Spots Red.***	***N. Spots***	***Spots Red.***	***N. Spots***	***Spots Red.***
P1	30195	7368	76%	6886	77%	6389	79%
P2	15186	5957	61%	6962	54%	4526	70%
P3	12429	3946	68%	3563	71%	4158	67%
P5	14132	4651	67%	4787	66%	3234	77%
P6	49469	9119	82%	8627	83%	8178	83%
P9	12919	4991	61%	4801	63%	3925	70%
P10	83661	14231	83%	13402	84%	14502	83%
P11	17852	5169	71%	4455	75%	4535	75%
P12	10744	2200	80%	2766	74%	1684	84%
P13	8776	3005	66%	2857	67%	1699	81%
P14	13748	3015	78%	3074	78%	2291	83%
P17	18406	5381	71%	5141	72%	4456	76%

TABLE 4.1: Comparison of the total number of spots and percentage of spots reduction between clinical plans and plans for each configuration (Fixed Grid, Air, Water) for each patient. The *Spots Red.* column is referred to the reduction of the total number of spots of the selected configuration with respect to the corresponding clinical plan.

4.2.4 Plans' Robustness Evaluation

As we mentioned in the previous chapter, plans are optimized using an hybrid optimization, which takes into account range uncertainties. However, robustness for geometrical shifts must be evaluated as well. To assess the plans' robustness, we analyzed the robustness DVHs generated by FIonA when running the *Calculate robustness DVHs* function. In our case, we considered plans to be robust if the robustness DVH for the worst-case

scenario of the CTV satisfied the condition V95% > 95%. The evaluation of the robustness was limited to Fixed Grid and Air configuration plans, as from a first general analysis, all Water configuration plans were not considered clinically acceptable.

All the Fixed Grid plans resulted robust according to our criteria, except for plans for Patient 5 and Patient 17, for which V95% values were slightly below the set threshold. For this configuration, the mean value of V95% for the CTV in the worst-case scenario was 96.39% (range 94.68% - 99.50%). For Air plans, instead, only 3 of 12 plans met the robustness requirements, while the remaining plans were demonstrated not to be robust, with a mean value of V95% for the CTV in the worst case scenario of 92.86% (range 87.07% - 97.10%). The comparison CTV V95% for the worst-case scenario between Fixed Grid and Air configurations of prescribed values for each patient are shown in Figure 4.9.

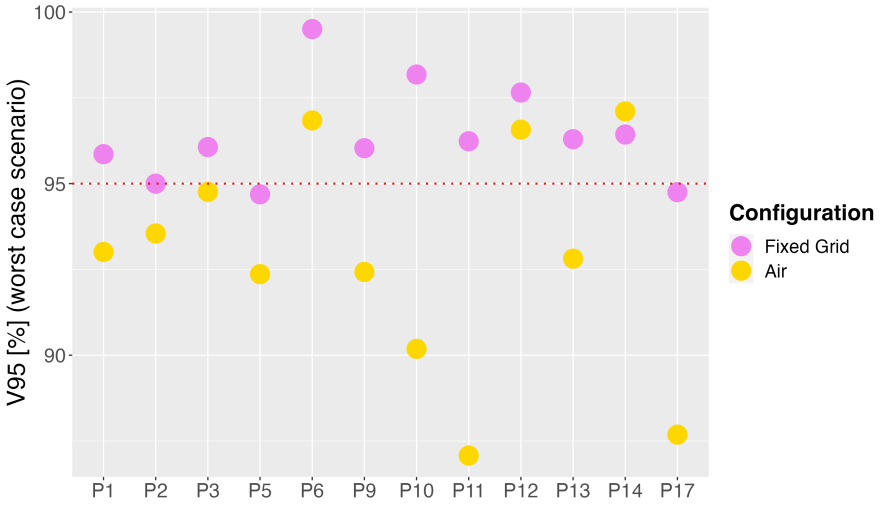

FIGURE 4.9: CTV V95% values for the worst case scenario of plans made with the Fixed Grid and Air configurations for all patients. The red dotted line represents the threshold for satisfying robustness criteria (V95% > 95%).

Additionally, we evaluated the robustness of plans for both the Fixed Grid and Air configurations in terms of target coverage within different breath-hold stages by recalculating the planned dose distribution on a CT scan acquired during a different breath-hold. Results showed that the prescription for CTV coverage was still satisfied for the plans of these patients, meaning that plans were robust between different breath holds for target coverage.

4.2.5 Plans with Increased Energy Step Factor (ESF)

All the results presented above are relative to plans created using an ESF equal to 3. However, by looking at Table 4.1, we noticed that Patient 1, Patient 6 and Patient 10 showed the highest number of spots, as these patients have the biggest PTV volumes. Hence, for these patients we created an additional plan setting the ESF = 5 to further reduce the total number of energy layers, and thus, total number of spots, keeping all the other settings unchanged. We did that only for the Fixed Grid configuration, as from preliminary results, this was the configuration that showed the best results. We compared both the DVHs and the number of spots between plans created with ESF = 3 and plans with ESF = 5 for these patients. The comparison of DVHs can be seen in Figure 4.10.

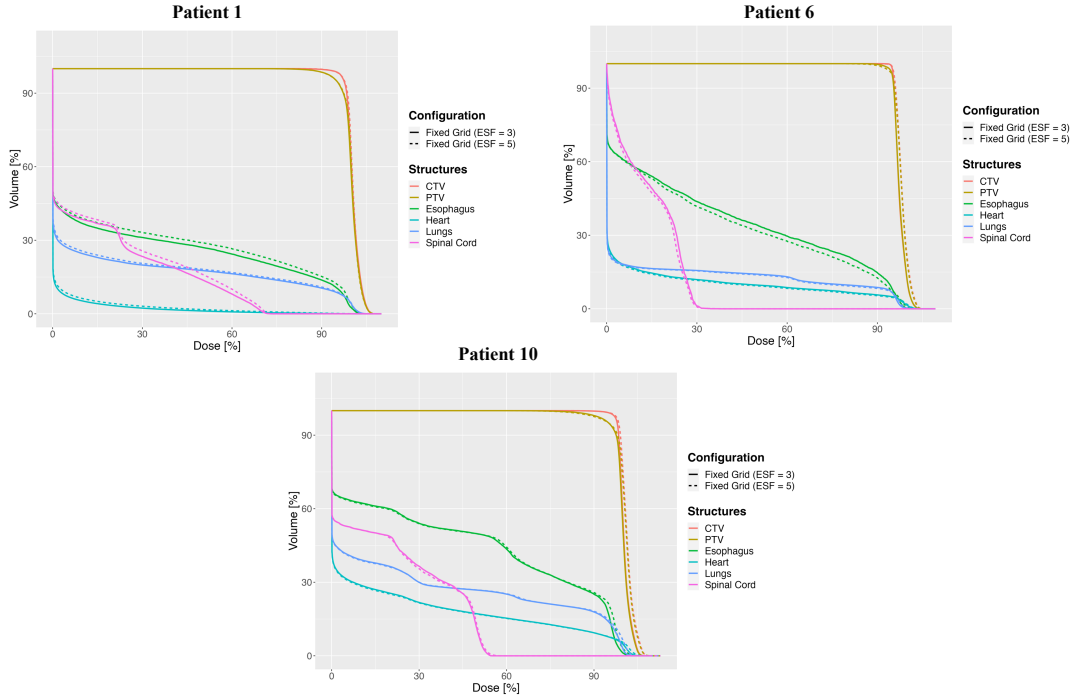

FIGURE 4.10: DVHs comparison between plans created for the Fixed Grid configuration by setting the ESF = 3 and ESF = 5 for Patient 1, Patient 6 and Patient 10.

DVHs for the target appear to be almost overlapped between plans for ESF = 3 and ESF = 5 for all three patients, with Patient 10 showing to deliver slightly more dose to the PTV for the plan made with ESF = 5 with respect to the plan with ESF = 3. DVHs for organs, instead, have a different behaviour between the three patients: indeed, for Patient 1 OARs DVHs for the plan with ESF = 5 show an higher dose with respect to

the plan with ESF = 3, while the opposite situation is found for Patient 6. For Patient 10, instead, DVHs of OARs are overlapped. Furthermore, all the plans made using ESF = 5 satisfied the medical prescriptions and met robustness requirements, and can thus be considered clinically acceptable.

Finally, we compared the number of spots between the two plans with ESF = 3 and ESF = 5 for each of the three patients (see Figure 4.11).

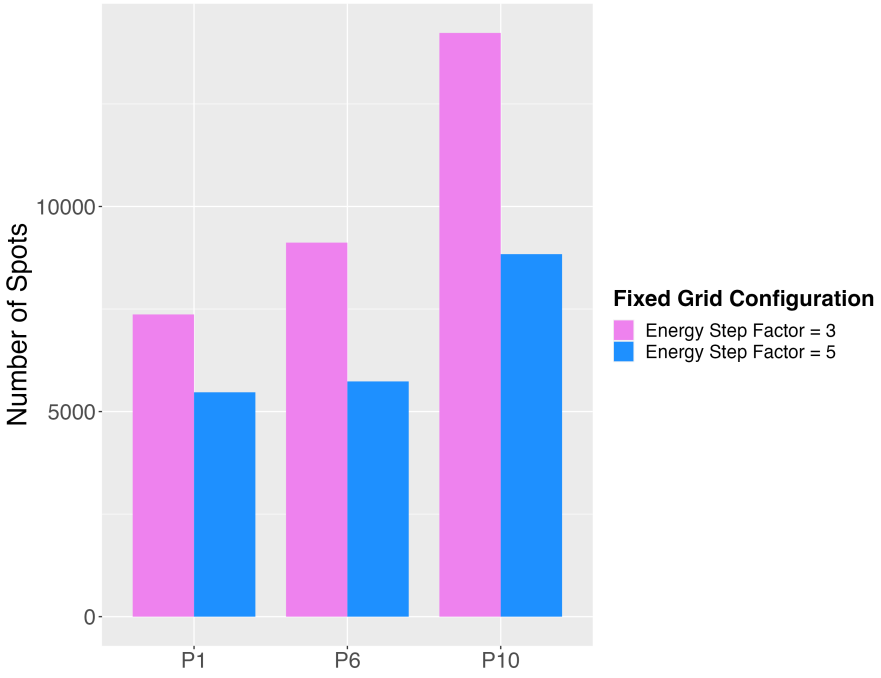

FIGURE 4.11: Comparison of the number of spots between plans created for the Fixed Grid configuration by setting the ESF = 3 and ESF = 5 for Patient 1, Patient 6 and Patient 10.

Table 4.2 shows the comparison of the number of spots between clinical plans and plans created using ESF = 3 and ESF = 5 for Patient 1, Patient 6 and Patient 10. By using an ESF = 5, the total number of spots for Patient 1 decreased by 26% with respect to the plan made with ESF = 3, while for Patient 6 the reduction was 37% and for Patient 10 it was 38%.

	Clinical	**Fixed Grid (ESF = 3)**		**Fixed Grid (ESF = 5)**	
Patient	***N. Spots***	***N. Spots***	***Spots Red.***	***N. Spots***	***Spots Red.***
P1	30195	7368	76%	5470	82%
P6	49469	9119	82%	5735	88%
P10	83661	14231	83%	8838	89%

TABLE 4.2: Comparison of the number of spots between clinical plans and plans created using the Fixed Grid configuration with an energy step factor (ESF) equal to 3 and 5 for Patient 1, Patient 6 and Patient 10. The *Spots Red.* column is referred to the reduction of the total number of spots of the selected configuration with respect to the corresponding clinical plan.

4.2.6 Plans Selection

After analyzing data from the comparison of performances between the different configurations, we selected clinically acceptable plans to use in the delivery time analysis. These plans must meet all medical prescriptions and demonstrate robustness to be considered clinically acceptable.

From this first comparison analysis, we observed that all the plans created with the Fixed Grid configuration for all patients are acceptable from a medical point of view, satisfying all medical prescriptions. Regarding robustness values, we considered Fixed Grid plans for Patient 2, Patient 5, and Patient 17 acceptable despite robustness values were slightly below the 95% threshold as the discrepancy was very low, while for all other patients robustness was above 95%. It is important to note that robustness remains a topic of discussion, and medical doctors and medical physicists hold varying opinions on this topic. This justifies our decision of not removing these plans from our analysis. For Air configuration plans, instead, only 3 plans out of 12 satisfy all medical prescriptions and robustness constraints (Patient 6, Patient 12 and Patient 14). Plans for Patient 3, Patient 5 and Patient 9 satisfy prescriptions, but do not meet the robustness requirement. However, also in this case, the value of V95% for the CTV in the worst-case scenario for these plans is not that far from the acceptability threshold, and we considered plans for these patients acceptable anyway for our final analysis for the same reasons explained above. Air plans for Patient 1, Patient 2, Patient 10, Patient 11, Patient 13 and Patient

17, instead, cannot be considered acceptable, as prescriptions on both OARs and PTV are not satisfied. Finally, all Water configuration plans are not acceptable due to the high overdosing of both organs at risk and the target volume.

To conclude, the only clinically acceptable plans are Fixed Grid plans for all patients, including plans created with ESF = 5 for Patient 1, Patient 6 and Patient 10, and Air plans for Patient 3, Patient 5, Patient 6, Patient 9, Patient 12 and Patient 14. These plans were the only ones considered for the analysis of the treatment delivery time.

4.3 Delivery Time Analysis

In this section, we present the results obtained from the calculation of delivery times for each plan and configuration that was considered clinically acceptable (see Section 4.2.6). In the first part, we evaluated delivery times distinguishing between patients who required patching and those who did not (i.e., Patient 5, Patient 12, Patient 13 and Patient 14). For patients without patching, we compared estimated values and measured values of the mean delivery time per field, while for patients with patching, we only calculated the estimated times required for dose delivery per patch per field. In the second part, instead, we focused on estimating and comparing the three contributions to the total delivery time (beam-on time, spots-changing time, and energy-changing time) between the different configurations. However, as mentioned before, reported values for the beam-on time and the spots-changing time are not precise and must thus be considered just as a rough approximation.

4.3.1 Delivery Times Calculation

For patients who did not require patching, i.e. Patient 5, Patient 12, Patient 13 and Patient 14, we compared the estimated delivery times (obtained from steering files) and the measured delivery times (obtained from Log files) of plans created with the Clinical, Fixed Grid and Air configurations. Table 4.3 reports the values obtained from the calculation of the measured and the estimated mean delivery times per field, and the time difference between the two situations.

Patient	**Plan**	**Mean Delivery Time per Field**		
		Measured [s]	***Estimated [s]***	***Difference [s]***
P5	Clinical	25.91	21.53	4.38
	Fixed Grid	15.88	15.09	0.79
	Air	-	-	-
P12	Clinical	18.95	15.12	3.83
	Fixed Grid	9.45	9.06	0.39
	Air	11.42	10.14	1.28
P13	Clinical	17.48	14.84	2.64
	Fixed Grid	12.38	12.18	0.20
	Air	-	-	-
P14	Clinical	24.10	20.10	4.00
	Fixed Grid	12.38	12.14	0.24
	Air	12.88	12.53	0.35

TABLE 4.3: Comparison between the measured and the estimated mean delivery times per field for each plan for patients who did not require patching. Reported values are averaged on fields. Missing values for Air plans were not calculated as they were not clinically acceptable for these patients.

The measured delivery times are slightly higher than the estimated ones. The biggest discrepancy is given by clinical plans, for which the difference in time between measured and estimated values is on average 4.07 s. If we consider instead plans for the Fixed Grid and Air configurations, the estimated values are more in accordance with the measured ones, with differences less than 1s on average for both configurations. Out of all the Clinical plans, only two patients have mean delivery times per field below 20 seconds. In contrast, both Fixed Grid plans and Air plans exhibit delivery times below 20 seconds for all patients. Consequently, these patients would be suitable for breath-hold in Gantry 2. The results clearly indicate a significant decrease in the mean delivery time per field for both Fixed Grid plans and Air plans compared to clinical plans. On average, the reduction in delivery time for both configurations is approximately over 30%, with Fixed Grid plans demonstrating a slightly higher reduction of around one second.

Additionally, we utilized both steering files and Log files to determine the different contributions to the mean delivery time for both estimated and measured values. However, steering files do not separate between the beam on time and the spots changing time.

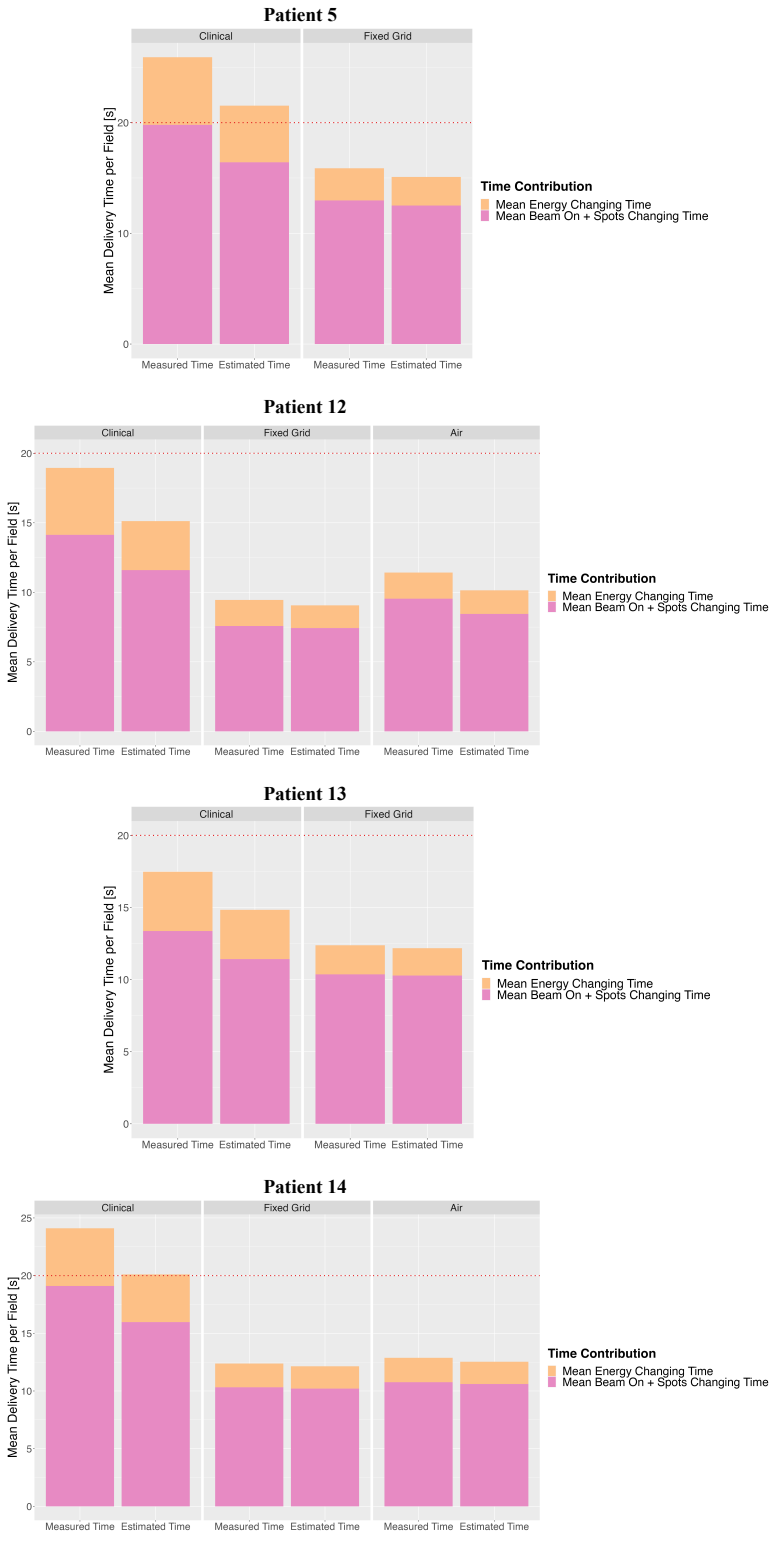

FIGURE 4.12: Comparison between measured and estimated mean delivery time per field for patients without patching, with visual representation of contributions to time from the mean energy changing time and mean beam on + spot changing time.

Consequently, we only computed the contributions due to the energy changing time and the sum of the beam-on and spots-changing time. Values are reported in Table A.1, while a visual representation of the contributions for both estimated and measured values can be seen in Figure 4.12. From the results, we notice that the contribution due to the sum of the beam-on time and the spots-changing time is under-estimated from steering files. The biggest difference is given by clinical plans, with an average of 2.75 s. For Fixed Grid and Air plans, instead, the average difference is below 1 s. If we instead look at the mean energy-changing time, we see that also in this case values are slightly under-estimated, and the difference between measured and estimated times for clinical plans is higher than the difference for the other two configurations. The disparity appears to escalate as the number of energy layers and spots increases.

For patients who required patching, i.e. Patient 1, Patient 2, Patient 3, Patient 6, Patient 9, Patient 10, Patient 11 and Patient 17, we only estimated delivery times per patch for each field from steering files. For our patients, a maximum of two patches were utilized per field. Table 4.4 reports the estimated delivery times of patches per field. It is important to note that not all fields required patching consistently, as for some patients only one or two fields required this division. Moreover, the subdivision into patches is not perfectly made such that patches are equal in size, but they could have different volumes. For these reasons, the reported values were not averaged across fields. As we can notice, in the majority of patients the estimated delivery times per patch for the clinical plans are above 20 seconds. Hence, they would not be feasible for breath-hold. In contrast, the Fixed Grid and Air plans showed significant reductions in delivery times per patch. For Fixed Grid plans, the delivery times are all below 20 seconds, with the exception of Patient 10, who had the biggest tumor volume. For this patient, delivery times are slightly above 20 seconds for two patches. The delivery times per patch for Air plans were similar to those of Fixed Grid plans, with slightly longer times for most plans. However, the difference in delivery times was only about 1 or 2 seconds. On average, for patients where it was possible to calculate the reduction in delivery time, both configurations achieved a reduction of over 40% in delivery time per patch.

Patient	**Plan**	**Delivery Time per Patch**					
		Field 0 [s]		***Field 1 [s]***		***Field 2 [s]***	
P1	Clinical	16.28	23.00	18.61	22.35	21.25	24.99
	Fixed Grid	10.89	14.64	11.76	12.91	10.81	13.21
	Air	-	-	-	-	-	-
P2	Clinical	23.59		26.29		16.35	18.57
	Fixed Grid	11.92	9.88	10.79	11.37	11.58	13.02
	Air	-	-	-	-	-	-
P3	Clinical	15.36	18.36	25.92		25.80	
	Fixed Grid	8.37	9.99	15.62		15,39	
	Air	9.22	11.48	10.22	10.79	8.68	11.57
P5	Clinical	20.44		21.78		22.37	
	Fixed Grid	14.58		15,08		15.62	
	Air	15.49		15.36		9.95	8.81
P6	Clinical	33.65	25.56	24.13	27.82	24.72	27.35
	Fixed Grid	15.51	11.94	12.88	15.30	12.42	14.55
	Air	16.30	11.22	13.75	15.74	12.64	15.51
P9	Clinical	12.18	17.37	11.07	17.48	26.40	
	Fixed Grid	9.50	13.37	8.46	13.21	7.96	12.17
	Air	10.11	13.68	8.98	13.04	8.68	11.92
P10	Clinical	52.38	35.33	51.00	37.98	40.05	41.60
	Fixed Grid	22.44	16.04	22.30	17.32	20.80	20.00
	Air	-	-	-	-	-	-
P11	Clinical	20.39	20.84	31.65		24.17	
	Fixed Grid	11.62	11.59	9.87	11.50	17.21	
	Air	-	-	-	-	-	-
P17	Clinical	31.75		30.97		24.79	15.28
	Fixed Grid	19.50		20,10		13.89	10.65
	Air	-	-	-	-	-	-

TABLE 4.4: Comparison of the estimated delivery times per patch for Clinical, Fixed Grid and Air plans. Fields for which patching was applied have two reported values, indicating delivery times for the two patches, while fields that did not required patching have only one reported value, indicating the delivery time of the whole field. Missing values for Air plans were not calculated as they were not clinically acceptable for these patients.

4.3.2 Comparison of Different Contributions to Total Delivery Time

In the second part of the analysis, for each plan we attempted to estimate the three distinct contributions to the mean delivery time per field: the energy-changing time, the spots-changing time, and the beam-on time. In this phase, however, we aimed to obtain more generalized results by disregarding the impact of patching. To achieve this, we estimated the total delivery time from steering files by subtracting the contributions attributed to patching, as if patching had not been implemented. It is important to note that the calculated values for the beam on time and spots changing time are not entirely precise but rather approximations, as they were derived based on an estimation of the spots changing time per spot. Nonetheless, these approximations can still be useful in visualising the time reduction for each contribution.

Figure 4.13 shows the mean delivery times per field for clinical, Fixed Grid and Air plans for each patient. In the plot, the different contributions due to the energy-changing time, the spots-changing time and the beam-on time can be visualized. Numerical values of the mean delivery times and single contributions per field are reported in Table A.2 for each patient. If we look at time contributions individually, we can see that the beam on time is quite similar between the three different plans (clinical, Fixed Grid and Air) for the same patient. Indeed, the dose delivered is the same, i.e., 2 GyRBE per fraction. By looking instead at the dead time, which is given by the sum of the spots-changing time and the energy-changing time, we notice that the dead time for Fixed Grid and Air plans highly decreased with respect to Clinical plans thanks to the RF.

Tables 4.5 and 4.6 report the reduction of contributions for Fixed Grid and Air plans with respect to clinical plans. In Table 4.5, the combined sum of the beam-on time and spots-changing time is highlighted, while Table 4.6 focuses on the contribution of energy-changing time. We decided to solely present the combined sum of these two contributions and refrain from providing separate estimations for beam-on time and spot-changing time. Again, this choice is due to the fact that steering files offer accurate measurements specifically for this combined sum. Considering only the plans of patients deemed acceptable, we see that for Fixed Grid plans, the combined sum of the beam on time and spots changing time is reduced on average by 30% (10% - 53%) with respect to clinical plans, while for Air plans the reduction is 27% (range 7% - 48%).

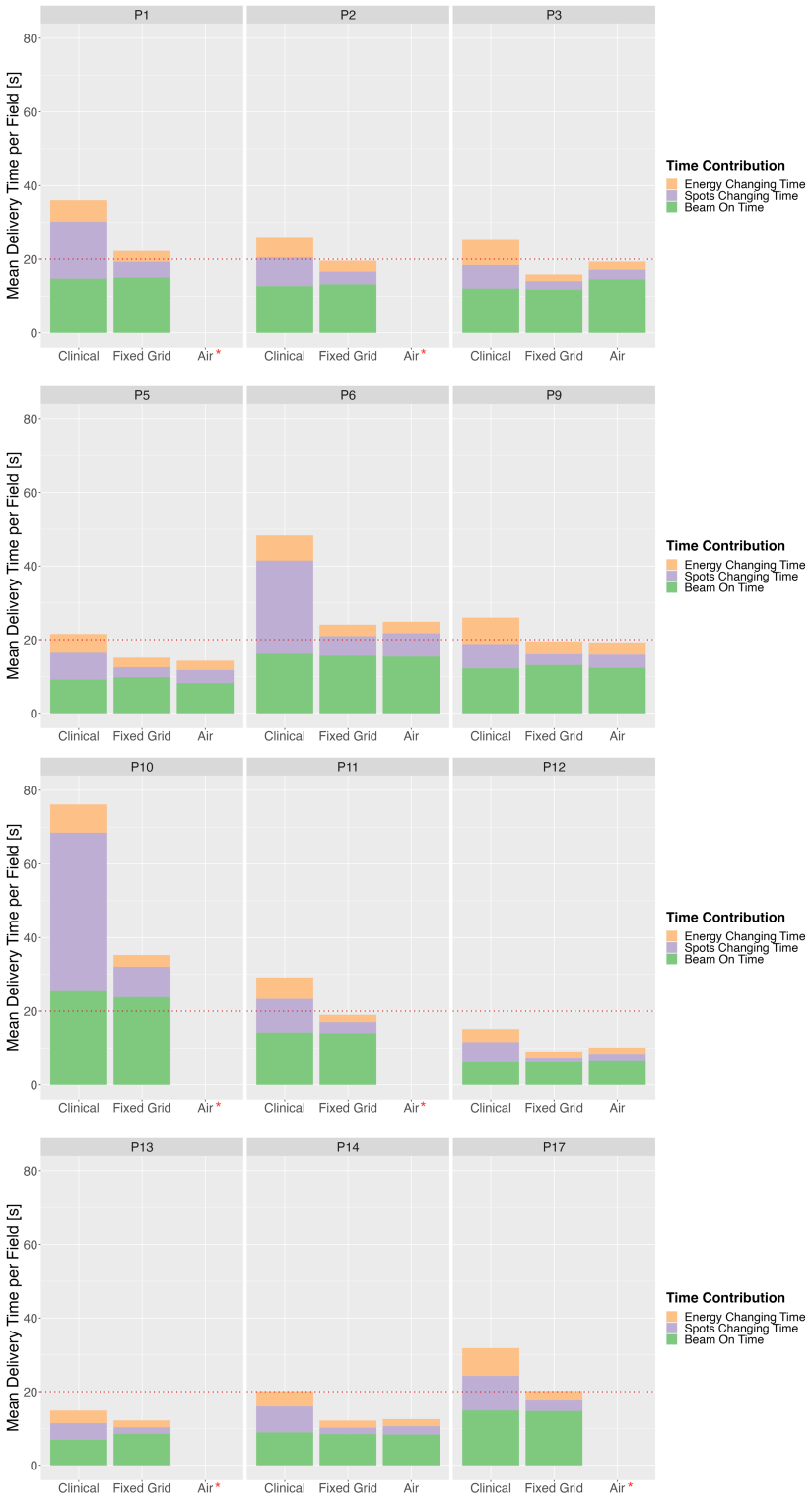

FIGURE 4.13: Comparison of estimated delivery times between clinical plans and Fixed Grid and Air configuration plans for each patient. Rough estimates of each contribution to the mean delivery time are shown in different colours. Air plans labelled in red indicate that they were not clinically acceptable and were thus removed from the analysis.

By comparing only the two configurations with the RF, instead, Fixed Grid plans have a mean beam on time and spots changing the time on average 6% lower than Air plans. The comparison of delivery times reduction has been made only for Patient 3, Patient 5, Patient 6, Patient 9, Patient 12 and Patient 14 as for other patients Air plans were not acceptable.

	P1	**P2**	**P3**	**P5**	**P6**	**P9**
Fixed Grid	36%	19%	24%	24%	49%	15%
Air	-	-	7%	28%	48%	15%

	P10	**P11**	**P12**	**P13**	**P14**	**P17**
Fixed Grid	53%	27%	36%	10%	36%	26%
Air	-	-	27%	-	34%	-

TABLE 4.5: Reduction [%] of the combined sum of the beam on time and spots changing time for Fixed Grid and Air plans with respect to clinical plans for each patient. Missing values for Air plans were not calculated as they were not clinically acceptable for these patients.

Finally, by looking at results for the energy changing time, the reduction for Fixed Grid plans with respect to clinical ones is on average 56% (range 45% - 73%), while for clinically acceptable Air plans the average reduction is 55% (range 51% - 68%). By comparing only the two configurations with the RF, instead, Fixed Grid plans have a mean energy changing time of an average 3% lower than Air plans.

	P1	**P2**	**P3**	**P5**	**P6**	**P9**
Fixed Grid	50%	47%	73%	50%	55%	51%
Air	-	-	68%	51%	54%	54%

	P10	**P11**	**P12**	**P13**	**P14**	**P17**
Fixed Grid	58%	66%	54%	45%	53%	69%
Air	-	-	52%	-	53%	-

TABLE 4.6: Reduction [%] of the energy changing time for Fixed Grid and Air plans with respect to clinical plans for each patient. Missing values for Air plans were not calculated as they were not clinically acceptable for these patients.

4.3.3 Estimated Delivery Times for Plans with Increased Energy Step Factor (ESF)

The delivery times analyzed earlier were referred to plans created with an ESF = 3. In this section, we analyze the delivery times for Fixed Grid plans made with an ESF = 5 for Patient 1, Patient 6 and Patient 10 and compare results with respect to clinical plans and Fixed Grid plans with ESF = 3. The delivery times per patch are reported in Table 4.7. The results reveal that, for these patients, using the Fixed Grid configuration with an ESF = 5 reduces the delivery time per patch on average by 7% with respect to using an ESF = 3. The most significant reduction was observed for Patient 10, who had the largest tumor volume, with a maximum reduction of the delivery time per patch of 2 seconds. On average, the time reduction between clinical plans and Fixed Grid plans with ESF = 3 for these patients is 48%, while the reduction between clinical plans and Fixed Grid plans with ESF = 5 is 52%.

Patient	**Plan**	**Delivery Time per Patch**					
		Field 0 [s]		***Field 1 [s]***		***Field 2 [s]***	
P1	Clinical	16.28	23.00	18.61	22.35	21.25	24.99
	Fixed Grid (ESF = 3)	10.89	14.64	11.76	12.91	10.81	13.21
	Fixed Grid (ESF = 5)	10.66	14.34	11.57	12.83	10.69	12.06
P6	Clinical	33.65	25.56	24.13	27.82	24.72	27.35
	Fixed Grid (ESF = 3)	15.51	11.94	12.88	15.30	12.42	14.55
	Fixed Grid (ESF = 5)	13.72	10.44	11.63	13.91	11.14	13.18
P10	Clinical	52.38	35.33	51.00	37.98	40.05	41.60
	Fixed Grid (ESF = 3)	22.44	16.04	22.30	17.32	20.80	20.00
	Fixed Grid (ESF = 5)	20.19	14.49	21.15	15.44	18.79	18.33

TABLE 4.7: Comparison of the estimated delivery times per patch for Clinical plans and Fixed Grid with ESF = 3 and ESF = 5. Reported values per field indicate the delivery times per patch for that field.

The comparison of the contributions to the mean delivery time per field between clinical plans, Fixed Grid configuration plans (with ESF = 3) and Fixed Grid plans with ESF = 5 is shown in Figure 4.14. Also in this case, each single contribution to the mean delivery time has been calculated following the same steps described earlier, and it has to be considered an approximation. As we can roughly see from the plots, the further

reduction of the number of energy layers and the number of spots did not decrease much the overall mean delivery time per field. Estimated values for each contribution for the three plans are reported in Table A.3.

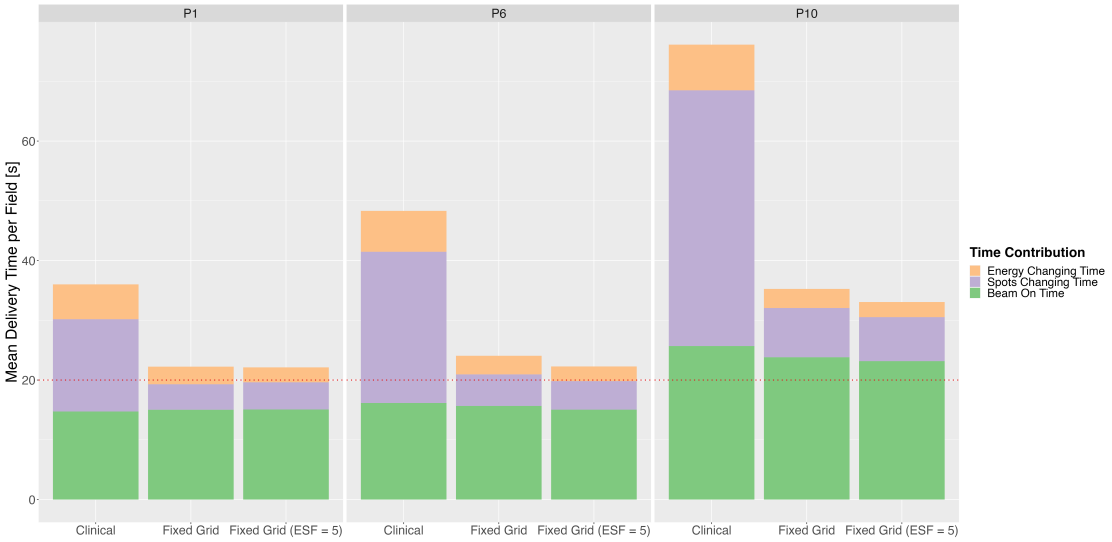

FIGURE 4.14: Comparison of the mean delivery time per field between clinical plans, Fixed Grid configuration plans (with ESF = 3) and Fixed Grid plans with ESF = 5 for Patient 1, Patient 6 and Patient 10.

Chapter 5

Discussion

The novelty of this study lies in the combination of the use of the RF with different spot positioning techniques to reduce the treatment delivery time. Indeed, many studies have been carried out to investigate the behaviour of the RF for PBS for spots reduction in order to decrease the total treatment delivery time (Maradia et al. [32], Fujitaka et al. [34], Wang et al. [35]), and many more focused on the performances of plans using different spot placement techniques (Rehman et al. [29], N. Bizzocchi [31]). However, to our knowledge, the idea of combining these two setups has never been investigated before.

This chapter focuses on the two main analyses made in this study: the comparison between plans made by using the Ridge filter and the three different spot positioning techniques, and the calculation of mean delivery times for clinically acceptable plans created with these setups, comparing them to plans created using the conventional PSI setup. We will investigate the implications of our results, examining their significance within the context of the research topic. Furthermore, we will address any limitations or challenges encountered during the study, acknowledging their potential impact on the validity and generalizability of these findings.

5.1 Plans' Comparison Between the Fixed Grid, Air and Water Configurations

The first part of our work focused on the comparison of the performances between plans created by combining the use of the RF with three different spot positioning algorithms: spot positioning on a fixed grid (Fixed Grid configuration) and energy-dependent spot positioning based on beam's size in air at the isocenter (Air configuration) and in water at the Bragg peak (Water configuration). The spot positioning algorithms we used are the same investigated by N. Bizzocchi in his work [31], as they were developed at PSI. In our case, however, plans were created using the RF as well.

5.1.1 Target Coverage and Spots Positioning

For each patient, we compared the DVHs of the three different configurations. If we look at Figures 4.3 and 4.4, a clear observation emerges: plans made with the Water configuration exhibit significantly higher dose delivery to both the CTV and PTV compared to the Fixed Grid and Air plans. This trend is consistent across all patients involved in the study. The underlying cause for this disparity can be attributed to the initial target coverage of Water plans prior to dose normalization. Indeed, the target coverage in Water plans was initially quite low, in the range approximately of 60% to 80%, leading to a subsequent dose shift after the normalization process. As a result, the target ended up being overdosed (see Figure 4.6), exacerbating the disparity in dose delivery between the different plan configurations. The same observation can be made also for Air plans for Patient 2, Patient 10, Patient 11 and Patient 17, even if less pronounced with respect to Water plans. Indeed, also for these plans, the initial target coverage was quite below the prescribed value.

The reason for the low target coverage for these plans can be attributed to how the TPS places spots when defining fields with the different spot positioning algorithms. As previously mentioned, in the Fixed Grid configuration the distance between spots remains unchanged at different depths, while for the Air and Water configurations, the distance between spots depends on the beam's energy. A general comparison between the three configurations of the arrangement of spots inside the target volume for different energy layers without the RF can be seen in Figure 3.9. The same trend of spot distance

is obtained also when using the RF. It is important to note that without the RF, spots are placed on each energy layer, with energy layers separated by 2.5 mm. However, when utilizing the RF, the Bragg peak broadening increases as it passes through. For this reason, placing spots on each energy layer would not be optimal, and our plans have been created by providing the TPS with an energy step factor equal to 3 meaning that energy layers (and consequently spots) are spaced 3 $\times$ 2.5 mm in the field's direction. However, if we look at the spots arrangement for the Air and Water plans when using the RF, several more energy layers were skipped by the TPS when placing spots in the whole target. This is evident from Figure 5.1.

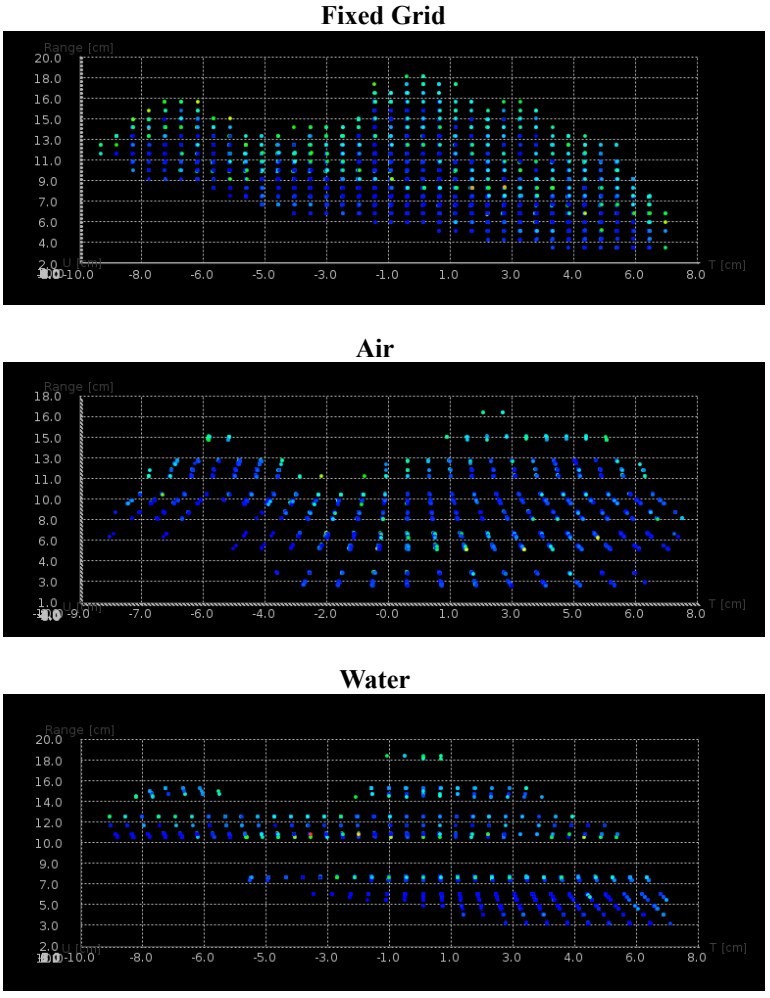

FIGURE 5.1: Visual representation of the spot positioning for different energy layers performed by FIonA for the three different configurations when the RF is applied for Patient 1. On the horizontal axis (T [cm] and U [cm]) the plans perpendicular to the direction of the field are reported, while on the vertical axis (Range [cm]) the depth inside the patient is reported.

One possible explanation for this behaviour could be related to the way the TPS assigns initial weights to the spots during the definition of fields. These initial weights will then be refined through the optimization process. If certain spots receive low initial weights, the TPS may automatically remove them, or even eliminate the entire energy layer, as it considers them ineffective or unnecessary. This can also occur if the number of spots within an energy layer is too low. Remarkably, an interesting observation can be made for Air and Water configurations: the energy layers skipped by the TPS were consistently at approximately the same depths within each patient for all Air plans, and similarly for all Water plans. As we can notice from Figure 5.1, the overall number of energy layers used by the Water configuration plan is much lower when compared to the other two configurations. Moreover, these skipped layers correspond to the depth at which the beam size reaches its minimum, resulting in spots being positioned in the closest proximity possible. Consequently, these layers contain a higher density of spots, and the TPS assigns lower weights to them. Eventually, the TPS might have decided to remove these layers, as they were considered less influential in achieving the desired treatment objectives. However, the underlying reasons for this particular behaviour of the TPS when placing spots based on the beam's size in air and water when utilizing the RF (and thus an increased ESF) still remain unclear and need further investigation.

5.1.2 Organs at Risk Sparing

Upon closer examination of the DVHs for organs at risk in Figures 4.3 and 4.4, no consistent trend is observed across all patients regarding a configuration that consistently delivers a higher dose to the OARs compared to the other configurations. Nevertheless, within each specific patient, there is always a particular configuration that delivers more dose to the OARs in comparison to the other two. This behaviour can be attributed to the spot margins set by the TPS and the position of the tumor inside the patient with respect to organs at risk. In the process of spot placement, the TPS not only positions spots within the target volume but also outside the target within a predefined margin, which can be manually set. This margin is essential to make sure that the target volume is completely covered. When utilizing a spot positioning algorithm based on a fixed grid, the margin set is constant across all energy layers since the spots are placed at a fixed distance. However, this margin varies depending on the energy used (and thus the depth inside the patient) for spot placement based on the beam's size in air and in

water. For spot positioning based on beam's size in air, at lower energies, the margins are larger, while at higher energies, the margins are smaller. For spot positioning based on beam's size in water, instead, at lower energies, the margins are larger, they reach a minimum width at intermediate energies and then increase again. Consequently, if an OAR is located in close proximity to the target, the dose delivered to that OAR will be influenced by its depth within the patient. Plans with larger margins at that particular depth will result in a higher dose being delivered to the close organs. However, additionally to that, also the direction of treatment fields significantly impacts the dose delivered to the OARs. All these factors come together to explain the different values obtained when checking prescriptions on organs (see Section A.1).

To gain a more comprehensive understanding of how the position of organs relative to the tumor influences the delivered dose, a 3-dimensional representation of them can be seen in Figure 5.2. For instance, when considering prescriptions on the esophagus (Figure A.1), it is apparent that the highest mean dose to this organ was delivered to Patient 2, Patient 5, Patient 9, Patient 10, Patient 11, Patient 14, and Patient 17. Indeed, the tumor grew near or around the esophagus in these specific patients, resulting in a higher mean dose delivered to the organ compared to patients where the tumor is located further away from the esophagus. Another argument could be made for the maximum dose delivered to the spinal cord. If we look at the prescriptions for the maximum dose delivered to this organ (see Figure A.2), we notice that Patient 1, Patient 3, Patient 9 and Patient 10 receive the highest dose. This outcome primarily results from the orientation of the treatment fields rather than the proximity of the tumor to the spinal cord. In fact, by referring to Figure 3.2, it is apparent that the fields' directions overlap with the spinal cord, leading to a higher dose being delivered to this organ, even if the tumor is not in close proximity (see Figures 5.2 and 5.2). In the case of the lungs, the mean dose delivered is influenced not only by the tumor's position and the orientation of the treatment fields but also by the size of the tumor, since we are considering tumors located inside this organ. Indeed, if we consider for example Patient 10, which has the largest tumor volume, the combination of these three factors leads to a significantly higher delivered dose compared to other patients. On the other hand, Patient 12, Patient 13, and Patient 14 received the lowest mean dose to their lungs. This is primarily due to the small size of their tumors, which subsequently leads to a lower dose being delivered to the organ. Moreover, in these patients, the tumor is not located inside the lungs but

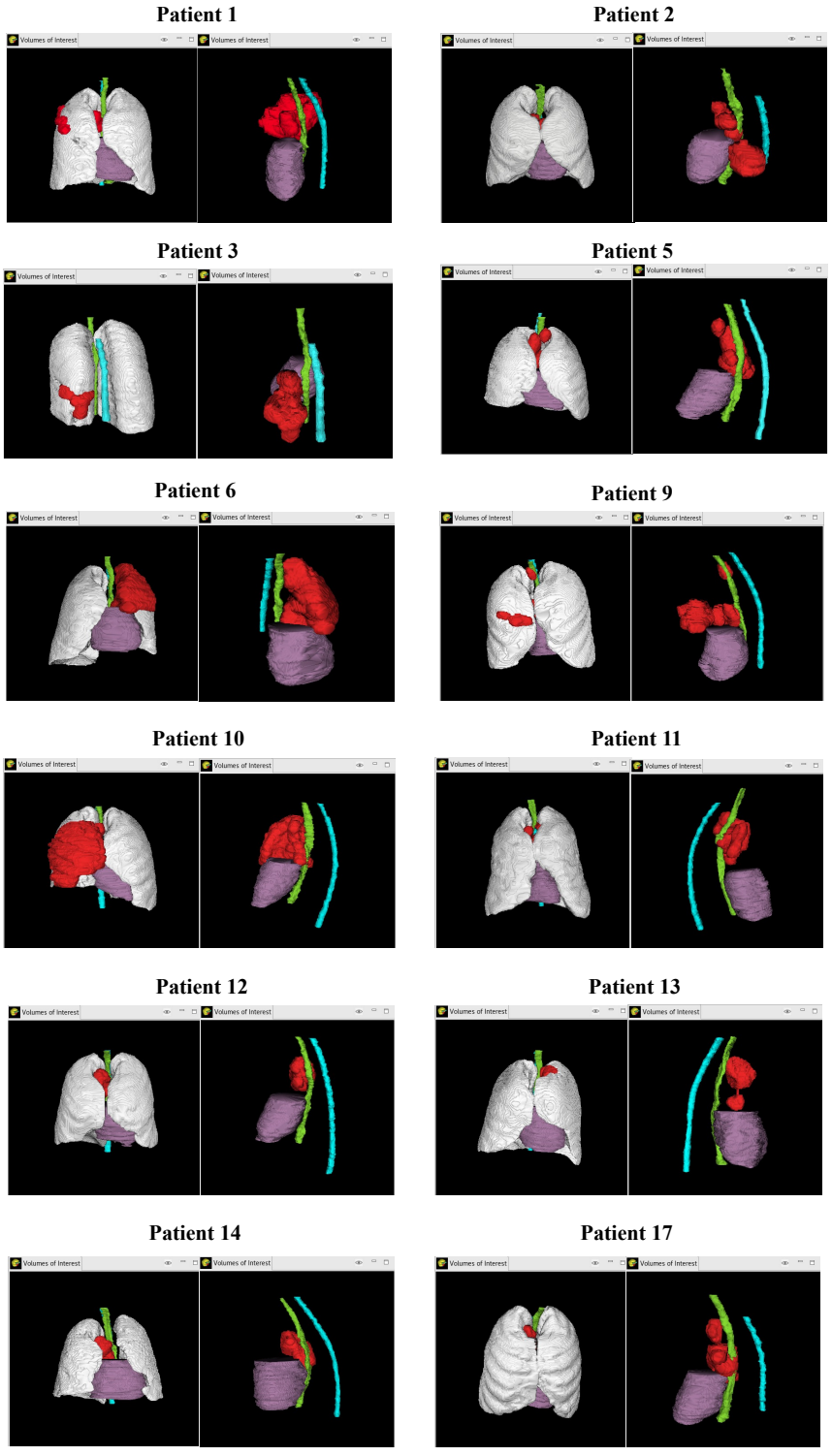

FIGURE 5.2: 3D representation of the position of the tumor volume with respect to the organs at risk for our cohort of patients. Images were created by PSI's treatment planning system FIonA. The target volume (PTV) is shown in red. Organs at risk are colored as follows: heart in purple, esophagus in green, spinal cord in blue and lungs in white.

it grew around the esophagus. Further, when the treatment fields are directed in such a way that the angles between them are wider, the dose administered to the organ will increase. This is because a larger area will be irradiated, resulting in a higher dose being delivered to the lungs, as can be seen in Patient 2, Patient 9, Patient 10 and Patient 17. For the heart, finally, the highest dose is delivered to Patient 2, Patient 6, Patient 10 and Patient 17. The main reason related to these outcomes can be attributed to the directions of fields. For these patients, the tumor is located near the heart, and the treatment fields are directed towards it. This results in the distal penumbra playing a significant role in increasing the dose to the organ. Nevertheless, it is important to note that in general, the dose to the heart remains well below the threshold prescriptions since the tumors are situated away from the heart rather than directly in close proximity or around it.

5.1.3 Comparison of the Number of Spots

This next section aims at comparing the differences in terms of the number of spots for the three different configurations used to design plans. It has to be reminded that all plans have been created using a fixed margin for the Fixed Grid configuration plans, while for the Air and Water the margin was energy dependent.

Plans for Patient 1, Patient 3, Patient 6, Patient 9, Patient 10, Patient 13, and Patient 14 were created with a SMF that resulted in a comparable margin width to the one used for the Fixed Grid configurations at 150 MeV. This decision was made because 150 MeV represented the mean energy value in our range, and we would expect similar margins on average compared to the Fixed Grid plans. Indeed, for these patients, the overall margin widths were quite similar among the three configurations. When considering the total number of spots in these plans, we observed a consistent trend for each patient across the different configurations (see Figure 4.8). The Fixed Grid plans consistently exhibited the highest number of spots, while the Water configurations consistently had the lowest number. This behaviour is clear if we look at Figure 3.8: indeed, while at intermediate energies the spots distance using the spots positioning based on the beam's size in water is similar to the spots distance used with the spot positioning on a fixed grid, for lower and higher energies the distance increases, due to the different interactions of the beam inside water. Indeed, at low energies, the beam's size is the

same the beam's size in air, while at higher energies the scattering contribution becomes relevant and the beam's size increases. These results are in accordance with what has been found by N. Bizzocchi [31]. Also in his work, the total number of spots in plans created using spot positioning based on the beam's size in water was significantly lower compared to plans where spots were placed using a fixed grid approach. However, in [31] the difference in terms of the number of spots between the plans with the different algorithms was greater compared to our results. Indeed, in his work, the spots reduction of plans using the spot placement in water was found to be on average greater than 50% with respect to plans which used spots placement on a fixed grid, while in our case the reduction between these two configurations was only approximately 19% on average. This is probably due to the presence of the RF, which already greatly reduces the number of spots, and a further reduction would not be optimal for the plans designed to reach the required target coverage. Additionally to that, the lower number of spots for Water plans with respect to Fixed Grid plans can also be attributed to the TPS selectively excluding specific energy layers for these plans, as previously mentioned. However, it is worth noting that for Patient 3 and Patient 10, the number of spots of the Water plans exceeded that of the other two configurations. This discrepancy can be attributed to the spots arrangement created by the TPS for these two plans. Upon examining the 3-dimensional distribution of spots, we found that the margins set by the TPS were actually larger than the ones we would have expected. This discrepancy can likely be attributed to the TPS's decision to employ larger spot margins in order to enhance the coverage of the target. Moreover, for these plans the TPS tried to place spots outside the target to reach the required coverage, due to the lack of a high number of energy layers. This behaviour might arise when the TPS has an excessive number of constraints and a limited number of degrees of freedom. Consequently, the system may prioritize certain factors while disregarding others, leading to the placement of spots outside the target volume. However, if we exclude these two plans, the overall trend observed is evident.

If we consider instead Patient 2, Patient 5, Patient 11, Patient 12 and Patient 17, we have to remember that Air plans for these patients were created by increasing the SMF. This has been made to increase the target coverage of these plans, as the choice of an SMF like for other plans lead to low values of CTV V95%. As a result, the overall number of spots for these Air plans increased as well. For Patient 2, Patient 5, Patient

12 and Patient 14, the number of spots was even higher than for Fixed Grid plans, while for Patient 11 and Patient 17, the number of spots was still lower than the number of spots for the Fixed Grid configuration. Nevertheless, it is worth mentioning that also for these patients the Water configuration plans consistently exhibited the lowest number of spots, aligning with the findings reported by N. Bizzocchi [31].

5.1.4 Robustness Evaluation

As previously mentioned, plans have been optimized using a hybrid robustness optimization, for which plans were optimized against range uncertainties. However, robustness for geometrical shifts had to be evaluated as well. This analysis has been performed only for plans created for the Fixed Grid and Air configurations, as from a preliminary analysis, Water configuration plans have been excluded since they resulted in a high overdose to the target volume. All Fixed Grid plans successfully met the robustness constraint, except for Patient 2, Patient 5, and Patient 17 (as illustrated in Figure 4.9). However, most of the Air plans did not demonstrate robustness against geometrical shifts. This discrepancy can be attributed to the correlation between plans' margins and the energies used to reach the tumor inside the patient. Generally, larger margins lead to more robust plans by ensuring greater target coverage. Nevertheless, for Air plans, as energy increases, margins decrease due to the smaller distance between spots. Consequently, plans that aim at treating tumors at greater depths (thus using higher energies) become less robust against geometrical shifts. This is evident when examining Patient 5, Patient 9, Patient 10, Patient 11, Patient 13, and Patient 17, whose Air plans exhibit the lowest D95% values for the CTV in the worst-case scenario. However, it is important to note that the direction of the fields also plays a role in plans' robustness, as fields coming from below are more robust compared to fields coming from the sides of the body. This factor could be relevant in the case of Patient 11, Patient 13 and Patient 17.

5.2 Delivery Time Analysis

In the second phase of this work, our focus shifted towards calculating the delivery time (per field or per patch) for each treatment plan that was considered clinically acceptable. The purpose was to evaluate the feasibility of utilizing the breath-hold

technique in PSI's Gantry 2 with these plans and calculate the time reduction that results from using these configurations with respect to plans that are currently used at the PSI's CPT. Additionally to that, we aimed at investigating the relative impact of the three components (beam-on time, spots-changing time, and energy-changing time) that contribute to the total delivery time.

5.2.1 Delivery Times of Plans

As previously stated, when treating larger tumors with PSI's Gantry 2, the small size of the nozzle window necessitates the use of the patching technique. This procedure requires longer treatment delivery times per field, primarily due to the need for moving the table between one patch and the next one to align the volume with the nozzle, while the gantry is kept in a fixed position. Thus, delivering an entire field dose within one single breath-hold would be very challenging for a patient, as the total delivery time would be high. For this reason, if we would like to implement the breath-hold technique in Gantry 2 for the treatment of large tumors which require patching, one possibility would be to apply one breath-hold per patch.

Our patient cohort exhibited a diverse range of tumor volumes, spanning from very small volumes (e.g., Patient 12, Patient 13, and Patient 14) to larger ones (e.g., Patient 1, Patient 6, and Patient 10) (see Table 3.1). The division of the target volume into one or two patches is determined by the steering files generator (SFGen), depending on the extent of spots distribution. The use of different spots positioning algorithms, however, results in different spot extents, primarily due to the disparities in spot margins set by the TPS during spot placement. Consequently, within the same patient, certain configurations might necessitate the division of target into patches, while others do not. This behaviour is evident in Fixed Grid plans for Patient 2 and Patient 9, as well as in Air plans for Patient 3 and Patient 9. In these cases, clinical plans for certain fields did not require the division of the target into two patches. Furthermore, as indicated in Table 4.4, it is evident that not all fields for each plan necessitated the division of the target volume into patches. This discrepancy mainly depends on the tumor's extension within the direction of the field. In principle, to avoid patching, one could consider selecting field directions in a way that, if possible, the tumor's size along that specific

direction does not require patching. However, opting for such field directions may not achieve the desired target coverage or, worse, damage organs at risk.

To measure the delivery times for each plan, we conducted our analysis by distinguishing patients with tumors that did not require patching from those with tumors that did. Initially, we estimated the delivery time from steering files specifically for patients without patching (Patient 5, Patient 12, Patient 13, and Patient 14) and compared these estimates with the measured times obtained from Log files, which are created when performing measurements in Gantry 2. The main purpose of this procedure was to ensure that the estimated delivery times and the actual delivery times did not differ significantly. Additionally, it allowed us to rely solely on the steering files to obtain accurate estimates of delivery times per patch for other patients, as the calculation of the delivery times for patched volumes from Log files presented challenges. From Figure 4.12 and Table 4.3, we notice that while for Fixed Grid and Air plans the estimated and measured times are very similar, for clinical plans the difference is significantly higher. This is related to both the energy changing time and the sum of the beam-on and spots-changing time, which steering files under-estimate. The main factor contributing to the disparity between the measured and estimated delivery times is the presence of systematic errors in the estimation of the energy-changing time per layer and spots changing time per spot, which are present in all plans. However, in the case of clinical plans, which typically involve a significantly larger number of spots and energy layers compared to the other two configurations, the errors accumulate for each layer and, as a result, the total error becomes more pronounced and evident. Considering our focus on the delivery times for the Fixed Grid and Air plans, however, we find these results satisfactory, as the difference between the measured and estimated delivery times for our configurations is negligible, with a difference of less than one second.

By looking at Tables 4.3 and 4.4, we can notice that the use of the Fixed Grid or Air configurations significantly reduced the delivery time per field and per patch in comparison to plans created with clinical settings. Specifically, for all Fixed Grid and Air plans, the delivery times remain below the 20 seconds threshold, with the exception of Patient 10, where the delivery times slightly exceed 20 seconds due to the larger tumor size. In contrast, the delivery times for clinical plans are above the set timing threshold. However, it is worth noting that currently, at the PSI's clinics breath-hold is not performed and reported values for clinical plans do not represent delivery times

for current procedures. Indeed, the only motion mitigation techniques employed in the clinics during proton therapy treatments are rescanning and gating. These techniques enable patients to breathe freely while receiving the treatment, with the dose being delivered generally twice with half of the intensity during predetermined phases of the breathing cycle. This procedure significantly increases the overall treatment duration, with field durations typically lasting a few minutes depending on the size of the tumor, compromising the comfort of the patient during the treatment. At PSI, only two cases of lung tumors have been treated so far using a combination of gating and rescanning techniques. For one of these cases, the target volume was divided into three separate PTVs to optimize coverage and enhance treatment effectiveness. The volumes of these PTVs were 650 cc, 380 cc, and 703 cc, respectively, with each PTV divided into two patches. By using the steering files, we were able to calculate the delivery times per patch per field for each of these targets. The dose delivery per patch varied from 35 seconds to 50 seconds. However, it's important to consider that the total dose was not delivered continuously; it involved pauses due to gating, and the dose had to be rescanned twice. As a result, the total duration of treatment delivery per field extended to few minutes. By implementing a breath-hold technique, the treatment duration would significantly decrease since the dose would be administered only once at full intensity.

Finally, we created additional Fixed Grid plans for Patient 1, Patient 6, and Patient 10, who had the largest tumor volumes. These plans used an energy step factor of 5 in order to further minimize the energy changing time and the spots changing time. However, by looking at Table 4.7, we observed that the delivery times per patch for the Fixed Grid plans with an ESF = 5 did not decrease significantly. The reduction was at most 2 seconds per patch for Patient 6 and Patient 10, who had the largest tumor volumes, while for Patient 1 the reduction was less than 1 second. This lack of significant improvement can be attributed to the fact that, as shown in Figure 4.14, the primary factor contributing to the total delivery time is now the beam-on time, and skipping few more energy layers or spots doesn't lead to a significant further reduction.

5.2.2 Comparison of Different Contributions to Total Delivery Time

As the last step of our work, we estimated the delivery times of the three contributions to time for all clinically acceptable plans. When calculating the times from steering

files, we removed the contributions for patching, and obtained timing values for mean delivery times per field and for each contribution as if patching is not applied. We made this decision mainly because we wanted to generalize our work also to other gantries and see which of the three contributions to time contributes more to the total delivery time. However, it is important to note once again that the estimations of the beam-on time and spots-changing time reported in Table A.2 and visualized in Figure 4.13 are not highly accurate, as the steering files provide more precise measurements for the combination of the two. Nonetheless, our intention was to present general findings and highlight the extent to which these factors contribute to the overall time, as well as the reduction achieved by implementing RF technology and employing different spot placement algorithms.

By looking at Figure 4.13, it is possible to notice that the beam-on time remains constant across all plans since the total dose delivered is consistent at 2 GyRBE per fraction. To be more precise, the beam-on time for plans created using the RF should be slightly lower compared to plans that do not employ the RF. This discrepancy arises from the fact that when using the RF, higher energies are utilized, which have an higher transmission and consequently a slightly lower beam-on time. The primary factor contributing to the overall delivery time for clinical plans in the majority of cases is the dead time, which accounts for both the energy-changing time and the spots-changing time. On the other hand, for Fixed Grid plans and Air plans, the beam-on time plays a more significant role in the overall delivery time, as the use of the RF and different spot positioning algorithms has significantly reduced the dead time.

The estimated delivery times obtained in our study are based on the characteristic times of Gantry 2. However, these results may vary for other facilities, as each facility has its own unique timing values. In principle, they could potentially utilize our findings as a reference to estimate their specific delivery times using the characteristic times of their gantries. Nevertheless, it is worth mentioning that certain factors might cause slight variations in the results. For instance, while Gantry 2 exhibits a relatively short energy-changing time of approximately 150 ms, other facilities could have different timings. Indeed, for cyclotron-based facilities, the energy-changing time ranges from 80 to 900 ms. However, for most synchrotron-based facilities, it is even slower ranging from 200 to 2000 ms [33]. Furthermore, also the spots-changing time or the technique used to scan the beam within the target might differ from facility to facility. Indeed, an alternative

approach that could be adopted is the raster scanning technique, which differs from spot scanning by continuously scanning the beam along the target instead of moving it spot by spot. This technique has been shown to significantly reduce delivery time. In a study conducted by Sun et al. [50], a comparison was made between the raster scanning and spot scanning methods. The results demonstrated a substantial reduction in the total delivery time when employing the raster scanning method. Specifically, a reduction of 53% was observed when irradiating a cubical target, and a reduction of 29% was observed in a pelvic case. However, it is important to note that in order to achieve these shortened delivery times with the raster scanning method, a sophisticated dose control strategy is necessary to ensure accurate dose distribution.

Chapter 6

Conclusions and Outlook

6.1 Conclusions

The purpose of this thesis was to evaluate the advantages and limitations of employing a Ridge filter in combination with different spot placement techniques and to investigate the feasibility of delivering a complete field dose within a single breath-hold. To do that, we tried to answer two main questions: What is the optimal configuration in terms of clinical acceptance and time reduction when comparing the Ridge filter in combination with various spot placement algorithms? Is it possible to reach a mean treatment delivery time per field or per patch < 20 seconds in PSI's Gantry 2?

In the first part of our analysis, the three different configurations, named Fixed Grid, Air, and Water configurations, were evaluated based on their performance in meeting clinical acceptability criteria for treatment plans. The Fixed Grid configuration demonstrated the highest level of clinical acceptability, as plans for all the 12 patients from our cohort satisfied the medical prescriptions and were robust according to our constraints. However, this configuration resulted in the highest number of spots being placed by the TPS. In contrast, the Air configuration showed mixed results, with half of the plans considered clinically acceptable and the remaining either lacking robustness, not satisfying prescriptions or both. The variability in acceptability can be attributed to factors such as the tumor's proximity to critical organs and the TPS's spot placement strategy, which employed variable margins depending on the beam energy. The Water configuration, instead, did not yield any acceptable plans. The initial target coverage was

insufficient, in the range of 60-80%, resulting in high overdosing of both the target and nearby organs at risk after dose normalization. This inadequacy in target coverage can be traced back to issues with the TPS, including problematic spot placement and the removal of too many energy layers, leaving the TPS with limited degrees of freedom during optimization. However, the underlying reasons that lead the TPS to act in this way would need deeper investigation. To summarize, the most favourable configuration in terms of clinical acceptance is achieved by combining the Ridge filter with the spot placement algorithm based on a fixed grid. Nevertheless, it is important to acknowledge that the choice to use the Fixed Grid configuration involves a tradeoff. This approach is considered conservative, as it employs a traditional spot placement algorithm that places the highest number of spots, which is currently used in the clinics at PSI. However, it is also the most effective approach.

The second part of this study revealed that combining the RF technique with different spot positioning algorithms significantly reduced the dead time (spots-changing time and energy-changing time) compared to the clinical setups currently used at PSI's CPT, with the beam-on time contributing the most to the total delivery time for our configurations. Regarding the feasibility of performing breath-hold in PSI's Gantry 2, results showed that, among the clinically acceptable plans we selected for timing analysis, i.e. plans that satisfied clinical prescriptions and robustness constraints, all plans had delivery times (per field or per patch) below 20 seconds. Thus, delivering an entire field dose within one single breath-hold would be feasible for small tumors (approximately smaller than 100-150 cc) while for more extended tumor volumes where the patching technique is utilized, it would be feasible to perform one breath-hold per patch. Nevertheless, to do that, it is crucial to evaluate plans' robustness to ensure consistency in the delivered dose across different breath-holds. Finally, based on our results, other facilities could potentially derive delivery times and determine time reductions specific to their own facilities by considering the characteristic timings of their equipment. Additionally, since the majority of other facilities, unlike Gantry 2, do not utilize patching, it would be interesting to explore the feasibility of performing breath-hold within an entire field dose for larger tumors.

In conclusion, our findings demonstrate that the optimal setup, considering both clinical acceptance and time reduction, involves combining the Ridge filter with the spot positioning algorithm based on the fixed grid, and that with this configuration it is possible

to achieve average delivery times per field or per patch of less than 20 seconds enabling breath-hold techniques with PSI's Gantry 2.

6.2 Outlook

The combination of the Ridge filter with various spot positioning algorithms has yielded promising results for using the breath-hold technique. Notably, for PSI's Gantry 2, treatment plans with delivery times per field (or per patch, depending on the extension of the tumor's volume) below 20 seconds were achieved, making it feasible for a delivery within a breath-hold. The implementation of these configurations significantly reduced the dead time contribution (spots-changing time and energy-changing time) to the delivery time, with the beam-on time being the only contribution left on which we could act. A possible way to further reduce the delivery time would be to decrease the contribution due to the beam-on time by using high-intensity beams. This is currently being investigated for Gantry 2 at PSI: Maradia et al. [51] demonstrated that by employing alternate beam optics imaging, the beam transmission through PSI's Gantry 2 may be enhanced by 30-40%, thus reducing the beam-on time. Furthermore, to improve our results in terms of both delivery time and target coverage, we could think of employing an alternative approach when reducing the number of selected energy layers when placing spots by utilizing an "intelligent" energy selection system. Currently, we employ a systematic removal of energy layers, retaining one layer every three layers due to the larger size of the Bragg peak. However, by employing an optimization algorithm that accounts for the number of energy layers employed and removes them in an appropriate way, more promising outcomes might be achieved. Finally, future investigations should focus on understanding the main reasons behind the underlying causes of the suboptimal behavior of the treatment planning system when utilizing the spot placement algorithm based on the beam's size in water at the Bragg peak in combination with a larger energy step factor. Understanding and addressing these issues could contribute to improving the performance of the TPS and improving the overall quality of treatment plans.

Appendix A

Appendix

A.1 Prescriptions Fulfillment

Below are reported the values for prescriptions on organs at risk between the three different configurations. The different values between the different patients are due to the position of the organ with respect to the target volume: the closer the organ is to the tumor, the higher the dose that it will receive. Thus, it is not possible to define a general trend for these values.

A.1.1 Esophagus Prescriptions Evaluation

Figure A.1 shows the values of Dmean and V74.00 GyRBE of the esophagus for plans with the three different configurations for all the patients. For medical prescriptions to be satisfied, these values should assume values of Dmean $<$ 34.00 GyRBE and V74.00 GyRBE $<$ 1.0 cc for this organ. As can be seen below, for Dmean all Fixed Grid plans satisfy the requirement. For Air plans, instead, only Patient 17 does not satisfy it, as for Patient 2, Patient 5, Patient 9, Patient 10 and Patient 17 for Water plans. For V74.00 GyRBE, instead, the prescription is satisfied by all Fixed Grid plans, and by 9 of 12 Air plans, with Patient 2, Patient 11 and Patient 17 not meeting the requirement. For Water plans, instead, only 3 of 12 plans satisfy the prescription, which are Patient 3, Patient 6 and Patient 12.

FIGURE A.1: Esophagus prescriptions evaluation: comparison of Dmean values (on the left) and V74.00 GyRBE values (on the right) between the Fixed Grid, Air and Water configurations for each patient. The red dotted line represents the threshold for satisfying the prescription.

A.1.2 Spinal Cord Prescriptions Evaluation

Figure A.2 shows the values of Dmax and V50.00 GyRBE of the spinal cord for plans with the three different configurations for all the patients. For medical prescriptions to be satisfied, these values should assume values of Dmax $<$ 54.00 GyRBE and V50.00 GyRBE $<$ 0.03 cc for this organ. As it can be seen below, for Dmax all plans for all configurations satisfied this requirement, with the exceptions for Water plans for Patient 1 and Patient 9. For V50.00 GyRBE, instead, the prescriptions is satisfied by all plans for all configurations, with the exception of Patient 1 and Patient 9. Indeed, for Patient 1 none of the configurations meets the requirements, with the Fixed Grid and Air plans slightly exceeding the threshold, while for Patient 9 only the Water plan does not satisfy the prescription.

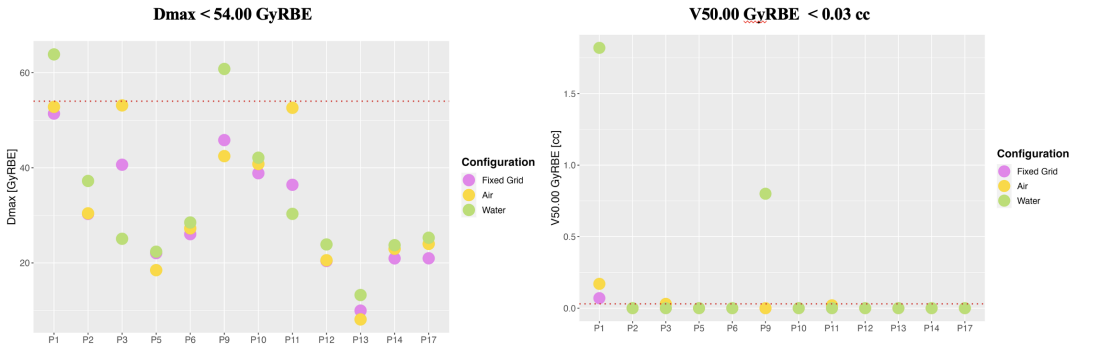

FIGURE A.2: Spinal Cord prescriptions evaluation: comparison of Dmax values (on the left) and V50.00 GyRBE values (on the right) between the Fixed Grid, Air and Water configurations for each patient. The red dotted line represents the threshold for satisfying the prescription.

A.1.3 Lungs Prescriptions Evaluation

Figure A.3 shows the values of Dmean, V5.00 GyRBE and V20.00 GyRBE of the lungs for plans with the three different configurations for all the patients. For medical prescriptions to be satisfied, these values should assume values of Dmean $<$ 20.00 GyRBE, V5.00 GyRBE $<$ 60.00% and V20.00 GyRBE $<$ 37.00% for this organ. As can be seen below, for Dmean all plans for all configurations satisfied this requirement, with the exception of the Water plan for Patient 10. For V5.00 GyRBE, instead, the prescriptions is satisfied by all plans for all configurations. Finally, for V20.00 GyRBE all plans for all configurations satisfied the prescriptions with the exception of the Air plan for Patient 17.

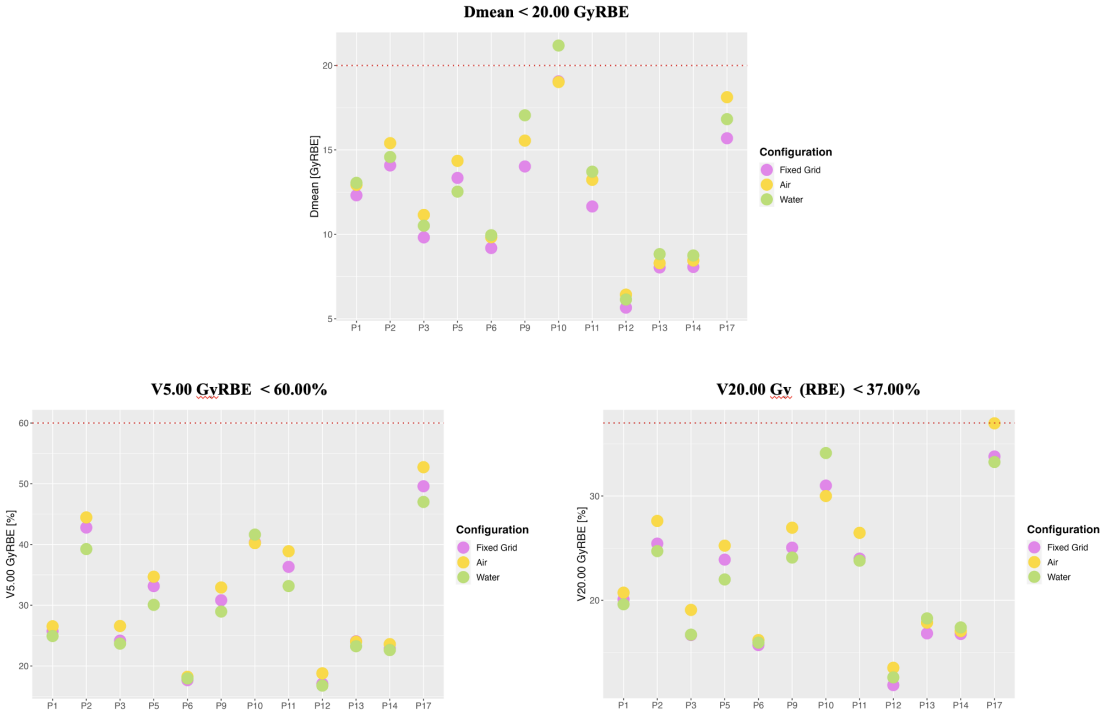

FIGURE A.3: Lungs prescriptions evaluation: comparison of Dmean values (on the top), V5.00 GyRBE values (on the bottom left) and V20.00 GyRBE values (on the bottom right) between the Fixed Grid, Air and Water configurations for each patient. The red dotted line represents the threshold for satisfying the prescription.

A.1.4 Heart Prescriptions Evaluation

Figure A.4 shows the values of V30.00 GyRBE and V45.00 GyRBE of the heart for plans with the three different configurations for all the patients. For medical prescriptions to be satisfied, these values should assume values of V30.00 GyRBE $<$ 50.00% and V45.00

GyRBE < 35.00% for this organ. As can be seen below, both V30.00 GyRBE and V45.00 GyRBE prescriptions were satisfied by all plans for all configurations.

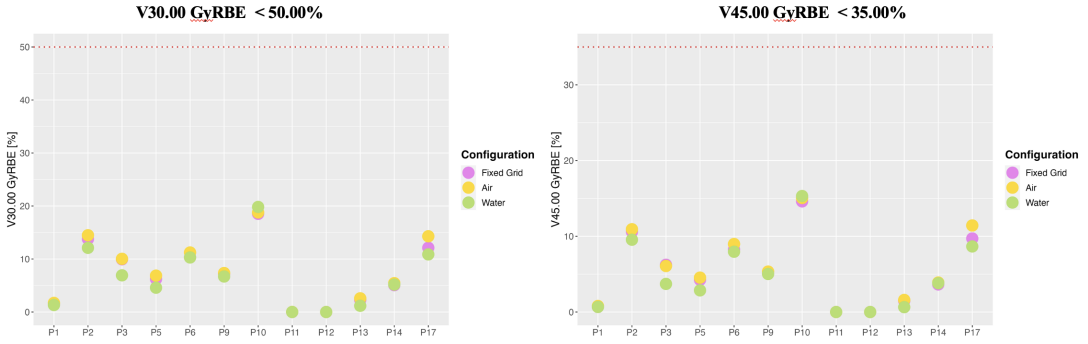

FIGURE A.4: Heart prescriptions evaluation: comparison of V30.00 GyRBE values (on the left) and V45.00 GyRBE values (on the right) between the Fixed Grid, Air and Water configurations for each patient. The red dotted line represents the threshold for satisfying the prescription.

A.2 Measured Delivery Times

Tables A.1 report the values for the combined sum of mean beam on time and spots changing time (upper table) and for the mean energy changing time (lower table) for patients who did not require patching. In each table, measured values obtained from Log files and estimated values obtained from steering files are compared for each configuration and for each patient, showing the time difference between the calculated values. The "difference" column have been calculated by subtracting estimated times from measured times.

A.3 Estimated Contributions to Delivery Times

Table A.2 reports estimated values of contributions to the mean delivery times calculated from steering files for each patient. The mean delivery times for volumes with patching were estimated by removing from steering files the timing contributions due to this procedure. The values reported for the beam on time and the spots changing time separately are a rough approximation, since they were derived by using assumptions on the mean spots changing time/spot measured from Log files. Values for the mean delivery time and the energy changing time, instead, can be considered precise, as the can be directly obtained from steering files.

Patient	**Plan**	**Mean Beam On + Spots Changing Time**		
		Measured [s]	***Estimated [s]***	***Difference [s]***
P5	Clinical	19.80	16.42	3.38
	Fixed Grid	12.97	12.51	0.46
	Air	-	-	-
P12	Clinical	14.14	11.60	2.54
	Fixed Grid	7.58	7.43	0.15
	Air	9.54	8.45	1.10
P13	Clinical	13.37	11.42	1.95
	Fixed Grid	10.36	10.28	0.08
	Air	-	-	-
P14	Clinical	19.10	15.97	3.13
	Fixed Grid	10.32	10.21	0.11
	Air	10.76	10.61	0.16

Patient	**Plan**	**Mean Energy Changing Time**		
		Measured [s]	***Estimated [s]***	***Difference [s]***
P5	Clinical	6.11	5.11	0.99
	Fixed Grid	2.90	2.58	0.32
	Air	-	-	-
P12	Clinical	4.81	3.52	1.29
	Fixed Grid	1.87	1.63	0.24
	Air	1.88	1.70	0.18
P13	Clinical	4.11	3.42	0.69
	Fixed Grid	2.02	1.90	0.12
	Air	-	-	-
P14	Clinical	5.00	4.13	0.87
	Fixed Grid	2.06	1.93	0.13
	Air	2.11	1.93	0.18

TABLE A.1: Comparison between the measured and the estimated mean beam on + spots changing time (upper table) and mean energy changing time (lower table) for each plan for patients which did not required patching. Missing values for Air plans were not calculated as they were not clinically acceptable for these patients.

A.4 Estimated Contributions to Delivery Times for Plans with ESF = 5

Table A.3 reports estimated values of contributions to the mean delivery times calculated from steering files for Clinical plans and Fixed Grid plans made using an ESF = 3 and ESF = 5 for Patient 1, Patient 6 and Patient 10. The mean delivery times were

estimated by removing from steering files the timing contributions due to patching. The values reported for the beam on time and the spots changing time separately are a rough approximation, since they were derived by using assumptions on the mean spots changing time/spot measured from Log files. Values for the mean delivery time and the energy changing time, instead, can be considered precise, as the can be directly obtained from steering files.

Patient	Plan	Mean Delivery Time [s]	Beam On Time [s]	Spots Changing Time [s]	Energy Changing Time [s]
P1	Clinical	36.01	14.73	15.45	5.83
	Fixed Grid	22.24	15.03	4.27	2.94
	Air	-	-	-	-
P2	Clinical	26.04	12.71	7.77	5.56
	Fixed Grid	19.59	13.20	3.45	2.94
	Air	-	-	-	-
P3	Clinical	25.21	12.06	6.36	6.79
	Fixed Grid	15.86	11.76	2.29	1.81
	Air	19.34	14.55	2.62	2.18
P5	Clinical	21.53	9.19	7.23	5.11
	Fixed Grid	15.09	9.82	2.69	2.58
	Air	14.28	8.23	3.52	2.53
P6	Clinical	48.32	16.16	25.31	6.84
	Fixed Grid	24.06	15.67	5.28	3.11
	Air	24.86	15.38	6.34	3.14
P9	Clinical	25.98	12.21	6.61	7.17
	Fixed Grid	19.53	13.13	2.89	3.51
	Air	19.25	12.39	3.53	3.33
P10	Clinical	76.14	25.69	42.81	7.64
	Fixed Grid	35.25	23.82	8.24	3.19
	Air	-	-	-	-
P11	Clinical	29.13	14.20	9.13	5.79
	Fixed Grid	18.98	14.02	2.99	1.97
	Air	-	-	-	-
P12	Clinical	15.12	6.10	5.50	3.52
	Fixed Grid	9.06	6.16	1.27	1.63
	Air	10.14	6.41	2.03	1.70
P13	Clinical	14.84	6.93	4.49	3.42
	Fixed Grid	12.18	8.54	1.74	1.90
	Air	-	-	-	-
P14	Clinical	20.10	8.94	7.03	4.13
	Fixed Grid	12.14	8.46	1.75	1.93
	Air	12.53	8.35	2.26	1.93
P17	Clinical	31.82	14.86	9.42	7.54
	Fixed Grid	20.18	14.74	3.12	2.32
	Air	-	-	-	-

TABLE A.2: Comparison of values for the total delivery times and single contributions to time (beam on time, spots changing time and energy changing time) between plan and for each patients. Reported values are mean values on fields. Missing values for Air plans were not calculated as they were not clinically acceptable for these patients.

Patient	**Plan**	**Mean Delivery Time [s]**	**Beam On Time [s]**	**Spots Changing Time [s]**	**Energy Changing Time [s]**
P1	Clinical	36.01	14.73	15.45	5.83
	Fixed Grid (ESF = 3)	22.24	15.03	4.27	2.94
	Fixed Grid (ESF = 5)	22.12	15.07	4.56	2.49
P6	Clinical	48.32	16.16	25.31	6.84
	Fixed Grid (ESF = 3)	24.06	15.67	5.28	3.11
	Fixed Grid (ESF = 5)	22.28	15.04	4.78	2.45
P10	Clinical	76.14	25.69	42.81	7.64
	Fixed Grid (ESF = 3)	35.25	23.82	8.24	3.19
	Fixed Grid (ESF = 5)	33.06	23.16	7.37	2.53

TABLE A.3: Comparison of values for the total delivery times and single contributions to time (beam on time, spots changing time and energy changing time) between Clinical plans and Fixed Grid plans with ESF = 3 and ESF = 5. Reported values are mean values on fields.

Bibliography

[1] World Health Organization. Cancer. URL https://www.who.int/news-room/fact-sheets/detail/cancer.

[2] National Cancer Institute (NIH). What is cancer? URL https://www.cancer.gov/about-cancer/understanding/what-is-cancer.

[3] H. Paganetti, C. Grassberger, and G. C. Sharp. Physics of particle beam and hypofractionated beam delivery in nsclc. *Semin Radiat Oncol.*, 31(2):162–169, 2020. doi: https://doi.org/10.1016/j.semradonc.2020.11.004.

[4] J. Gorgisyan, P. Rosenschold, and A. Lomax. Feasibility of pencil beam scanned intensity modulated proton therapy in breath-hold for locally advanced non-small cell lung cancer. *Int J Radiat Oncol Biol Phys.*, 99(5):1121–1128, 2017. doi: https://doi.org/10.1016/j.ijrobp.2017.08.023.

[5] R. F. Hill, P. J. Keall, W.A. Beckham, and M.D. Perez. Photon buildup in orthovoltage x-ray beams. *Australas Phys Eng Sci Med.*, 21(2):51–6, 1998.

[6] Harald Paganetti. *Proton Therapy Physics*. Medical Physics and Biomedical Engineering. CRC Press, 2012.

[7] Provision Healthcare. Proton therapy advantages. URL https://provisionhealthcare.com/about-proton-therapy/advantages-of-proton/.

[8] M. Schwarz. Treatment planning in proton therapy. *Eur. Phys. J. Plus*, 126(67), 2011. doi: https://doi.org/10.1140/epjp/i2011-11067-y.

[9] Professor A. Lomax. PSI's Winter School lecture: Treatment Planning for Pencil Beam Scanning. .

[10] S. St. James, C. Grassberger, and H. Lu. Considerations when treating lung cancer with passive scatter or active scanning proton therapy. *Translational Lung Cancer Research*, 7(2), 2018. doi: https://doi.org/10.21037/tlcr.2018.04.01.

[11] D. Meer. PSI's Winter School lecture: Active Scanning Beam 1: Modulating Delivery.

[12] O. Gjyshi, T. Xu, and Z. Liao. Toxicity and survival after intesity-modulated proton therapy versus passive scattering proton therapy for nsclc. *J. Thorac Oncol.*, 16(2): 269–277, 2021. doi: https://doi.org/10.1016/j.jtho.2020.10.013.

[13] M. Chuong, S. Badiyan, and R. Nichols. Pencil beam scanning versus passively scattered proton therapy for unresectable pancreatic cancer. *J. Gastrointest Oncol.*, 9(4):687–693, 2018. doi: https://doi.org/10.21037/jgo.2018.03.14.

[14] G. S. Yoo, J. Il Yu, and H. Won. Comparison of clinical outcomes between passive scattering versus pencil-beam scanning proton beam therapy for hepatocellular carcinoma. *Radiother Oncol.*, 146:187–193, 2020. doi: https://doi.org/10.1016/j.radonc.2020.02.019.

[15] Particle Therapy Co-Operative Group. Patients statistics. URL `https://www.ptcog.site/index.php/patient-statistics-2`.

[16] William P. Levin and Thomas F. DeLaney. *Charged Particle Radiotherapy*. Elsevier, 2016. ISBN 978-0-323-24098-7.

[17] J. S. Chiang, N. Y. Yu, and T. T. Sio. Proton beam radiotherapy for patients with early-stage and advanced lung cancer: a narrative review with contemporary clinical recommendations. *J Thorac Dis.*, 13(2):1270–1285, 2021. doi: https://doi.org/10.21037/jtd-20-2501.

[18] B. Qiu, Y. Men, J. Wang, and Z. Hui. Dosimetry, efficacy, safety and cost-effectiveness of proton therapy for non-small cell lung cancer. *Cancers (Basel)*, 13(18):4545, 2021. doi: https://doi.org/10.3390/cancers13184545.

[19] S. Lazarev, K. Rosenzweig, and C. B. Simone 2nd. Where are we with proton beam therapy for thoracic malignancies? current status and future perspectives. *Lung Cancer*, 152:157–164, 2020. doi: https://doi.org/10.1016/j.lungcan.2020.12.025.

[20] S. R. Gameiro, A. S. Malamas, and J. W. Hodge. Tumor cells surviving exposure to proton or photon radiation share a common immunogenic modulation signature, rendering them more sensitive to t cell-mediated killing. *Int J Radiat Oncol Biol Phys.*, 95(1):120–130, 2016. doi: https://doi.org/10.1016/j.ijrobp.2016.02.022.

[21] Y. Han. Current status of proton therapy techniques for lung cancer. *Radiation Oncology Journal*, 37(4):232, 2019. doi: https://doi.org/10.3857/roj.2019.00633.

[22] A. Schreuder and J. Shamblin. Proton therapy: what is needed in the next ten years? *Br J Radiol.*, 93(1107):20190359, 2019. doi: https://doi.org/10.1259/bjr.20190359.

[23] J. Boda-Heggemann, A. C. Knopf, and F. Lohr. Deep inspiration breath hold-based radiation therapy: A clinical review. *Int J Radiat Oncol Biol Phys.*, 94(3):478–92, 2016. doi: https://doi.org/10.1016/j.ijrobp.2015.11.049.

[24] K. Raman. 4d scan and respiratory gating. URL `https://www.slideshare.net/skothu/4d-scan-and-respiratory-gating`.

[25] R. Underberg, F. Lagerwaard, and S. Senan. Benefit of respiration-gated stereotactic radiotherapy for stage i lung cancer: an analysis of 4dct datasets. *Int J Radiat Oncol Biol Phys.*, 62(2):554–60, 2005. doi: https://doi.org/10.1016/j.ijrobp.2005.01.032.

[26] D. Georg, M. Hillbrand, and R. Potter. Can protons improve sbrt for lung lesions? dosimetric considerations. *Radiother Oncol.*, 88(3):368–75, 2008. doi: https://doi.org/10.1016/j.radonc.2008.03.007.

[27] M. J. Parkes, S. Green, and T. H. Clutton-Brock. Safely prolonging single breath-holds to ¿5min in patients with cancer; feasibility and applications for radiotherapy. *Br J Radiol.*, 89(1063):20160194, 2016. doi: https://doi.org/10.1259/bjr.20160194.

[28] C. Grassberger, S. Dowdell, and H. Paganetti. Motion interplay as a function of patient parameters and spot size in spot scanning proton therapy for lung cancer. *Int J Radiat Oncol Biol Phys.*, 86(2):380–6, 2013. doi: https://doi.org/10.1016/j.ijrobp.2013.01.024.

[29] M. Rehman, O. Zeidan, and K. Erhart. Dosimetric comparison of various spot placement techniques in proton pencil beam scanning. *Int J Part Ther.*, 9(1):54–63, 2022. doi: https://doi.org/10.14338/IJPT-21-00022.1.

[30] S. Van de Water, M. F. Belosi, and A. Lomax. Shortening delivery times for intensity-modulated proton therapy by reducing the number of proton spots: an experimental verification. *Phys Med Biol.*, 65(9):095008, 2020. doi: https://doi.org/10.1088/1361-6560/ab7e7c.

[31] N. Bizzocchi. Advanced spot and energy layer positioning strategies for proton pencil beam scanning: implementation and evaluation. Paul Scherrer Institute. 2021.

[32] V. Maradia, I. Colizzi, and S. Psoroulas. Universal and dynamic ridge filter for pencil beam scanning particle therapy: A novel concept for ultra-fast treatment delivery. *Phys Med Biol.*, 67(22), 2022. doi: https://doi.org/10.1088/1361-6560/ac9d1f.

[33] A.C. Giovannelli, V. Maradia, and A. Lomax. Beam properties within the momentum acceptance of a clinical gantry beamline for proton therapy. *Med Phys.*, 49: 1417– 1431, 2022. doi: https://doi.org/10.1002/mp.15449.

[34] S. Fujitaka, T. Takayanagi, and T. Terunuma. Reduction of the number of stacking layers in proton uniform scanning. *Phys Med Biol.*, 54(10):3101–11, 2009. doi: https://doi.org/10.1088/0031-9155/54/10/009.

[35] X. Wang, Y. Li, and X. Zhu. Synchrotron-based pencil beam scanning nozzle with an integrated mini-ridge filter: A dosimetric study to optimize treatment delivery. *Cancers (Basel)*, 9(12):170, 2017. doi: https://doi.org/10.3390/cancers9120170.

[36] R. Liu, S. Charyyev, and L. Lin. An integrated physical optimization framework for proton stereotactic body radiation therapy flash treatment planning allows dose, dose rate, and linear energy transfer optimization using patient-specific ridge filters. *International Journal of Radiation Oncology Biology Physics*, 2023. ISSN 0360-3016. doi: https://doi.org/10.1016/j.ijrobp.2023.01.048.

[37] Center for Proton Therapy Paul Scherrer Institute. Patients numbers, . URL `https://www.psi.ch/en/protontherapy/patients-numbers`.

[38] Center for Proton Therapy Paul Scherrer Institute. Gantry 1, . URL `https://www.psi.ch/en/protontherapy/gantry-1`.

[39] E. Pedroni, D. Meer, and S. Zenklusen. Pencil beam characteristics of the next-generation proton scanning gantry of psi: design issues and initial commissioning results. *Eur. Phys. J. Plus*, 126(66), 2011. doi: https://doi.org/10.1140/epjp/i2011-11066-0.

[40] Center for Proton Therapy Paul Scherrer Institute. Therapy facilities, . URL `https://www.psi.ch/en/protontherapy/therapy-facilities`.

[41] Center for Proton Therapy Paul Scherrer Institute. Gantry 2, . URL `https://www.psi.ch/en/protontherapy/gantry-2`.

[42] Center for Proton Therapy Paul Scherrer Institute. Gantry 3, . URL `https://www.psi.ch/en/protontherapy/gantry-3`.

[43] Center for Proton Therapy Paul Scherrer Institute. Optis 2, . URL `https://www.psi.ch/en/protontherapy/optis-2`.

[44] Dr A. Aitkenhead. Treatment Planning Systems for Proton Therapy.

[45] L. Evans. The robustness of the daily adaptive proton therapy optimization algorithm for tumors in the head, 2021.

[46] *Flexible Ion-planning Application: FIonA - Technical Manual*. Paul Scherrer Institute, April 2023.

[47] Martina Bonomi. FIonA Plans Analysis. URL `https://github.com/martibonomi/FIonA-Plans-Analysis`.

[48] Professor A. Lomax. ETH Lecture: Treatment Plan Evaluation. .

[49] P. M. DeLuca, A. Wambersie, and G. Whitmore. Prescribing, recording, and reporting proton-beam therapy: Contents. *J. ICRU*, 7(2):NP–NP, 2007.

[50] X. Sun, Y. Li, and Y. Pu. Shortening the delivery time of proton therapy by real-time compensation method with raster scanning. *Nuclear Science and Techniques*, 33(6):73, 2022. doi: https://doi.org/10.1007/s41365-022-01051-9.

[51] V. Maradia, A.C. Giovannelli, A.L. Lomax, D. Meer, S. Psoroulas, J.M. Schippers, and D.C. Weber. A Novel Beam Optics Concept to Maximize the Transmission Through Cyclotron-based Proton Therapy Gantries. In *Proc. IPAC'21*, number 12 in International Particle Accelerator Conference, pages 2477–2479. JACoW Publishing, Geneva, Switzerland, 2021. ISBN 978-3-95450-214-1. doi: 10.18429/JACoW-IPAC2021-TUPAB407.